MASTER THESIS

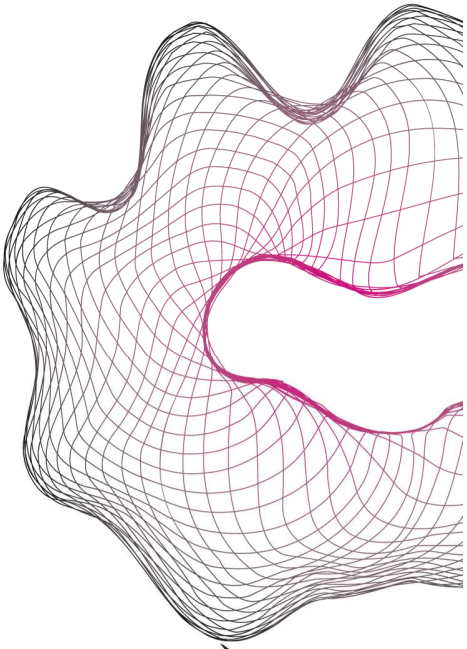

DESIGN OF A STATICALLY BALANCED FULLY COMPLIANT GRASPER USING THE RIGID BODY REPLACEMENT METHOD

A.J. Lamers

FACULTY OF ENGINEERING TECHNOLOGY

MECHANICAL ENGINEERING

MECHANICAL AUTOMATION AND MECHATRONICS

EXAMINATION COMMITTEE

prof. dr. ir. J.L. Herder (chairman)

J.A. Gallego Sanchez Msc

ir. K.P.G. Folkersma

prof. dr. ir. A. de Boer

DOCUMENT NUMBER

-

UNIVERSITY OF TWENTE.

22-06-2012

preface

Sinds 42 het antwoord is op de ultieme vraag over het leven, het universum, en alles [1], kan men zich afvragen of het beter is om antwoorden te hebben of vragen. Of (geen van) beide. De vragen houden je bezig. De antwoorden maken het dagelijks leven gemakkelijker, en geven voor korte duur rust. Ze blijken opgebouwd te zijn uit tig nieuwe vragen. In dit werk komt ten minste 1 antwoord voor. Een robuust stuk metaal dat meegeeft bij de kleinste aanraking. Genoeg reden voor genoeg nieuwe vragen.

Ik wil graag het IMR lab op de TU Delft bedanken voor de aandacht, tijd en ruimte die ik gekregen heb om te ontdekken en te leren. In het bijzonder Just Herder en Juan Gallego. Ook bedank ik Gerard Dunning, Sergio Pellegrini, Pieter Pluimers, Jos Lassooij, Nima Tolou, Lodewijk Kluit en Johan Rob, het was erg leuk en leerzaam om met jullie te werken en op te trekken.

Enschede was onmisbaar. Met regelmaat reisde ik af naar Twente en kon altijd rekenen op een gezellig weerzien en vanzelfsprekende gastvrijheid. Dat is mij veel waard. Mooi!

Dank,

Toon Lamers

Since 42 is the answer to the ultimate question of life, the universe and evertything [2] one could wonder if it is beter to have questions or answers. Or (neither of) both. The questions leave you occupied. The answers make daily life more comfortable, and give rest for the shoft term. They appear to be composed out of many new questions. In this work at least one answer can be found. A robust piece of metal that moves along with the slightest touch. Consequently enough new questions may be posed.

I want to thank the IMR lab at the TU Delft for the attention, time and facilities I received in order to explore and learn. Special thanks to Just Herder and Juan Gallego. Also thanks to Gerard Dunning, Sergio Pellegrini, Pieter Pluimers, Jos Lassooij, Nima Tolou, Lodewijk Kluit en Johan Rob, it was a pleasure to work and meet with you.

Enschede was essential. Frequently I traveled to Twente and always encountered a hospitable and joyful environment. That is worth a lot to me. Great!

Thanks,

Toon Lamers

[1] het boek ”Het Transgalactisch Liftershandboek” door Douglas Adams
[2] the book ”The Hitchhiker’s Guide to the Galaxy” by Douglas Adams

Abstract

Monolithic and thus fully compliant surgical graspers are promising when they provide equal or better force feedback then conventional graspers. In this work a fully compliant grasper is designed to have zero stiffness and the capability to obtain zero operation force. The design problem is addressed by taking a building block approach, in which a pre-existing positive stiffness compliant grasper is compensated by a negative stiffness balancer. The design of the balancer is conceived from a 4-bar linkage and explores the Rigid-Body-Replacement method as a novel design approach towards static balancing. Design variables and sensitivities are determined through the use of a pseudo rigid body model. Final dimensions are obtained using rough hand calculations. Justification of the pseudo rigid body model as well as the set of final dimensions is done by non linear finite element analysis. Experimental validation is done through a titanium prototype of 40 [mm] size having an unbalanced positive stiffness of 62.3 [N/mm] showing that a force reduction of 98.92 [%] is achievable over a range of 0.6 [mm]. While hysteresis is approximately 1.32 [%]. The behavior can be tuned from monostable to bistable. The Rigid-Body-Replacement method was proved successful in the design of a statically balanced fully compliant grasper, widening the design possibilities for this kind of mechanisms.

Contents

Chapter 1

Introduction

1.1 Background

In this work the application of statically balanced fully compliant (SBFC) mechanisms is proved valuable in the development of a grasper for minimal invasive surgery. Statically balanced compliant mechanisms are mechanisms which achieve motion due to elastic deformation of slender parts, but without requiring any external work. The elastic potential remains constant through the range of motion. Important design requirements for surgical tools are high force feedback and high sterilisability. Ideally this means removing all hinges which are present in conventional tools used today. This can be done by designing a fully compliant grasper. But then elasticity will disturb force feedback instead. Here a statically balanced fully compliant mechanism would meet all design requirements. And besides that the monolithic character of statically balanced fully compliant mechanisms also creates opportunities for the design of a inexpensive single piece disposable tool.

1.2 Problem statement

Design of compliant mechanisms is not an easy task. As expressed by Howell [6], the design of compliant mechanisms considering only kinematic requirements is challenging enough. Adding the static balancing requirement will in general add even more complexity to the design of the compliant mechanism. The problem is that for this new class of mechanisms no established general design method exists yet [3]. And known so far no successful prototype has been presented yet of a statically balanced fully compliant surgical grasper [11].

1.3 Literature review

In 1997 the urge for high force feedback was recognized and aimed for by designing a rolling contact mechanism replacing the conventional hinged surgical grasper by Herder et al [7]. In 2000 it was realized by van den Berg and Herder [4] that friction, wearing, lubrication, etc. could be eliminated by moving towards a zero stiffness compliant design, with the added benefits of sterilizability and reduced assembly costs. While a prototype was made, it was not a fully compliant design, it consisted of a positive stiffness compliant gripper compensated by a rolling contact mechanism. The balancing mechanism compensates for the elastic forces of the compliant grasper. Later in 2004 Stapel and Herder [10] proposed a feasible solution for a fully compliant version but no prototype was made. De Lange et al. [9] proposed in 2008 a design based on topology optimization, without a proving prototype. In 2009 Tolou and Herder [11] developed a mathematical model for partially compliant bistable segments in order to

facilitate the design of a partially compliant balancing mechanism. In 2010 fully compliant balancing segments (negative stiffness building blocks) are introduced by Hoetmer et al [5]. A prototype was created using these segments but exceeded the yield stress due to the pre-loading force.

In literature devoted to the development of this SBFC surgical grasper attention is payed to the design methodology aswell as the specific design problem itself. Known so far, the proposed and developed methodologies did not deliver a real world solution for the SBFC surgical grasper. In general not much design examples of SBFC mechanisms are described in literature, the design methodology seems to be undeveloped. See appendix A for a literature review. Allthough there is a vast amount of literature on designing compliant mechanisms [2], the field of designing SBFC mechanisms seems relatively unexplored [3].

1.4 Objective

The objective of this work is the design and prototyping of a statically balanced fully compliant grasper. The design approach is based on the exploration of the Rigid-Body-Replacement method (RBR) as a novel way to design statically balanced compliant mechanisms.

1.5 Structure

This work is structured as follows. The method chapter begins treating the design criteria, followed by a chronological description of the taken design steps and concluding with the method of evaluation. The evaluation method focuses on the obtained design itself using FE analysis, the experimental setup and the taken design approach (RBR method). The results chapter presents the FE predictions for the final design, the measurement results and a validation of the derived pseudo rigid body model used in the rigid body replacement method. In the conclusion chapter assessment of the design criteria and the design approach will be done. The discussion chapter focuses on the recommendations and perspectives of the obtained design as well as the design approach.

Chapter 2

Method

2.1 Criteria

A grasper for minimally invasive surgery should achieve high force feedback and high sterilizability, staying within a certain size and weight allowing for easy manual operation and handling. The sterilizability requirement can be met by choosing for a monolithic and thus fully compliant mechanism. High force feedback can be obtained by implying static balance. The size requirement can be accomplished by looking for the smallest allowable monolithic geometry satisfying a certain balance quality. It is assumed that meeting the size requirement means meeting the light weight requirement. The requirements can then be summarized in two main criteria discussed next.

The power transmission criterion defined by equation 2.1 accounts for the static balance property. As long as at each time instance the input power is equal to the output power, no energy will be stored or lost in the mechanism during any motion. When any other external dissipating (damping) or accumulating (driving) effects are neglected the elastic potential must remain constant. This is a necessary and sufficient condition for static balance. Since there is no typical value known for the power occuring in surgical applications, it is suggested to consider the next properties:

- The energy needed to deform the unbalanced mechanism against the balanced mechanism
- The ratio between the maximal change in force in both cases, called the force reduction factor, defined as: $(1 - F_2/F_1) \cdot 100[\%]$. see figure 2.1.
- The energy needed to pre-load the mechanism against the energy used to balance the mechanism
- The hysteresis of balanced and unbalanced mechanism

All mentioned properties will be investigated in this work.

The size requirement defined by equation 2.2 and its quantification is adopted from Stapel [10]. The requirement is based on the size of a cylinder in which the design should fit. When this is the case then the mechanism is assumed to be acceptable for application in a surgical handcraft tool. The length of the cylinder is undetermined but certainly subjected to the same goal.

$$\frac{P_{out}}{P_{in}} = 1 \tag{2.1}$$

$$\text{size} \leq \varnothing 40 \tag{2.2}$$

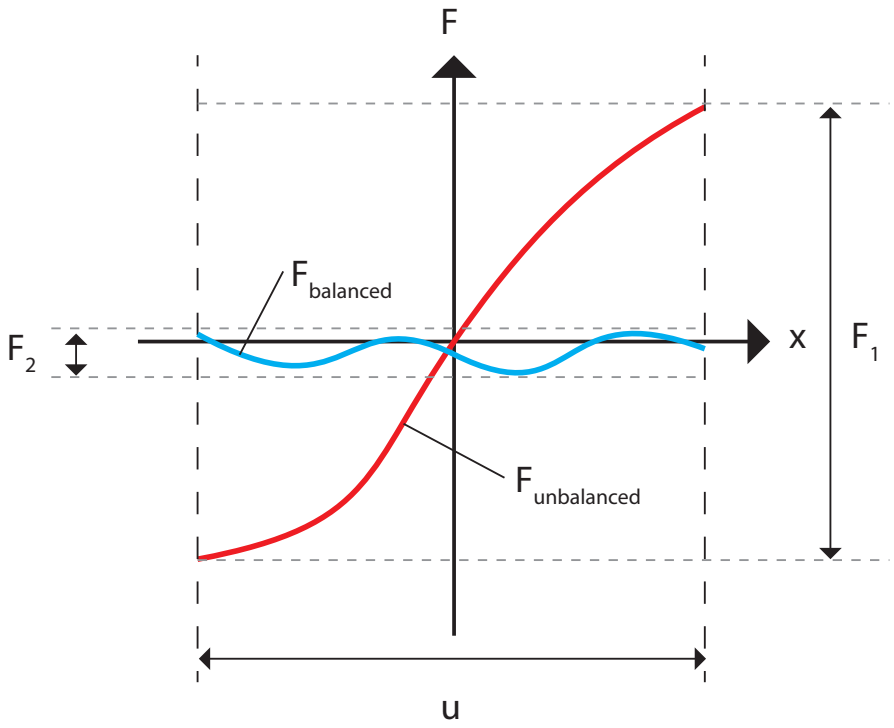

Figure 2.1: Definition of the force reduction factor: $(1 - F_2/F_1) \cdot 100[\%]$.

2.2 Design

The design problem is addressed by taking a building block approach. A fully compliant negative stiffness mechanism is designed by using the rigid body replacement method. The design variables and sensitivities are determined through the use of a pseudo rigid body model. Non linear finite element analysis is used to evaluate the pseudo rigid body model. A prototype was fabricated using wire EDM. Validation of the models is done through measurement of the prototype.

A prototype is manufactured and measured to validate the experiment is performed to validate

2.2.1 building block approach

In this work it is assumed that one deals with a pre-existing compliant mechanism having near constant positive stiffness over a range of motion. When a mechanism with equal but negative near constant stiffness is connected, a zero stiffness mechanism will result. This is called the building block approach (see the literature review in appendix A). Now if the building blocks (positive stiffness and negative stiffness) are physically connected to each other from an equilibrium configuration (zero force), then the resultant zero stiffness entails neutral stability along the entire range of motion. Neutral stability is a necessary and sufficient condition for static balancing that implies zero stiffness and zero force. This condition is derived from the more fundamental condition, the constant potential energy criterion.

In our case the pre-existing positive stiffness is the compliant grasper proposed by van den Berg [12], see figure 2.2. This grasper was specifically designed for minimal invasive surgery and satisfies the applicable set of requirements for this purpose. So the design of the grasper itself will not be considered in this work. A negative stiffness balancing mechanism will be designed to compensate for the positive stiffness of the grasper. The grasper and balancer need to be manufacturable out of one single piece of material. Typical properties of the grasper are :

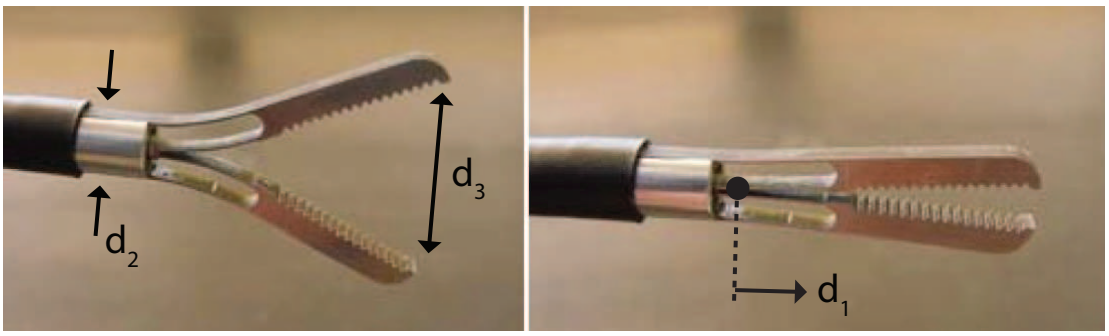

Figure 2.2: Compliant grasper designed by van den Berg [4] in open and nearly closed configuration.

- actuation displacement range: $d_1 = [-0.3...0.3]$ [mm]
- actuation force deflection behavior: linear
- actuation stiffness: 50 [N/mm] (material: orthopedic stainless steel)
- size: fits in a $d_2 = \varnothing 5$[mm] tube when closed
- max open: $d_3 = 10$ [mm]

2.2.2 negative stiffness

Negative stiffness rises from elastic systems that exhibit unstable equilibrium points. Most elastic bodies naturally reside in a state of stable equilibrium, even for large perturbations. Elastic structures are in fact in most cases designed to do so. However it is known that the transition from stability to instability can occur under certain loading conditions. For simple geometry and infinitesimal displacements this transition of the force deflection relation can be modeled analytically and solved explicitly for some cases. An example of this is the constant cross section cantilever beam, axially and laterally loaded that is presented in appendix C.

For design purposes it is beneficial to have more freedom of shape than just the simple beam shape. However more complex geometric shapes means in many cases loosing the simple analytical description. In those situations it is likely that one has to rely on non linear finite element modeling to analyze the stability transition and to study the unstable behavior. Consider for example the design of a 6 DOF statically balanced stage by Dunning [1]. In this design so called ”bistable buckling beams” are used as balancing elements. To study the unstable behavior of those elements extensive use of finite element analysis was necessary. This makes analysis often a computational demanding matter, while contribution to the understanding of the behavior is relatively small.

2.2.3 rigid body replacement method

A simplification of modelling negative stiffness may be obtained by using the rigid body replacement method. The Rigid-Body-Replacement method (RBR) assumes that a compliant mechanism can be designed by first designing a rigid body mechanism. Once the kinematics is determined, a proper replacement of rigid elements by flexible element provide with a compliant solution with a close kinematic behavior. When force deflection requirements are included, it is needed to account for the stiffness in the rigid body model. Normally, stiffness is modeled by the use of torsion springs. When the rigid body is composed of pin jointed rigid links, the RBR method makes extensive use of the Pseudo-Rigid-Body model (PRB) to translate the rotating links into deflecting cantilever beams. See figure 2.3.

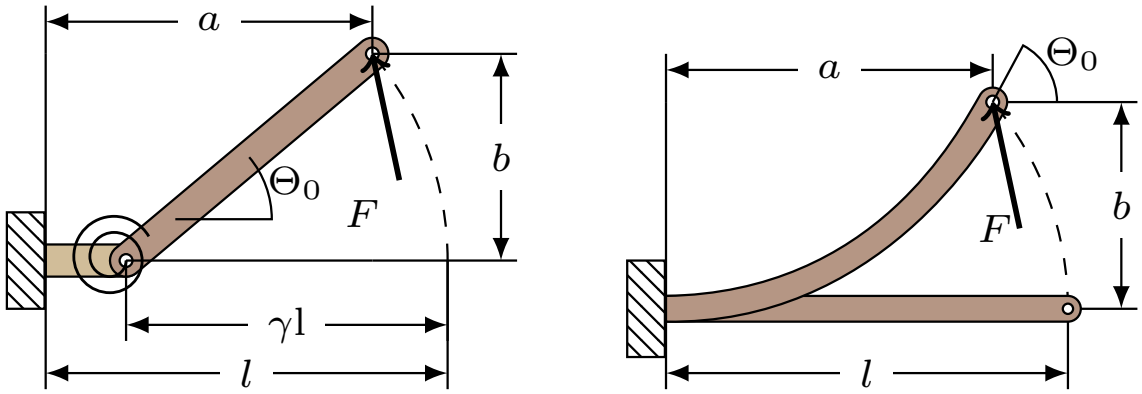

(a) rigid link mechanism

(b) compliant mechanism

Figure 2.3: The pseudo rigid body model for a distributed compliance [6]

The PRB model allows approximating the kinematic and dynamic behavior of the flexible model with a relative small set of kinematic and equilibrium equations, even for large deflections. This means a computational advantage compared to non linear finite element modeling while still being fairly compatible with the designer's intuition. For these reasons the rigid body replacement method is used in this work. Thereby the problem of finding an elastic structure having negative stiffness shifts to finding a rigid body mechanism having negative stiffness. Once found, it has to be converted to an elastic mechanism.

2.2.4 topology

In the case of the surgical grasper the balancer requires to be a 1 degree-of-freedom (DOF) system with straight line motion. The simplest solution providing 1 DOF is the four bar linkage. There are several straight line motion solutions, like Watt's linkage or Burmester's linkage, but in most of these the motion is dimension dependent, therefore it is opted for a rocker-coupler-slider linkage. This is illustrated in figure 2.4

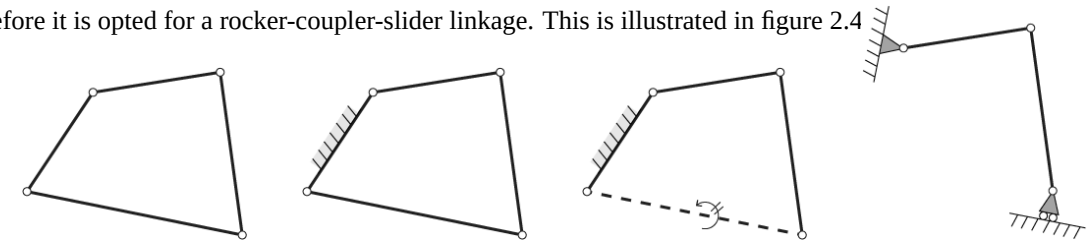

(a) Four bar kinematic chain.

(b) A four-bar linkage is created by grounding one link from the kinematic chain.

(c) Replacement of a pin joint by a sliding joint.

(d) rocker slider mechanism

Figure 2.4: Obtaining the rocker slider topology for the rigid link mechanism.

2.2.5 design variables

Torsion springs must be applied in all 3 hinges of the rocker slider mechanism in order to create the possibility to replace the rigid bodies by compliant segments. See illustration 2.5. The mechanism exhibits negative stiffness when (i) the torsion stiffness in hinge A is larger than in hinges B an C, and (ii) the pre-loading displacement at hinge A is in a vertical downward direction. In this section the behavior of the force in point C over a horizontal displacement range of point C is investigated for changes in model parameters.

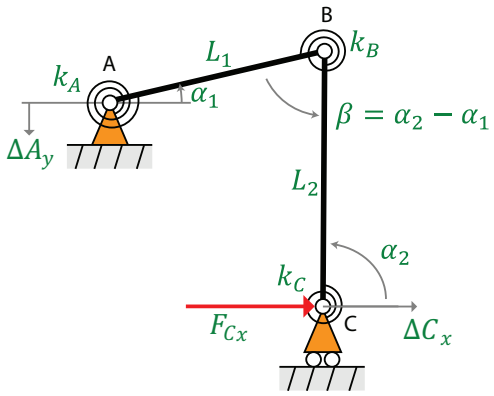

Figure 2.5: The rocker slider mechanism having torions springs.

Table 2.1: Model parameters for rocker slider mechanism.

torsion stiffness [Nmm/rad]	$k_A = 100 \cdot 10^3$ $k_B = k_C = 1 \cdot 10^3$
link lengths [mm]	$L_1 = 20$ $L_2 = 15$
initial coordinates of hinges A and C [mm]	$\langle A_{xi}, A_{yi} \rangle = \langle 0, 15 \rangle$ $\langle C_{xi}, C_{yi} \rangle = \langle 20, 0 \rangle$
range of motion [mm]	$\Delta C_x = [-3...3]$
pre-loading displacement [mm]	$\Delta A_y = -1$

For this mechanism the force displacement function can be explicitly found at point C in the horizontal direction:

$$F_{Cx} = f(C_x) \text{ with } C_x = C_{xi} + \Delta C_x \tag{2.3}$$

See appendix D for the derivation of this function. The pre-loading is done by adding a negative value to the initial y-coordinate of point A.

$$A_{yi} + \Delta A_y \tag{2.4}$$

To study the behavior of the mechanism, a representative approximate set of values is chosen for the model parameters in the following way. See table 2.1. The origin of the coordinate system is placed such that coordinates A_{xi} and C_{yi} are zero. Link 1 and 2 are about equal in length. As the size requirement restricts dimensions to be below 40 [mm] a typical link length is set to the half of this value (for reasons explained in section 2.2.6). Considering that hinges B and C are likely to be replaced by elastic joints some space needs to be reserved for this, that is why L_2 is chosen a bit smaller than L_1. Prescribing L_1 and L_2 to be perpendicular makes the geometry fully determined. The torsion stiffness in hinge A is chosen such that F_{Cx} shows realistic values (in the range of 15 to 20 [N] based on the typical values listed in section 2.2.1), values for hinge B and C are chosen much lower. The magnitude of the range of motion ΔC_x and the pre-loading displacement ΔA_y are chosen such values that they dont differ to much from the initial stress free geometry while non linear behavior is still visible. Now the model is fully determined and the force displacement graphs can be investigated through equation 2.3.

For this purpose a graphical user interface was programmed which shows interactively how the force deflection graph is affected by changes in the model parameters through sliders. See appendix E for a screenshot and the numerical scheme used in this graphical user interface. A detailed study was performed (see appendix F), the main

results will be summarized below. Dotted lines in the configuration plots represent the stress free configuration, continuous lines represent the actual configuration for $\Delta C_x = -3$ [mm] and the full pre-loading displacement $\Delta A_y = -1$. In the force deflection graphs the change of model parameter from initial to final value is indicated by lines with circles (initial) and by lines with squares (final). Dotted lines lying in between the initial and final graphs are incremental solutions.

Figure 2.6b presents the results of the incremental change of the pre-loading displacement until its final value. It can be observed that the system turns from stable to unstable. Figure 2.6a shows the corresponding geometry of the mechanism. The pre-loading displacement acts as a tuning parameter of the negative stiffness. During tuning the unstable equilibrium point shifts a little bit to the right side.

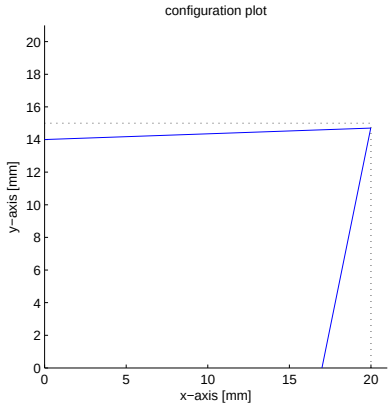

(a) Pre-loaded configuration.

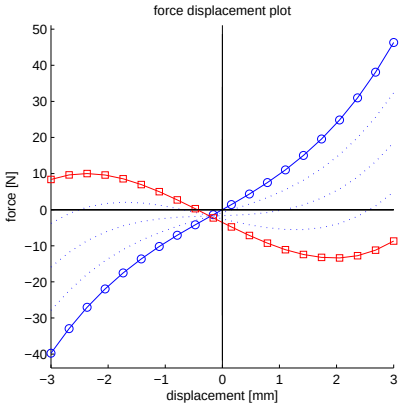

(b) Force displacement graph of F_{Cx} tuned by pre-loading displacement.

Figure 2.6: GUI simulation of rigid body mechanism, tuning the pre-loading displacement.

The negative stiffness will increase when torsion stiffness A increases relative to B and C. Nearly the same increasing effect is seen when link length L_1 is shortened while both links are kept perpendicular in the stress free configuration. This is illustrated in figure 2.7.

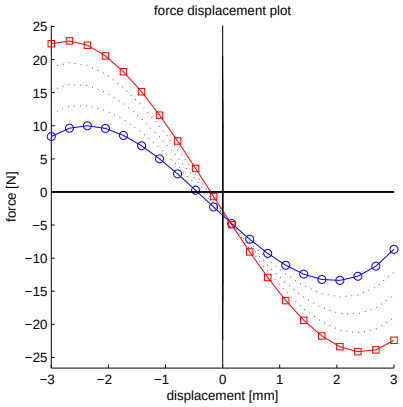

Figure 2.7: GUI simulation, effect of tuning torsion stiffness values and link lenght L_1

Varying the angle of link 2 around vertical orientation in the stress free configuration has significant influence on the behavior. Decreasing or increasing the angle from vertical orientation causes a large forward or backward shift of the force deflection graph. See figure 2.8.

The effects of changes in other model parameters seem to be relatively small and are therefore not discussed here. See detailed investigation in appendix F.

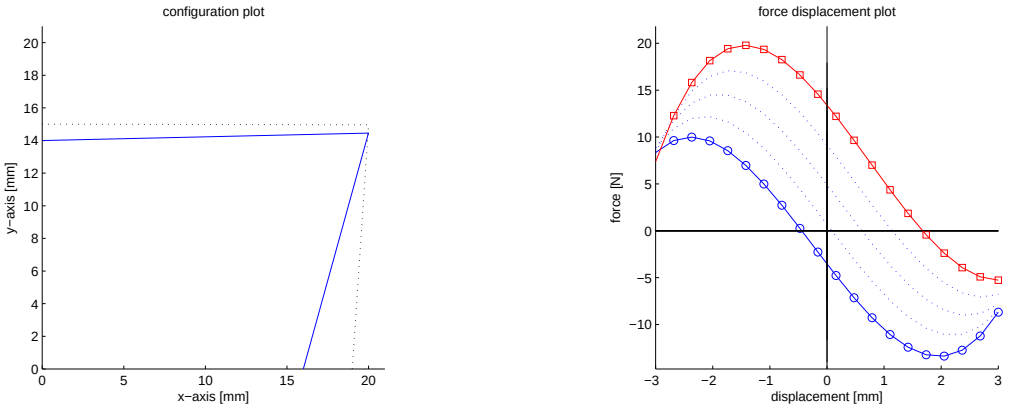

(a) Configuration for rotational offset of link L_2 in stress free configuration.

(b) Large shift of force displacement graph due to rotational offset.

Figure 2.8: GUI simulation of tuning rotational offset of link L_2.

From these observations the following conclusions can be drawn. When designing for negative stiffness the ratio between the stiffness in hinge A should be maximized relative to B and C. Both links may be perpendicular to each other in stress free configuration. Any deviation from perpendicularity only causes undesired shifting of the force deflection graph. The length of link 1 should be decreased. While the length of link 2 should be maximized to improve the linearity of the behavior, see appendix F.

2.2.6 monolithic design

After identifying the main design variables, a fully compliant geometry may be derived to replace the rigid body mechanism. See figure 2.9.

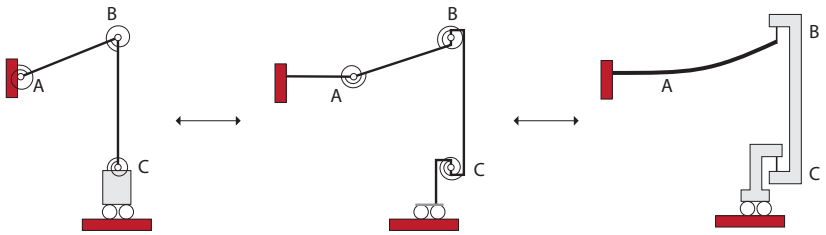

Figure 2.9: The rocker slider mechanism (on the left) converted to a version (in the middle) which may be replaced by a compliant geometry (on the right).

The torsion stiffness in hinge A should be high. The pre-loading displacement will then develop a high vertical force in hinge B, increasing the negative stiffness. This is proven in the last section of appendix D. To prevent high stresses a distributed compliance is chosen to replace link 1. See figure 2.10a.

Torsion stiffness in hinge B and C should be low. Lumped compliances are used to realize elastic joints that have well defined hinge locations. Several common solutions are available for lumped compliances [8]. To simplify the design process a leaf spring shape is chosen. In this case the joints should transmit a high vertical force in points B and C. Then compressive stresses are unwanted since they easily could buckle the slender leaf spring shape, thus a ”tensile setting” is applied. Finally link 2 is replaced by a rigid body having leaf spring shaped lumped compliances at both ends in a tensile setting as illustrated in the figures 2.10b and 2.9 on the right.

The resulting geometry is not fully compliant as can be seen in figure 2.9 on the right. Straight line guidance is still needed for horizontal displacement of point C. And when the pre-loading displacement ΔA_y is used for

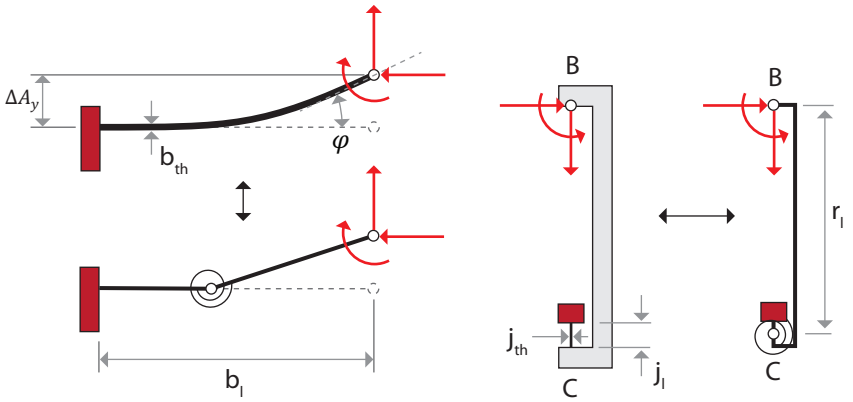

(a) A distributed compliance replacing hinge A

(b) A lumped compliance in a tensile setting, replacing hinge C. Also applied on hinge B.

Figure 2.10: Replacing the rigid bodies of the rocker slider mechanism.

tuning the negative stiffness then a straight line guidance for vertical displacement is needed at point A too. The design may be mirrored two times to get rid of the need for straight line guidance at both points. This is done over the horizontal axis and over the vertical axis. See figure 2.11.

A disadvantage of mirroring is that the size of the mechanism is doubled in two directions, for that reason link length 2 is initially taken less than half (15 [mm]) of the size requirement. On the other hand, the mirror operation over the vertical axis has as consequence (i) an equilibrium point insensitive to the shifting due to the pre-loading (see fig. 2.6b) and (ii) a four times increased negative stiffness. See appendix G for detailed information about mirroring.

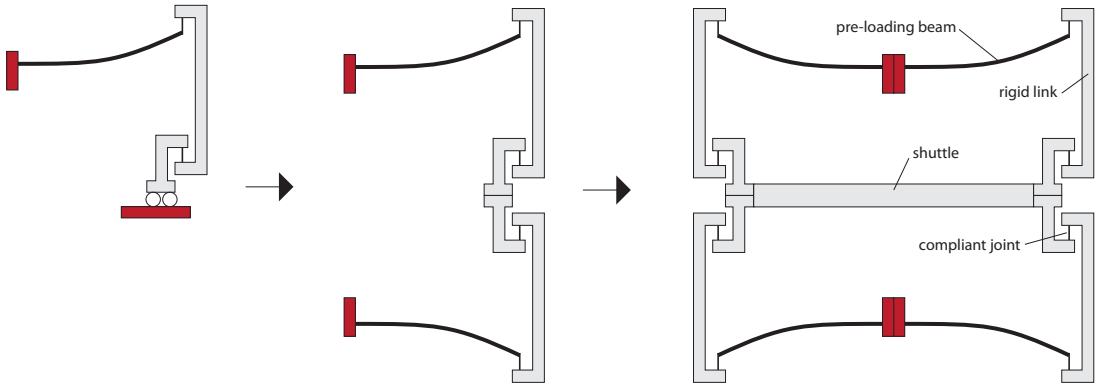

Figure 2.11: Mirroring the partial compliant solution vertically and horizontally.

2.2.7 dimensions

Final dimensions need to be obtained such that (i) it is suitable for the manufacturing method and (ii) for not exceeding the maximal allowable stress while maximal negative stiffness is exposed. This is done by some rough hand calculations as summarized below following the next line of thought.

The elastic joint is recognized as the most critical part of the mechanism. It has to transmit the maximal possible tensile force and in the mean time account for bending moments. The bending moments are generated by the pre-loading of the mechanism and by the movement through the whole range of motion. Applying a pre-loading displacement means that a rotational deflection occurs at the tip of the pre-loading beam (where it is connected to

the elastic joint) conveying the induction of a bending moment.

The resulting bending and tensile stresses (summed together) should stay below the allowable stress which is set to 500 [MPa]. The selected material is titanium grade 5, with a Young's modulus of 113.9 [MPa]. In order to maximize the tensile force the portion of bending stress should be minimal. This means that bending deformation should be kept small. Thus (i) having a small range of motion compared to the mechanism size and (ii) having small rotations at the tip of the pre-loading beam due to pre-loading. Since loading and deflection are meant to be in-plane, a relatively large out-of-plane thickness of $w = 6$ [mm] is chosen to prevent any out-of-plane deflection effects due to asymmetric loading.

Elastic hinge

Since the equivalent torsion stiffness needs to be minimized, the smallest producible thickness j_{th} is assumed for the elastic hinge (see figure 2.10b), which is about 0.2 [mm] in case of wire EDM. Taking a length thickness ratio of 10 makes the length $j_l = 2$ [mm] and by that guarantees slenderness of this elastic segment. The length r_l of the stiff part is limited by the design requirement of 40 [mm]. Extra space for the elastic hinges is needed, so a length of approximately 15 [mm] is taken into account. When a portion of 2/3 of the allowable stress is set for tensile stress then 1/3 is set for the bending stress. This results in a maximal allowable tensile force of 400 [N].

Pre-loading beam

The pre-loading beam is considered to be a one sided clamped beam with lateral loading at the tip (see figure 2.10a). So for small deflections the next force deflection relations from linear beam theory apply.

$$\Delta A_y = \frac{F \cdot b_l^3}{3 \cdot E \cdot I} \tag{2.5}$$

$$\varphi = \frac{F \cdot b_l^2}{2 \cdot E \cdot I} \tag{2.6}$$

$$I = \frac{1}{12} \cdot w \cdot b_{th}^3 \tag{2.7}$$

The load amounts 400 [N] as prescribed by the elastic hinge. Minimizing tip rotations can be achieved by designing a beam having low length/thickness ratio (b_l/b_{th}). For this reason the pre-loading displacement is assumed to be small but still tunable, that is $\Delta A_y = 0.2$ [mm]. Using formula 2.5 and 2.7 the length thickness ratio becomes then:

$$\frac{b_l}{b_{th}} = \sqrt[3]{\frac{\Delta A_y \cdot E \cdot w}{4 \cdot F}} \approx 4.40 \ \ [-] \tag{2.8}$$

Using 2.6 and 2.7 gives a tip rotation of approximately:

$$\varphi = \frac{6 \cdot F}{E \cdot w} \cdot \left(\frac{b_l}{b_{th}}\right)^2 \approx 6.80 \cdot 10^{-5} \ \ [\text{rad}] \tag{2.9}$$

Knowing this ratio, choosing a length b_l or thickness b_{th} gives the final dimensions of the prelaod beam. The length will be considered (rather then the thickness) since it was explored as a design variable in section 2.2.5. Decreasing the length will improve the negative stiffness, but also increase bending stresses. Another possible disturbing effect is rotation of the shuttle when pre-loaded. The length should be increased to avoid this. Another measure is taken to avoid this effect, that is the leaf springs at 1 and 2 acting as a straight line guidance, see figure 2.12. Thus after all increasing the length is prefered. In order to find a reasonable size of the mechanism a limit is

set to below 30 [mm]. Final dimensions become then: length 29.5 [mm] and thickness 6.8 [mm]. This results in to a bending stress of 260 [MPa].

To prevent stress concentrations at corners, a fillet of radius 0.45 [mm] is applied. In figure 2.12 the final design is shown. Leaf springs 3 and 4 are added for straight line guidance for measurement purposes, they can be omitted in case of application to a surgical tool.

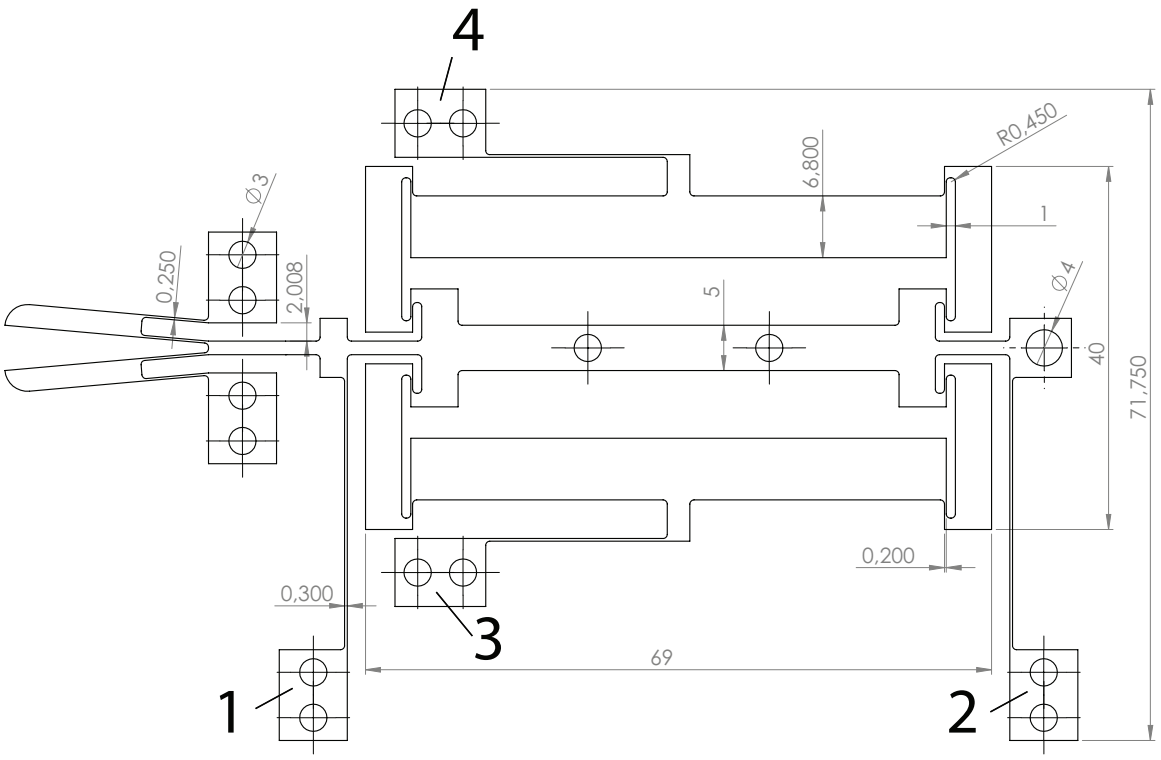

Figure 2.12: The final geometry of a monolithical statically balanced grasper. Main dimensions are shown.

2.3 Evaluation

2.3.1 Obtained design

To evaluate the obtained design a finite element model is used (non linear analysis) to predict the force deflection behavior of the balancer and the grasper individually, and to check for the maximal stresses. See appendix B for a detailed description. Also a linear pre-buckling analysis is done on the balancer model to check for unwanted low stiffness modes which may occur close to the pre-loading force, such as a rotational mode of the shuttle. See appendix H for details. Important results are summarized in section 3.

2.3.2 Experiment

Experimental validation of the design is done by measuring the force deflection characteristics of a manufactured prototype. The prototype is fabricated by wire electrical discharge machining. The displacement range is prescribed at point 7, see figure 2.13. At the same point the force F is measured. The next four load cases are measured.

1. force deflection graph of grasper: point 1 and 2 are fixed, point 3 and 4 are free. No pre-loading is applied at point 5 and 6.
2. force deflection graph of grasper and balancer: points 1,2,3 and 4 are fixed. No pre-loading is applied at point 5 and 6.
3. force deflection graph of grasper and balancer while pre-loaded. points 1,2,3,4 are fixed. At point 5 and 6 a pre-loading displacement is applied.
4. force deflection graph of balancer. Points 3 and 4 are fixed, 1 and 2 are free, pre-load is applied at 5 and 6.

See the 2 pictures below (figure 2.14) for the measurement setup. They show the monolithic design fitted in the measurement setup for the non pre-loaded state and the pre-loaded state. The levers (1,2) are used to pre-load the mechanism accurately by prescribing a displacement using the tuning screws (3,4). The pre-loading force is not measured. At point 5 the connecting rod to the force sensor and linear actuation stage can be seen. Important results are discussed in chapter 3. A detailed measurement report can be found in appendix L.

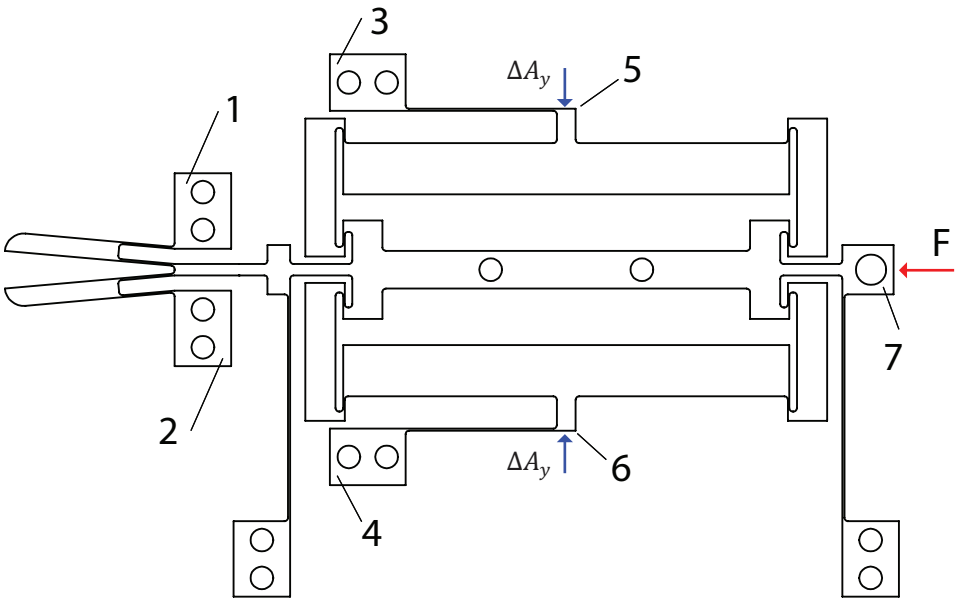

Figure 2.13: Schematic view of measurement method for different load cases.

2.3.3 Design approach

To evaluate the design approach the justification of using a rigid body mechanism for the behavioral study of the compliant mechanism is investigated. This is firstly done by a strain energy analysis using the finite element model. For specific parts of the model the strain energy is calculated, the distribution of strain energy over several parts is compared to the energy characteristics of the rocker slider mechanism. See appendix I for detailed information on the strain energy analysis. Secondly the pseudo rigid body modeling method is applied to the final design to obtain a more accurate force deflection graph from the rocker slider model (see appendix J). This graph is compared to the prediction of the finite element model. Additionally a sensitivity analysis for design variables is performed for the finite element model and the pseudo rigid body model. Those results are compared for both models with the experimental data, see appendix K. Important conclusions are summarized in chapter 3.

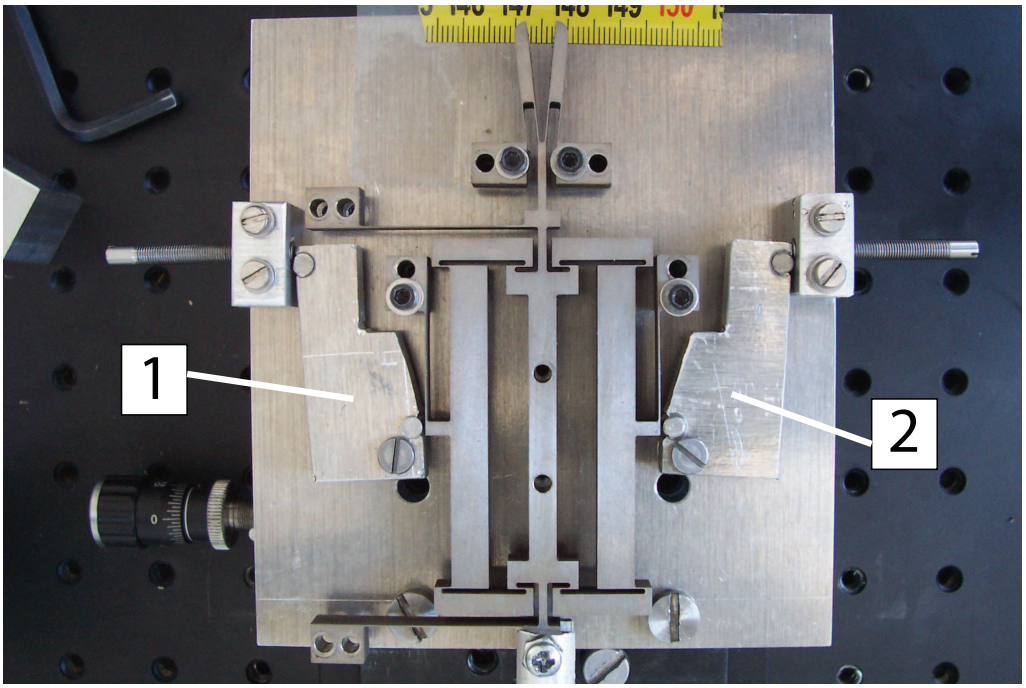

(a) Prototype in non pre-loaded state.

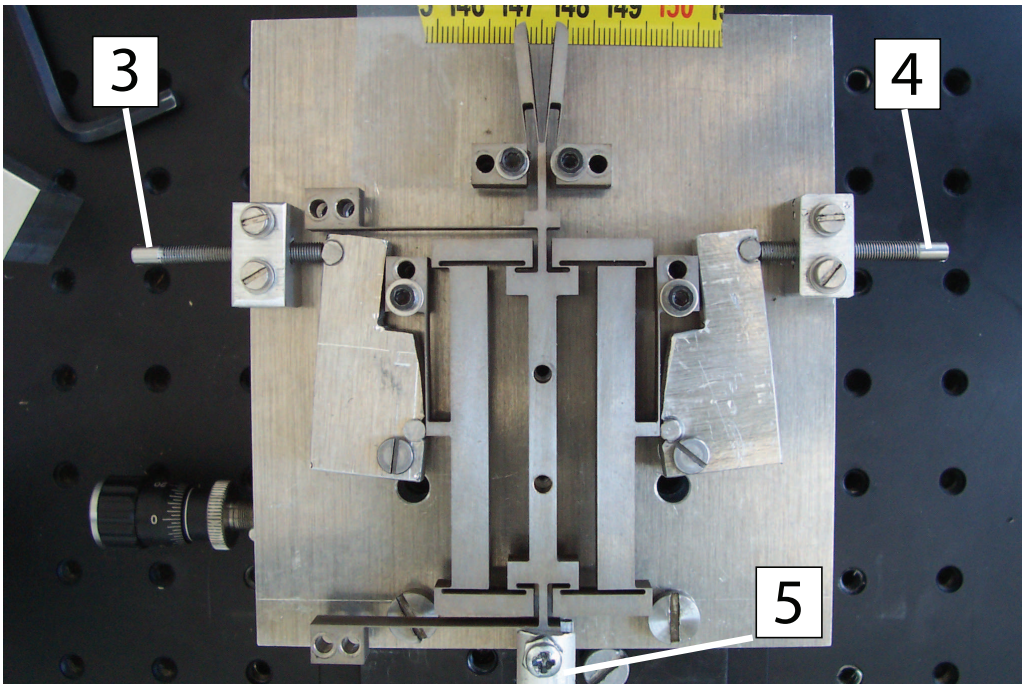

(b) Prototype in pre-loaded state.

Figure 2.14: Photos showing the measurement setup used to evaluate the different load cases.

Chapter 3

Results

3.1 Model predictions

Grasper and balancer are both individually modeled and analyzed through non linear finite element analysis using displacement control. The simulation shows that the balancer generates approximately enough negative stiffness to compensate the positive stiffness of the grasper. See figure 3.1. The maximal occurring equivalent stress is 555 [MPa] for the balancer and 531 [MPa] for the grasper. See appendix B for more details.

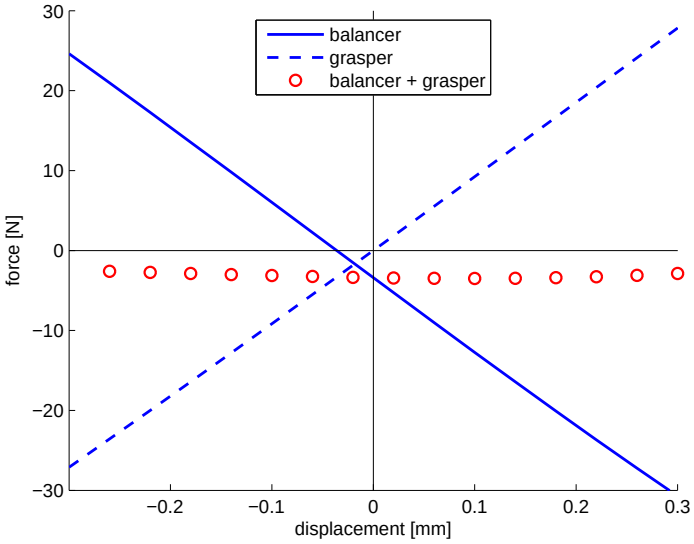

Figure 3.1: FE simulations of the balancer and the grasper individually. Both results are added afterwards to predict the behavior of the balanced mechanism.

3.2 Measurement of the prototype

The wire EDM fabricated design is pictured in figure 3.2.

Force deflection data resulting from the experiment as described in the section 2.3 (Evaluation) are plotted in figure 3.3. Detailed measurement information is contained in appendix K. The red circles in the graphs indicate the starting point (grasper is fully open) in the range of motion during measurement.

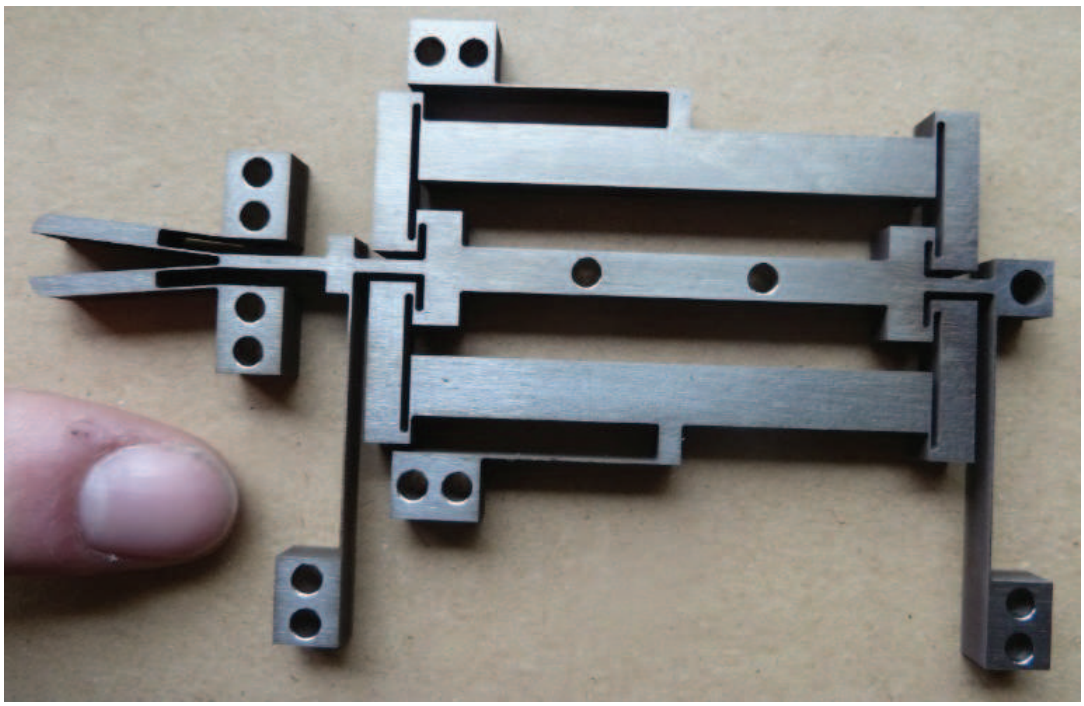

Figure 3.2: Prototype manufactured by wire EDM.

Table 3.1: The energy balance calculated based on measurement data.

case	remark	energy in [mJ]	energy out [mJ]	hysterisis [mJ]
case 1	unbalanced mechanism	5.6819	-5.5800	0.1019
case 2	constant positive force	0.8242	-0.7749	0.0492
case 3	constant negative force	1.5851	-1.5099	0.0752
case 4	bistable	0.5023	-0.4369	0.0653

In load case 1 and 2, see figure 3.3a, one can see the difference in positive stiffness of the grasper and the combination of grasper and balancer without pre-loading. The positive stiffness of the balancer alone is thus much lower than the grasper. Both load cases expose nearly linear behavior. When pre-loading is applied, see load case 3 in figure 3.3b, the positive stiffness is drastically influenced. The range of motion is taken smaller (0.6 instead of 0.8 [mm]) for reasons related to out-of-plane deflection. This is explained in the measurement report, see appendix L. The results in terms of energy and hysteresis are listed in table 3.1.

The results of load case 4 are figured in 3.4 and listed in table 3.2. The negative stiffness is approximated by the formula $k = \Delta F/\Delta x$ using the entire measurement range for ΔF and Δy. Pre-load displacement is incrementally raised to a value of approximately 0.25 [mm]. Thereby the negative stiffness of the balancer is clearly tuned. The position of the equilibrium point is hardly influenced by the pre-loading.

3.3 Model validation

3.3.1 Comparison between the measurement data and the model predictions

The experimental data is compared with the finite element model (see appendix B), and the pseudo rigid body model (see appendix J). The comparison is graphed in figure 3.5. For both models the same nominal set of parameters is used. These parameters are based on the dimensions of the final prototype and the estimated values

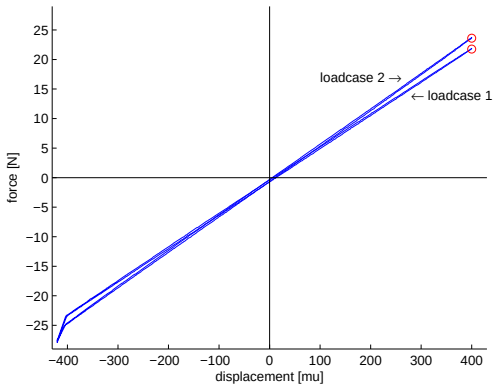

(a) Load case 1 having positive stiffness of 56 N/mm and load case 2 having 60 N/mm over a range of 0.8 mm.

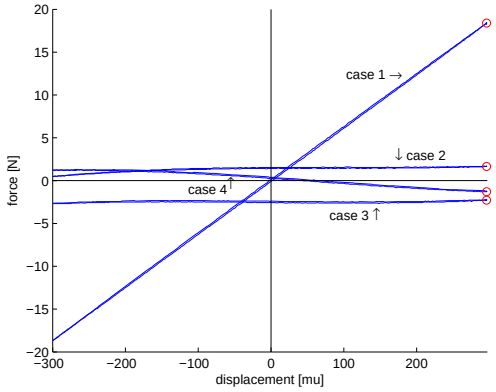

(b) Load case 3 showing different measurement results over a range of 0.6 mm, the unbalanced behavior (case 1), two constant force behaviors (case 2 and 3) and one bistable behavior (case 4).

Figure 3.3: Measurement results of different loadcases and settings.

Table 3.2: Negative stiffness and hysteresis values calculated based on measurement data.

nr	negative stiffness [N/mm]	linear correlation [-]	hysteresis [mJ]
1	-7.82	-0.99785	0.0159
2	-17.47	-0.99948	0.0539
3	-25.29	-0.99964	0.0786
4	-36.13	-0.99973	0.1273
5	-45.96	-0.99979	0.1953
6	-58.53	-0.99980	0.3297
7	-68.53	-0.99982	0.5149

of settings of the applied load case during the experiment. In theory the three results should be close to each other. But the comparison shows a significant deviation, however the measurement data and both models show the desired linear negative stiffness.

3.3.2 Sensitivity analysis

The design variables are changed in order to determine the sensitivities of both models. It is found that both models predict equal behavioral changes, in magnitude and shape, for all design variables individually (see appendix K). To illustrate this result two graphs are plotted predicting change of behavior due to a combination of assumed fabrication tolerances on the geometry for both models. See figure 3.6.

3.3.3 FE strain energy analysis

A strain energy analysis is performed on the finite element model. For specific areas (see figure 3.7) of the mechanism the strain energy is calculated in two states of loading. When the mechanism is pre-loaded in its initial stress free configuration and when the mechanism reaches the maximal deflection in its range of motion (while pre-loaded). When the elastic energy used for pre-loading is set to 100 [%] it is observed that area 1 has the largest energy release (-3.23 [%]). Area 3 and the combination of areas 5 and 6 release respectively -0.50 [%] and -0.25 [%]. Area 2 hardly releases or accumulates energy (0.00 [%]) while area 4 is consuming 0.05 [%].

The total released energy (-3.93 [%]) is very low compared to the provided energy through pre-loading (100 [%]). This is mainly caused by the assumed prematurely end stop limiting the range of motion to [-0.3...0.3] [mm].

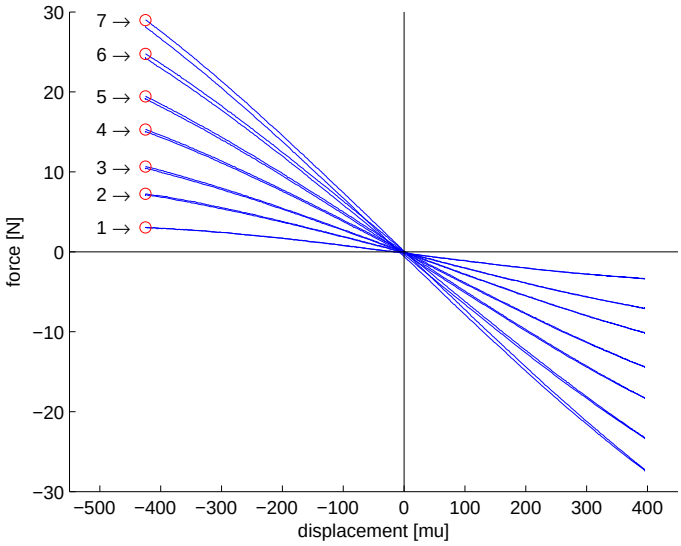

Figure 3.4: Load case 4 measured over a range of 0.82 [mm]

When full range of motion is considered (motion from one elastic stable equilibrium to the other: [-1.1...1.1] [mm]) the total released energy increases up to 83 [%], while maximal stress is raised to about 977 [MPa].

The result is that the pre-loading beam is mainly responsible for the energy storage and release and thus has an equal function compared to torsion spring A in the rocker-coupler-slider mechanism. Details of the energy analysis can be found in appendix I.

3.3.4 Linear pre-buckling analysis

Linear pre-buckling analysis results indicate that the balancer shows a buckling mode equal to the desired range of motion at relatively low critical load (57 [N]) compared to the predicted pre-loading force (330 [N], see appendix B). See figure 3.8. Since buckling modes are calculated under infinitesimal displacement assumptions their magnitude have no more physical meaning then just the initial shape of deformation. The zero stiffness mode is predicted correctly by the stress stiffening effect using only the linear stiffness matrix of the FE model. See details of this analysis in appendix H.

3.3.5 Numerical scheme for RBM simulation

A numerical scheme is developed which, combined with a graphical user interface, enables to quickly analyze the transition from stability to instability of elastic systems resulting from the rigid body replacement method. The effect of change in design variables on the unstable behavior can be studied with low computational effort compared to non linear finite element modeling. See appendix E for a detailed description of the developed numerical scheme and graphical user interface.

The low computational effort can be illustrated by comparing roughly the number of matrix inversions needed to obtain the same results. This is done for a resolution of the force deflection graph of 25 points in the displacement range and 25 points in the pre-loading displacement range.

- numerical scheme used for the PRB model takes 625 times a matrix inversion of a 6x6 sized matrix. See section equations in appendix E.

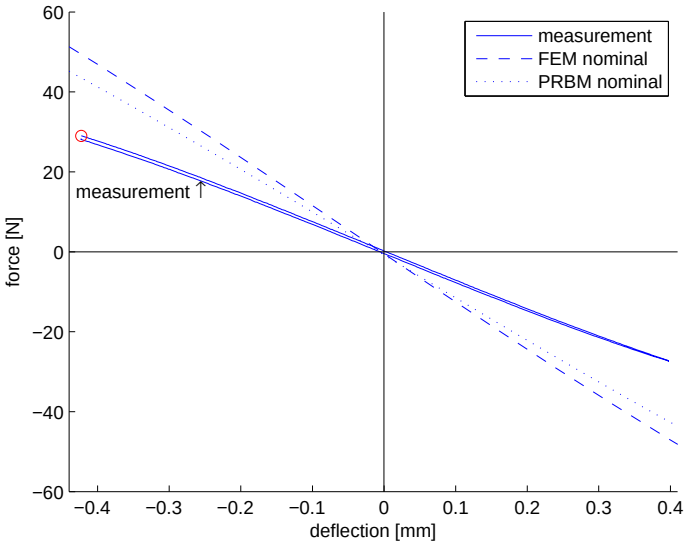

Figure 3.5: Comparison of measurement data and predictions by PRB model and FE model.

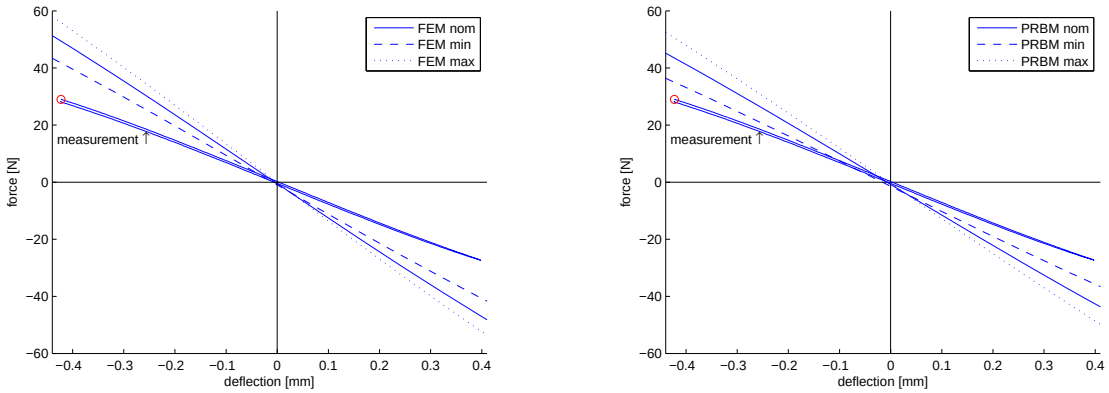

(a) Finite element model.

(b) Pseudo rigid body model.

Figure 3.6: Maximal expected change of behavior due to a combination of fabricational tolerances for both models

- the FE model takes 1875 times a matrix inversion of a 1292x1292 sized stiffness matrix. 1875 follows from 3 consequtive loadcases of each 25 steps, this should be repeated for each load step (25), thus $25 * 3 * 25 = 1875$. The matrix size follows from the number of nodes (646) having each 2 degrees of freedom, thus $2 * 646 = 1292$.

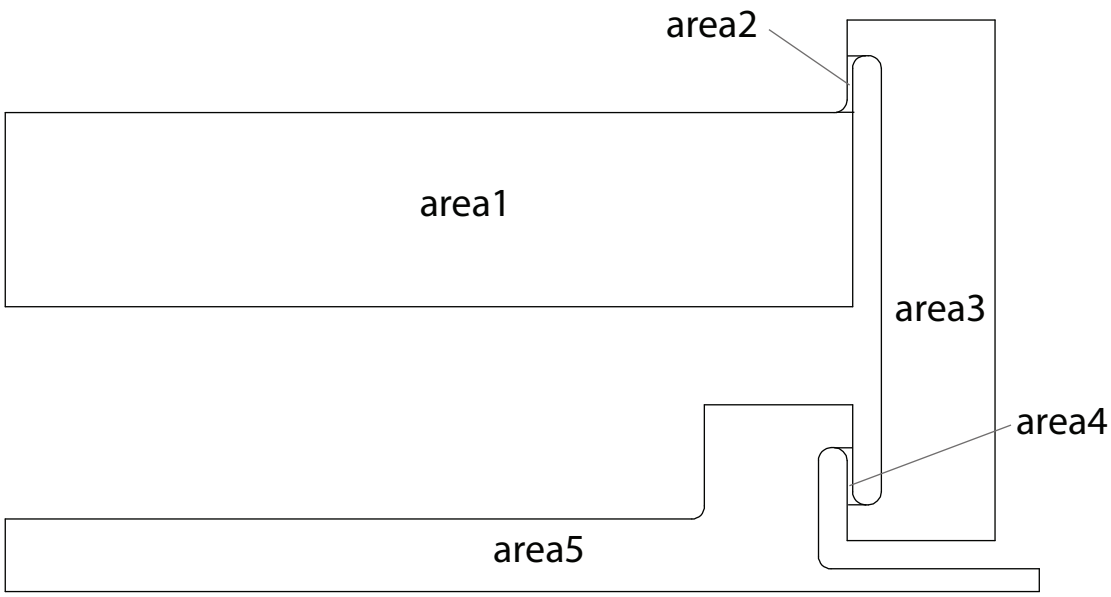

Figure 3.7: Definition of areas over which the strain energy is calculated.

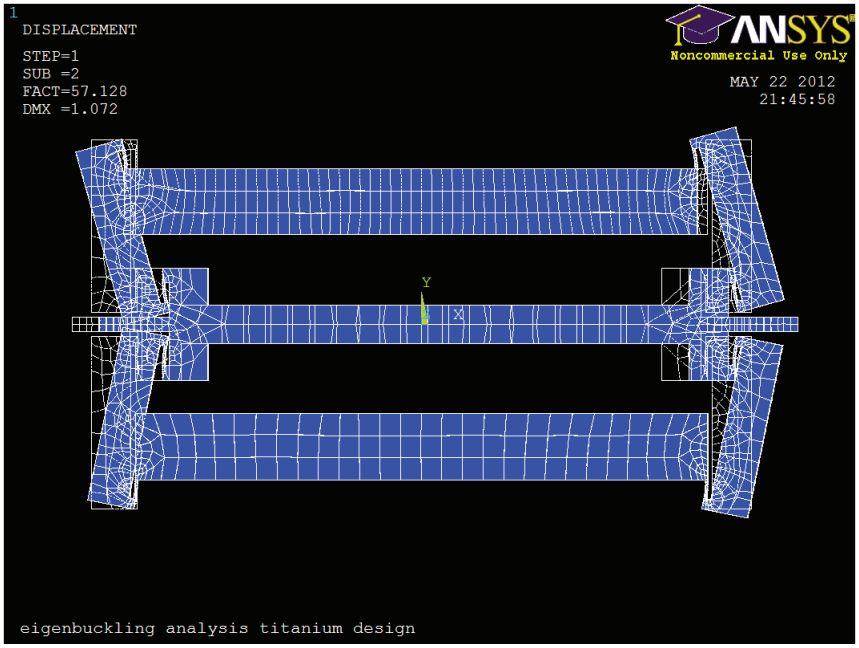

Figure 3.8: Buckling mode obtained from linear pre-buckling analysis.

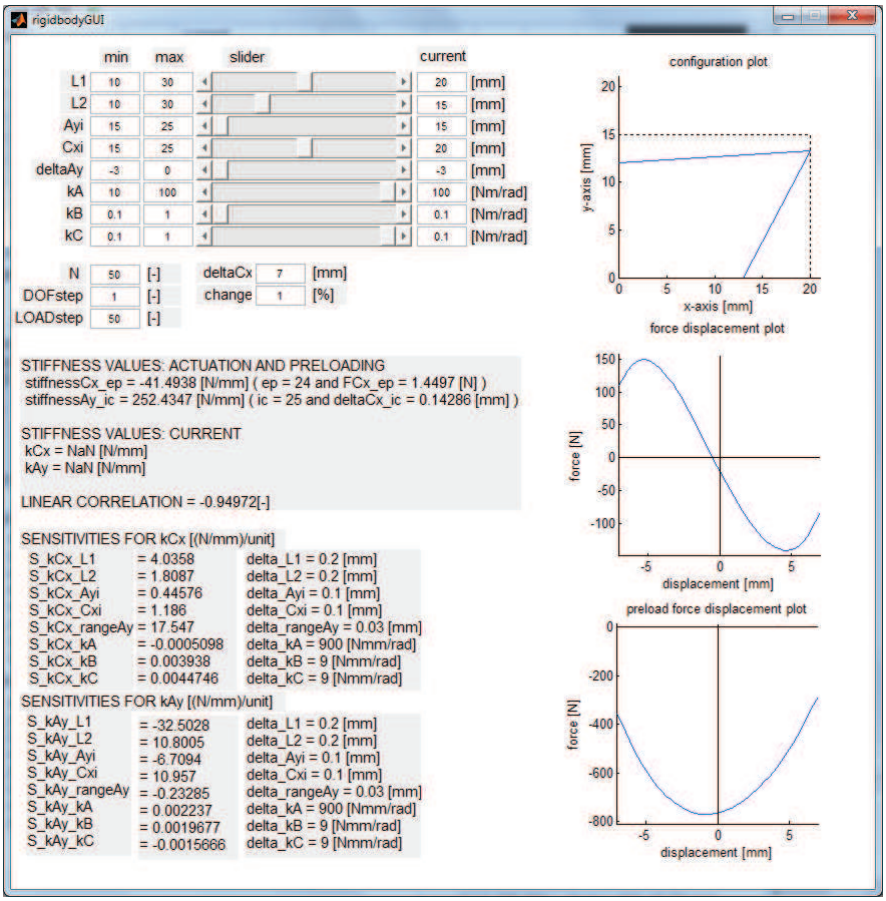

Figure 3.9: Screenshot of the GUI used for analysis of the crank slider mechanism.

Chapter 4

Conclusion

For the first time a statically balanced fully complaint grasper is successfully designed and prototyped using the rigid body replacement method. The prototype meets the size requirement of 40 [mm], when all leaf springs for straight line guidance are omitted. The low hysteresis value of 1.32 [%] combined with the high force reduction factor of 98.92 [%] (see figure 2.1) shows that this design can improve the force feedback of a compliant surgical grasper in a monolithic way. Although a zero force measurement was not obtained, the experimental results prove that this is certainly achievable when the equilibrium positions of the grasper and balancer are tunable with respect to each other. Then the force reduction will lead to near zero force over the required range of motion.

The novel design widens the perspective on the field of designing statically balanced fully compliant mechanisms. The nominal finite element and pseudo rigid body models predict similar behaviors with the same significant deviation from the experimental data. Both models show that the magnitude of uncertainty of the pre-loading displacement during the experiment has a large effect on the behavior. This behavior can drift into big deviations by considering uncertainty in material and geometrical parameters. The pseudo rigid body model comes close to the finite element model, since the pseudo rigid body model is a gross approximation a deviation as shown may be expected. The sensitivities for both models are similar. Their equivalence is supported by the strain energy analysis. Summarizing it can be concluded that the pseudo rigid body model is an accurate modeling method, provided that the deviation can be explained through the mentioned uncertainties. It is a modeling method that requires low computational effort and provides high intuitive support.

Chapter 5

Discussion

5.1 The design

There is a lot of space for improvement of the particular design presented in this work, since no optimization has been performed. Therefore it is expected that the size may be scaled down significantly. This might be achieved by choosing smaller dimensions for the pre-loading beam, or by choosing for a alternative solution for the pre-loading beam as shown in figure 5.1. The following steps may be taken towards down scaling:

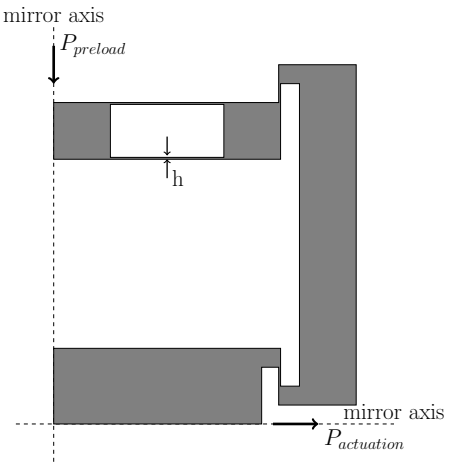

Figure 5.1: Replacing the pre-loading beam for a straight line guidance to prevent rotation at the tip. The leafspring thickness h can be designed for pre-loading displacement versus force.

- The lenght of the prelaod beam may be decreased significantly, since no rotational low stiffness mode of the shuttle is expected and the estimated bending stresses are quite low.
- From the sensitivity analysis it follows that decreasing the length of link 2 and increasing the length of the compliant joint will increase the negative stiffness.
- Mirroring over the horizontal axis might be omitted if straight line guidance is implied otherwise, see figure 5.2, reducing the overall size of the balancer.
- An optimal value for the joint thickness might be found, at which the negative stiffness is maximized, since the elastic joint transmits a large tensile force (maximum thickness) while accounting for the bending stresses (minimize thickness).

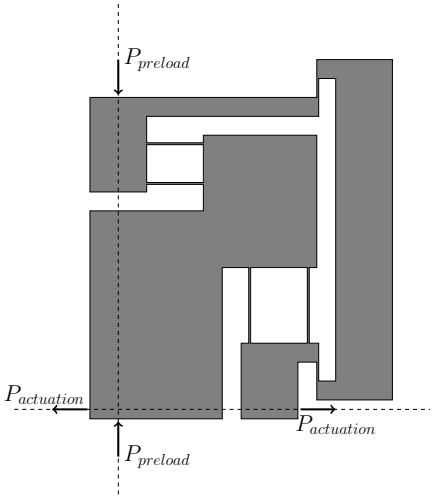

Figure 5.2: When mirroring is ommitted then straight line guidance of the shuttle and the pre-loading displacement can be achieved through adding the leafsprings as illustrated.

If the size is reduced while the negative stiffness and pre-loading force remain constant then this is the same as having a constant size and negative stiffness while the pre-loading force is decreased. Reducing the required pre-loading force also means decreasing the out-of-plane thickness of the design.

The required pre-loading displacement is very small which caused troubles in precise determination of its value during the experiment. Consequently the validation of both models was subject to large uncertainties. The pre-loading displacement can be increased easily by using the alternative solution in figure 5.1 through decreasing h. Also no problems are to be expected when a more convenient length thickness ratio (see equation 2.8) is assumed for the pre-loading beam.

Apart from improving the negative stiffness, steps can be taken towards the application to a surgical tool. Finding a simple way of switching the pre-loading on and off is recommended in order to avoid stress relaxation effects. Furthermore when negative stiffness is increased, adding more positive stiffness segments is allowed creating possibilities to develop a complete tool having compliant handles in a monolithic way. A preview of such a tool might look like figure 5.3.

Besides application in a surgical tool, the adjustability via pre-loading displacement of the constant negative stiffness of the balancer makes it an attractive alternative for the negative stiffness building blocks proposed by Hoetmer [5].

5.2 The method

A weak spot in the taken design approach is the determination of shapes and dimensions of the monolithic geometry. When a rigid body mechanism is designed (link lengths, torsion stiffness values and initial configuration are known) there is no guarantee that a replacing compliant version will be found which shows equivalent behavior. There is also no guarantee that when a compliant version is found it will be the best solution, and does not exceed the allowable equivalent stress. Thus the taken approach seems to have mainly an added value for the synthesis step in the design process.

To improve the added value, the model parameters of the rigid body mechanism might be coupled to predefined shapes in the software. Suppose that a distributed compliance is chosen to be replaced by a cantilever beam with constant cross section. Then the sensitivity of the behavior might be calculated directly for changes in the shape parameters. It will also become possible to predict a maximal stress value. When several standard shapes are

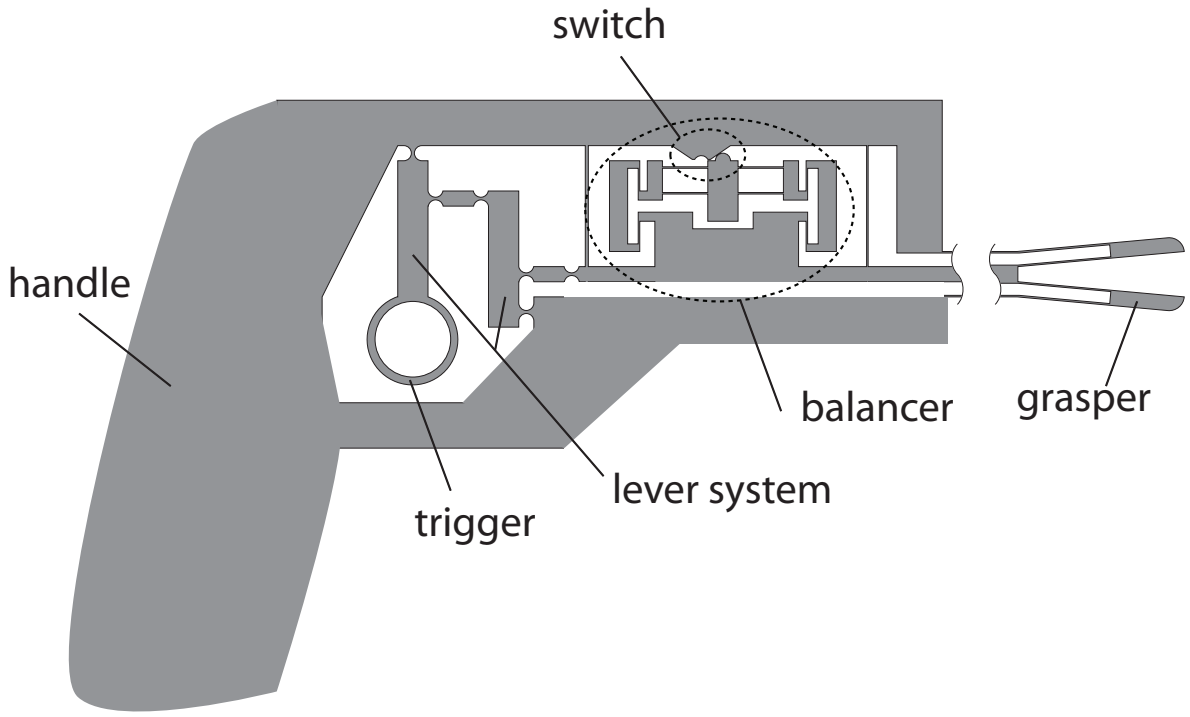

Figure 5.3: An impression of how the balancer might be applied in a surgical tool in the future.

defined in the software, the user can quickly determine which one fits best. The software might even automatically determine the best shape and propose it to the user.

Thus the software used in this work may be developed further to model the 4 bar mechanism in general. This allows for generation of many different mechanisms and configurations of which the behavior and replace ability with compliant segments can by analyzed quickly by the designer. This may be applied in the beginning of the design process of a SBFC mechanism. The proposed candidate solution may then be optimized to a final design based on its finite element model.

For the particular design presented in this work only small deflections are considered compared to the overall mechanism size. An application to large deflection mechanism might be proven valuable. Then the potential of rigid link mechanisms combined with the pseudo rigid body model to simulate non linear behavior through large deflections is fully exploited.

Appendix A

Review of design approaches for statically balanced compliant mechanisms

abstract

This paper aims to be an investigation of the state of the art of designing statically balanced compliant mechanisms. Often abbreviated as SBCM. SBCM are beneficial because they combine the advantages of a compliant mechanism (no backlash and sliding friction) and a statically balanced system (no external force is needed to achieve displacements). The mathematical criteria for static balance are known. One of them is that the stiffness matrix is singular. But there is no design method directly available to achieve this. Although there are several theoretic areas that relate to statically balanced compliant mechanisms via the more generally known property neutral stability. The objective is to make an inventory of related theoretical areas in the field of neutral stability. To see how areas are related and what their overlap is with statically balanced compliant mechanisms. To develop vision for design. This might lead to new ideas for approaches to a design method. One existing design approach is identified, the so called building block approach. Areas found to be related are: linear buckling, postbuckling, analysis of neutrally stable mechanisms, vibration isolation, exact constraint design, Non linear spring design. These areas indicate that design doesn't necessarily has to be seen as a building block problem. The conclusion is that neutral stability for some finite range can be achieved by applying a certain pre-stress distribution to a certain geometry. This translates into a stiffness matrix being singular. Two hints towards ideas in how to achieve singularity are mentioned: the first is based on exact constraint design and the second on a scalar stiffness description.

introduction: background

A mechanism is a physical structure, often composed out of several hinged parts, designed to transfer force and motion, see figure 1. Motion is typically achieved by relative movement of rigid parts through joints. A compliant mechanism (abbreviated with CM) achieves motion by elastic deformation of its own geometry, thus by lowering stiffness in one specific direction compared to all other directions, see figure 2. A statically balanced compliant mechanism (abbreviated with SBCM) achieves elastic deformation without applying any actuation force. Statically balanced compliant mechanisms are promising because of the advantages listed in Table 1 [1].

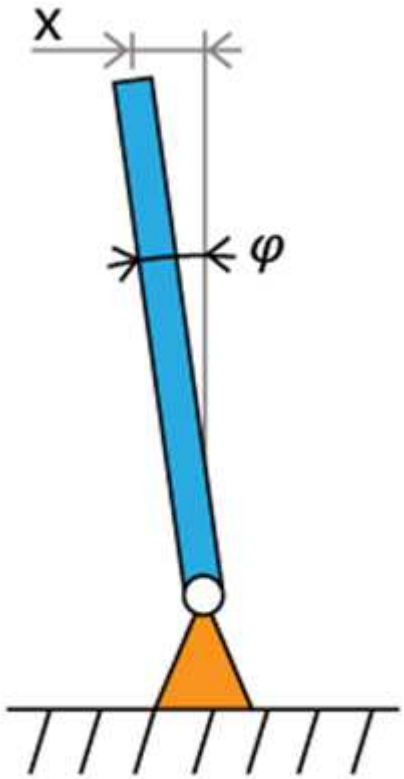

figure 1: mechanism

figure 2: compliant mechanism

The absence for the need of an actuation force to overcome the elastic deformation is a remarkable property, but nevertheless mechanically possible [2] [3]. The property of static balance is generally known in literature as neutral stability. Real world examples proving this property are discussed in Section 3. Unfortunately the advantages are counter acted by some disadvantages listed in Table 2.

Table 1: advantages of (statically balanced) compliant mechanisms	
advantages	**explanation**
CM: No backlash	Hinges and such are absent, motion is a result of elastic deformation.
CM: No sliding friction	
CM: Monolithic	Can be manufactured out of one piece, no assembly is needed.
SBCM: Energy efficient	No actuation force needed to deform elastically.
SBCM: Force feedback	Force feedback is convenient in case of human control of the mechanism [4].

Table 2: disadvantages of statically balanced compliant mechanisms	
disadvantages	**explanation**
Increase in size	A statically balanced compliant mechanism tends to be larger in size then the unbalanced version. This is discussed in Section 4.
Increase in hysteresis	Decreasing the demanded actuation force implies that possible occurring hysteresis effects become relatively more dominant [5].
Little understanding	Analysis is not straight forward which limits the understanding of the behavior. This is because compliant design is challenging by itself [6] and besides that nonlinear behavior is likely to be involved [7].Another limiting factor for understanding is that the property of neutral stability is in general not pursued as a design goal in literature. Being the border between stable and unstable behavior, neutral stability is naturally avoided in most cases [8].
No design methods	There are no design methods available. Mainly because of the little understanding of the behavior.

introduction: problem statement

The problem statement is formulated by first discussing what is known about SBCM, and then what still remains unknown.

What is known about static balance for compliant mechanisms ?

In [1] some criteria are derived which define static balance for a range of motion for a mechanism which may be compliant or not. The criteria apply in general for discretized mathematical models, for example a finite element model of a elastic structure. The vector $\underline{x}$ contains the degrees of freedom of the model which are displacements. A preliminary investigation is made to determine if the criteria suit the design methods for compliant mechanisms discussed in [6]. Three relevant criteria which are based on the principle of work [9] are listed in Table 3.

Table 3: criteria for statically balanced mechanisms for some range of motion $\underline{x}$

criterion	explanation	relation
Constant potential energy $U(\underline{x}) = \text{constant}$ **(1)**	Elastic energy is internally exchanged, no work is supplied to or generated by the system.	$U(\underline{x}) = \text{constant}$ **(2)**
Continuous equilibrium $\sum F_i(\underline{x}) = 0$ **(3)**	Internal elastic forces add up to a resultant force which is zero, irrespective of the motion.	$\underline{F} := \frac{\partial U(\underline{x})}{\partial \underline{x}}$ **(4)**
Zero stiffness $\det([K_t(\underline{x})]) = 0$ **(5)**	Stiffness relates force to displacement. When no force is needed to obtain displacement, stiffness is zero. The tangent stiffness matrix becomes singular. See remark below.	$[K_t] := \frac{\partial^2 U(\underline{x})}{\partial \underline{x}^2}$ **(6)**

Remark:

when no force is needed to obtain displacement for an elastic mechanism it is easy to see that then stiffness must be zero, especially for a one degree of freedom system:

$$k \cdot x = F \rightarrow k \cdot x = 0 \rightarrow x \neq 0 \text{ thus } k = 0 \quad \textbf{(7)}$$

It is less clear that for a multi degree of freedom system it also means that the tangent stiffness matrix must be singular. To see this, consider the next situation for a general linearized system which is only valid for small variations of displacements $\underline{\Delta x}$ and forces $\underline{\Delta F}$. Then the linear equation holds:

$$[K_t] \cdot \underline{\Delta x} = \underline{\Delta F} \quad \textbf{(8)}$$

Suppose that by magic the system gained some how the special property of neutral stability, then with zero load there should still be displacement unequal to zero possible. These displacements satisfy then the homogenous equation:

$$[K_t] \cdot \underline{\Delta x} = \underline{0} \quad \textbf{(9)}$$

So there are more solutions for $\underline{\Delta x}$ besides the trivial one: $\underline{\Delta x} = \underline{0}$. The non zero solutions for $\underline{\Delta x}$ form the so called null space of the matrix. This is only possible when the matrix is singular [10 - Private]. Or in other words when the system is linear dependent. The number of equations is less than the number of unknowns, so there is no unique solution possible and there is at least one free variable. When such a linear system is elaborated into the echelon form then it also can be seen that the determinant is zero [10]. Thus:

$$\det([K_t]) = 0 \quad \textbf{(10)}$$

What is not known ?

It is not known how the criteria can quickly lead to a large number of use full designs. A method is not directly available. Although there are several theoretic areas that relate to SBCM via the more generally known property of neutral stability.

introduction: objective

The objective is to make an inventory of related theoretical areas in the field of neutral stability. To see how areas are related and what their overlap is with SBCM. And eventually to develop vision for design of SBCM. This might lead to new ideas for approaches to a design method.

introduction: structure

This paper is structured as follows. In section 2 the search method will be described. In section 3 the results of the method will be presented. In section 4 the results will be discussed and in section 5 a final conclusion is stated.

method

Table 4 summarizes the sources and key words used in the search for literature. The keywords listed indicate the encountered fields, buckling and SBCM. Several combinations of the keywords where used, only search results of less then 50 items where accepted for further processing.

Table 4: sources and keywords used for literature research

Sources	Keywords
Scopus: http://www.scopus.com/ mainly scientific publications	zero stiffness, neutral stability, buckling, bifurcation, static balancing, compliant mechanisms
IMR: (research group TU Delft) mainly conference proceedings and scientific publications	
Other: (TU Delft Library, private book collection, internet) mainly books	

results

In this section the areas in literature found to be related to neutral stability are described and the relation is explained per area.

Area: linear buckling

In linear buckling analysis an eigenvalue problem is derived [11]. This eigenvalue problem can be derived from the tangent stiffness matrix of the system [12]. The tangent stiffness matrix can be represented by a sum of two matrices:

1. linear stiffness matrix: accounting for the linear stiffness
2. stress stiffness matrix: accounting for the (change of) stiffness induced by the preload force.

By dictating the tangent stiffness matrix to be singular the system of equations will exhibit the eigenvalue

problem. The eigenvalues correspond to the critical loads and the eigenvectors to the buckling modes. Having a singular stiffness matrix means having a null space spanned by the eigenvectors, as explained in the Table 3. This way linear buckling is related to SBCM. This analysis is only valid for infinitesimal displacements around one configuration.

Area: postbuckling

It is known that structures can carry loads exceeding their initial buckling load [13]. In post buckling the main interest lays in understanding the behavior of the structure after the initial buckling load is exceeded. Then the structure may become unstable or stable again. Positive, zero and as well negative stiffness can occur. Meaning that the force displacement relation is nonlinear. Limit points have zero stiffness, bifurcation points may branch into zero stiffness paths. Some conditions for zero stiffness bifurcation are studied in [14], they apply to simple truss system. Most other work encountered focus on the influence of imperfections on post buckling behavior and path calculation methods. Mainly column, truss, shell and plate like structures are considered.

For shell and plate structures [15], truss systems forming domes [16] bipath [17] hiearchy.

The equilibrium path described by the increasingly loaded structure (and thus increasingly deforming structure) also possibly covers zero stiffness (bifurcation) paths for a finite range of displacement. This possibility links to SB.

Area: design of statically balanced compliant mechanisms (SBCM)

A few attempts have been made to design SBC mechanisms.

- The earliest attempt found was in [3]. A proposal for a zero stiffness leaf spring guidance is made by compensating with negative stiffness.
- A longer design route was taken to end up with a SB laparoscopic grasper. In [18] a feasibility study is done for conceptual design using a negative stiffness building block to balance the grasper. In [19] another negative stiffness mechanism was conceptually designed and optimized. In [20] finally an equally design was made and prototyped.
- Then in [21] a design for SB flexure joint was made and prototyped by Morsch.
- In [5] a negatieve stiffness is designed together with a positive stiffness gripper for SB.
- A straight line guiding mechanism is designed and prototyped in [22]. A 2D mechanism having zero stiffness for a large finite range of motion, and positive stiffness in any other in plane direction.
- Recently a compliant finger is balanced in a large displacement range by a contra compliant mechanism in [23].

All these design attempts have in common that a positive stiffness is added to a negative stiffness and thus zero stiffness is approximated for a certain range of motion. Design is often done by optimization, by minimizing stiffness or actuation force over the range of motion. To realize negative stiffness often two fundamental types of mechanisms are used, a bi stable mechanism and an unstable mechanism. The first one can be compliant by itself, the second one not and is to be translated to a compliant equivalent.

Area: analysis of neutrally stable mechanisms

TENSEGRITY: In [24] a zero stiffness tensegrity structure is analyzed, in [25] a design of tensegrity mechanism zero stiffness is made an prototyped. The key property is the zero free length spring which replaces all of the tensioning cables. This combined with matrix analysis presented in [26] and a tangent stiffness matrix formation presented in [27] leads to a method to generate a family of tensegrity structures which are SB for a large range of motion. The structures discussed are pin jointed and thus not compliant. It is recommended to search for an equally generic theory for non-pin jointed structures.

SHELL: In [28] and [2] a neutrally stable elastic shell is presented. This is proven theoretically, and a prototype is made to illustrate its behavior in reality. The shell is a solid piece of flat metal which is plastically deformed in 2 different ways to create an initial stress distribution.

COMPOSITE SHELL: In [29] a composite shell is presented which is neutrally stable and its application in

deployable structures is discussed. Its neutral stability is achieved by plastically deforming two layers of non-ferro material and then glue them together in a concave way. In [30] an equal composite tape spring is presented.

Area: vibration isolation

Some work was encountered in the area of vibration isolation. In [31] [32] and [33] non linear springs are used to obtain so called quasi dynamic zero stiffness. In [31] negative stiffness is used to lower the natural frequency.

Area: exact constraint design

In [34] it is proven and validated that a certain misalignment in a parallel leaf spring guidance does lower the stiffness of the mechanism in some direction, because of residual stresses. This is considered to be undesirable for mechatronic purposes, because it leads to a drop in the second lowest natural frequency and therefore has a negative influence on feedback performance.
In [35] it is therefore motivated to consider static and kinematic indeterminacy when designing mechatronic systems. Fully determinate design, in this field referred to as “exact constraint design” is then strived for. A kinematic analysis based on singular value decomposition is used to predict any indeterminacy. Over or under constraints can be visualized based on information out of the SVD. In [36] the visualization of over constraints is related to imaginary stress distributions. This visual SVD analysis is applied to a concept design of a large stroke in plane elastic positioning mechanism.
The relation with SBCM can be distinguished when lowering stiffness (as a consequence of residual stresses) is considered as a desired result. Namely towards zero stiffness.

Area: Non linear spring design

In [37] the main contribution is a method to design nonlinear springs given a prescribed force displacement relation. Buckling behavior (by negative stiffness) is avoided strictly in this method but in the design of a constant force mechanism the stiffness is allowed to approximate zero for a range. Constant force mechanism can be used to balance other constant force mechanisms. A negative and positive constant force mechanism lead to a zero force zero stiffness mechanism. This may be achieved by using two equal nonlinear springs and pretension them both and connect the mechanically. A symmetric mechanism results, relating this area to SB.

discussion

Linear buckling leads to buckling modes which show zero stiffness or in other words: span a null space. Those modes are of interest when they comply with the desired SB range of motion. But these modes only account for infinitesimal displacements around the configuration for which the tangent stiffness matrix is derived. So a natural question to be answered next, would be, how to preserve the null space for the tangent stiffness matrix for a desired range of motion ?

Post buckling is closely related as it considers the nonlinear equilibrium path of the system. SBCM are very likely to be nonlinear because of the demand to design for a good size/range ratio, which implies large displacements relative to mechanism size. Besides, if it is assumed that neutral stability only can be achieved by pre-stressing a certain geometry, then the problem is per definition nonlinear.

The designed SBCM’s have all the common property that a positive stiffness is balanced by adding a mechanism with negative stiffness. This often leads to increase in size compared to the positive stiffness mechanism itself. Because lowering stiffness can also be achieved by residual stresses it is likely to think that there might be a more generic way to design for SB leading to more compact designs. For example to determine for a known geometry and desired range of motion the necessary prescribed displacement or pre load for the system.

The analysis of some compliant shell/tape mechanisms shows that some special combinations of geometry and initial stress distribution exhibit neutral stability. The theoretic analysis does confirm this, but

does not lead yet to a method for generating a large number of possible designs. In contrary, the tensegrity structure does generate a family of designs based on a geometric property, although not for compliant structures. The geometric property was found by considering kinematic analysis, static equilibrium and the zero free length spring in relation to the tangent stiffness matrix.

The exact constraint design approach leads to the observation that kinematic analysis can be used to visualize indeterminacy of compliant beam structures, besides truss structures. By over constraining a compliant a system it may be expected that the resulting stress distribution influences the stiffness. Then it might be possible to use this kinematic analysis to pursue static balance for a compliant mechanism out of beam elements.

The non linear springs mentioned in the area of vibration isolation might be covered by the last area non linear spring design. This method is a tool to design a spring for a prescribed load displacement function. Constant force mechanisms are designed to. One could investigate what happens in this method if the constant force is assumed to be zero. Maybe by extending the method with some extra condition it might lead to SBCM designs.

One could state that design for neutral stabililty can be considered at three levels:

1. Energy potential $U(\underline{x}) - \text{constant} = 0$
2. Static equilibrium $\frac{\partial U(\underline{x})}{\partial \underline{x}} = \underline{0}$
3. Zero stiffness $\det\left(\frac{\partial^2 U(\underline{x})}{\partial \underline{x} \cdot \partial \underline{x}}\right) = 0$

At each level the problem can be seen as finding a system that satisfies and maintains a desired nullspace for a range of motion, and in the mean time having a physical meaning for geometry and prestress. Talking in level number one in terms of energy we are close to the definition of the key property of a SBCM, talking in level number three in terms of stiffness we are close to the pre-stressed geometry of a mechanism.

At the first level it is possible to define continuous functions that satisfy the criterion of constant potential energy. In other words parameterizing the potential energy function. The functions should be defined such that they leave as much design freedom as possible when twice differentiated, and thus in the stiffness level.

The second level considers static equilibrium. In [26] static equilibrium and the kinematic description of truss systems is used to analyse indeterminacy. Schenk [24] used this to derive a geometric condition for the design of a family of statically balanced tensegrity structures. Using the kinematic tools from SPACAR for beam elements might lead to the identification of a family of statically balanced compliant mechanisms based on beam elements.

The third level can also be put into another view. Until now the condition for SB is translated to a matrix being singular. But many times it is also refered to as zero stiffness, because the scalar stiffness value experienced by an actuator is zero for a SB mechanism. Then it might be interesting to investigate how the corresponding stiffness matrix transforms into this scalar value zero.

conclusions

One elaborated approach for design was found, the building block method (positive + negative stiffness). Then there are some cases in which specific structures where theoretically analyzed or designed (tape springs, tensegrity structures). A related field that was found is buckling. Another field encountered is “exact constraint design”. The last two fields indicate that design doesn’t necessarily has to be seen as a mechanical addition of positive and negative stiffness. So the conclusion is that, in general, neutral

stability for some finite range can be achieved by applying a certain pre-stress distribution to a certain geometry. But there are no conditions known for geometry combined with pre-stress that allow for quick generation of a large number of different designs.

This observation motivates to develop an alternative design approach besides the building block method. Taking the analysis of tensegrity structures by Schenk as a lead, and using the kinematic SVD analysis tools from SPACAR together with still to be found tangent stiffness matrix formulations might provide a hint towards the development of a design method.

references

- [1] J. A. Gallego and J. Herder, "Criteria for the static balancing of compliant mechanisms," 2010.
- [2] K. A. Seffen and S. D. Guest, "Prestressed morphing bistable and neutrally stable shells," Journal of Applied Mechanics, Transactions ASME, vol. 78, pp. 0110021-0110026, 2011.
- [3] J. Van Eijk, "ON THE DESIGN OF PLATE-SPRING MECHANISMS," 1985.
- [4] J. Herder and P. A. van den Berg, "Statically balanced compliant mechanisms (sbcm's), an example and prospects," 2000.
- [5] K. Hoetmer, et al., "Negative stiffness building blocks for statically balanced compliant mechanisms: Design and testing," Journal of Mechanisms and Robotics, vol. 2, 2010.
- [6] J. A. Gallego and J. Herder, "Synthesis methods in compliant mechanisms: An overview," San Diego, CA, 2010, pp. 193-214.
- [7] J. W. A. Vaandrager, "Synthesis method for large deflection building blocks in compliant mechanisms, based on elastic potential," 2011.
- [8] S. P. Timoshenko and J. M. Gere, "Mechanics of materials, ISBN 0 7487 3998 X," 1999.
- [9] Young and Freedman, "Sears and Zemansky's University Physics: with modern physics, ISBN 0-8053-8684-X," 2004.
- [10] D. C. Lay, "Linear Algebra and its applications, ISBN 0-321-14992-0," 2003.
- [11] R. D. Cook, et al., "Concepts and applications of finite element analysis, ISBN 0-471-35605-0," 2002.
- [12] H. Grootenboer, "Eindige elementen methode in de werktuigbouwkunde ".
- [13] B. G. Falzon and M. H. Aliabadi, "Buckling and postbuckling structures experimental, analytical and numerical studies, ISBN 13 978-1-86094-794-0," 2008.
- [14] H. A. Mang, et al., "On the predictability of zero-stiffness postbuckling," ZAMM Zeitschrift fur Angewandte Mathematik und Mechanik, vol. 90, pp. 837-846, 2010.
- [15] E. A. De Souza Neto and Y. T. Feng, "On the determination of the path direction for arc-length methods in the presence of bifurcations and 'snap-backs'," Computer Methods in Applied Mechanics and Engineering, vol. 179, pp. 81-89, 1999.
- [16] I. M. Kani and A. Heidari, "Automatic two-stage calculation of bifurcation path of perfect shallow reticulated domes," Journal of Structural Engineering, vol. 133, pp. 185-194, 2007.
- [17] I. Kiyohiro, et al., "Bifurcation hierarchy of symmetric structures," International Journal of Solids and Structures, vol. 27, pp. 1551-1573, 1991.
- [18] A. Stapel and J. L. Herder, "Feasibility study of a fully compliant statically balanced laparoscopic grasper," Salt Lake City, UT, 2004, pp. 635-643.
- [19] N. Tolou and J. L. Herder, "Concept and modeling of a statically balanced compliant laparoscopic grasper," San Diego, CA, 2010, pp. 163-170.
- [20] D. J. B. A. De Lange, et al., "Design of a statically balanced compliant laparoscopic grasper using topology optimization," 2008.
- [21] F. M. Morsch and J. Herder, "Design of a generic zero stiffness compliant joint," 2010.
- [22] E. J. Rosenberg, et al., "An energy approach to a 2dof compliant parallel mechanism with self-guiding statically-balanced straight-line behavior," 2010.
- [23] J. W. A. Vaandrager, "Design of a statically balanced, large range of motion, compliant gripping mechanism," 2011.
- [24] M. Schenk, et al., "Zero stiffness tensegrity structures," International Journal of Solids and Structures, vol. 44, pp. 6569-6583, 2007.
- [25] M. Schenk, et al., "Design of a statically balanced tensegrity mechanism," Philadelphia, PA, 2006.
- [26] S. Pellegrino and C. R. Calladine, "Matrix analysis of statically and kinematically indeterminate

frameworks," International Journal of Solids and Structures, vol. 22, pp. 409-428, 1986.
- [27] S. Guest, "The stiffness of prestressed frameworks: A unifying approach," International Journal of Solids and Structures, vol. 43, pp. 842-854, 2006.
- [28] S. Guest and E. Kebadze, "A zero-stiffness elastic shell structure," 2010.
- [29] T. W. Murphey and S. Pellegrino, "A novel actuated composite tape-spring for deployable structures," Palm Springs, CA, 2004, pp. 260-270.
- [30] M. R. Schultz, et al., "Neutrally stable behavior in fiber-reinforced composite tape springs," Composites Part A: Applied Science and Manufacturing, vol. 39, pp. 1012-1017, 2008.
- [31] A. Carrella, et al., "On the force transmissibility of a vibration isolator with quasi-zero-stiffness," Journal of Sound and Vibration, vol. 322, pp. 707-717, 2009.
- [32] W. S. Robertson, et al., "Theoretical design parameters for a quasi-zero stiffness magnetic spring for vibration isolation," Journal of Sound and Vibration, vol. 326, pp. 88-103, 2009.
- [33] I. Kovacic, et al., "A study of a nonlinear vibration isolator with a quasi-zero stiffness characteristic," Journal of Sound and Vibration, vol. 315, pp. 700-711, 2008.
- [34] J. P. Meijaard, et al., "Analytical and experimental investigation of a parallel leaf spring guidance," Multibody System Dynamics, vol. 23, pp. 77-79, 2010.
- [35] R. G. K. M. Aarts, et al., "Flexible multibody modelling for the mechatronic design of compliant mechanisms," 2010.
- [36] F. Hoitzing, "Kinematic and dynamic modeling for the conceptual design of a 2-DOFs large stroke elastic positioning mechanism," 2010.
- [37] C. V. Jutte and S. Kota, "Design of nonlinear springs for prescribed load-displacement functions," Journal of Mechanical Design, Transactions of the ASME, vol. 130, pp. 0814031-08140310, 2008.

Appendix B

Non linear FEM analysis of balancer and grasper

A non linear finite element analysis was done to simulate the force deflection graph of the balancer and the grasper separately. See last four sections of this appendix for the FEM code used and detailed information about the models used. In the pictures (ref) below is illustrated:

- the model geometry
- the applied boundary conditions
- the element mesh
- solution: the deformed shape (scale 1:1) at maximum stress value
- solution: the stress distribution and maximum stress

Since all forces and displacements are planar, both models are considered to be in a plane stress situation. In the finite element package Ansys the element type PLANE82 is used. The simulation is done using displacement control. The results of both simulations are listed in the table below.

	balancer		**grasper**	
half range [mm]	0.3	0.5	0.3	0.5
linear correlation [-]	−0.99996		0.99993	
stiffness [N/mm]	$4 \cdot -23 = -92$		91	
maximum stress [MPa]	555	680	304	531
preload displacement [mm]	0.2		-	
maximum preload force [N]	−330		-	
comment				

In the table above a comparance is made between grasper and balancer. Both behave quite linear, considering the linear correlation coefficient. This allows to estimate the stiffness by deviding the change in force over the change in displacement over the entire range of motion. Multiplying the balancer times four (see justification in section below) generates enough negative stiffness to compensate the grasper. This result is achieved using a preload displacement of only 0.2 [mm] and having the resulting maximum stresses below 550 [MPa] when range of motion is restricted to the required 0.3 [mm].

Balancer

Because of symmetry only one fourth of the entire geometry is modeled. Boundary conditions are applied at the vertical and horizontal symmetry lines. The vertical line is displacement constraint in horizontal direction. The horizontal line is displacement constraint in vertical direction. 3 consecutive load cases are applied on top of the all ready applied boundary conditions:

1. first load case: prescribing a displacement at point 1 in vertical direction while point 2 is fixed in horizontal direction
2. second load case: prescribing a negative displacement (half range) in horizontal direction for point 2
3. third load case: prescribing a positive displacement (full range) in horizontal direction for point 2.

The maximum stress occurs at point 3 when the balancer is in left most position of the range of motion. It is assumed that the final result (force deflection graph) can be simply multiplied by 4 to model the entire geometry. Justification of this multiplication is discussed in appendix (ref to mirroring effects).

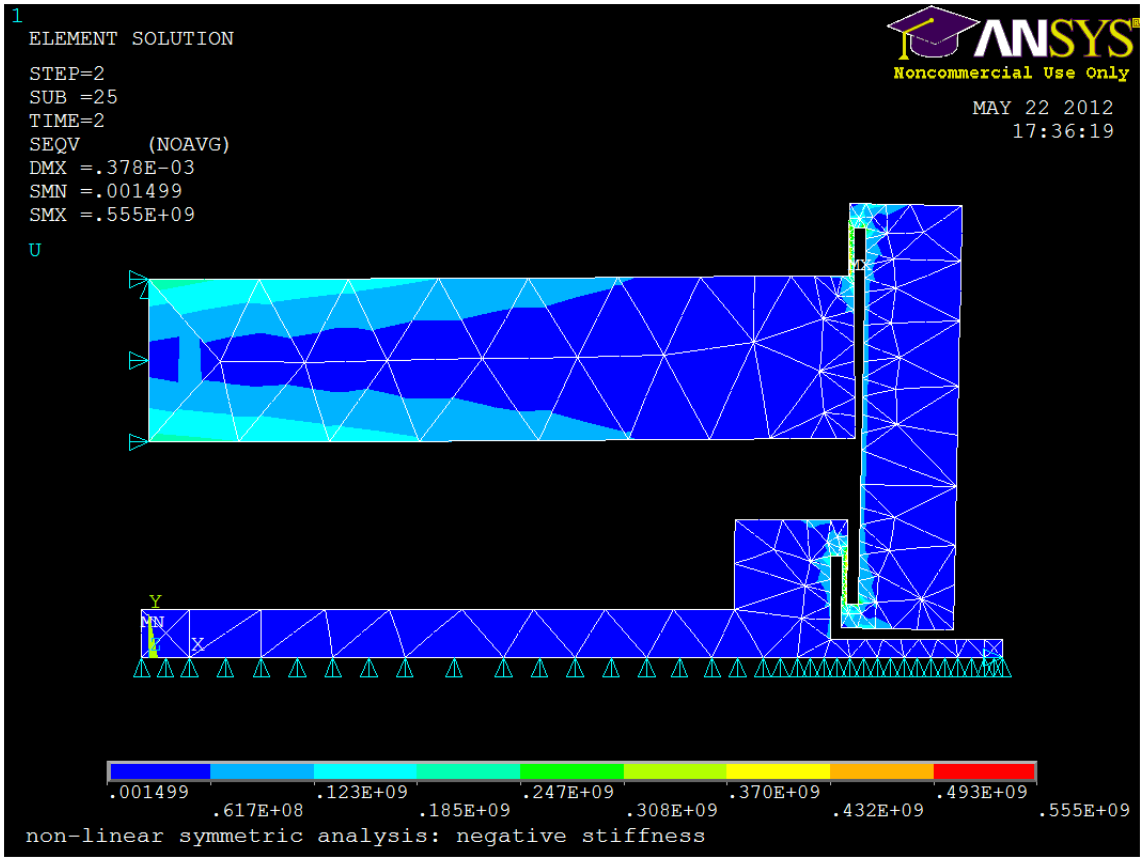

comment

The resulting force deflection graph is shown below (ref) for a displacement range of $[-0.3...0.3]$ [mm].

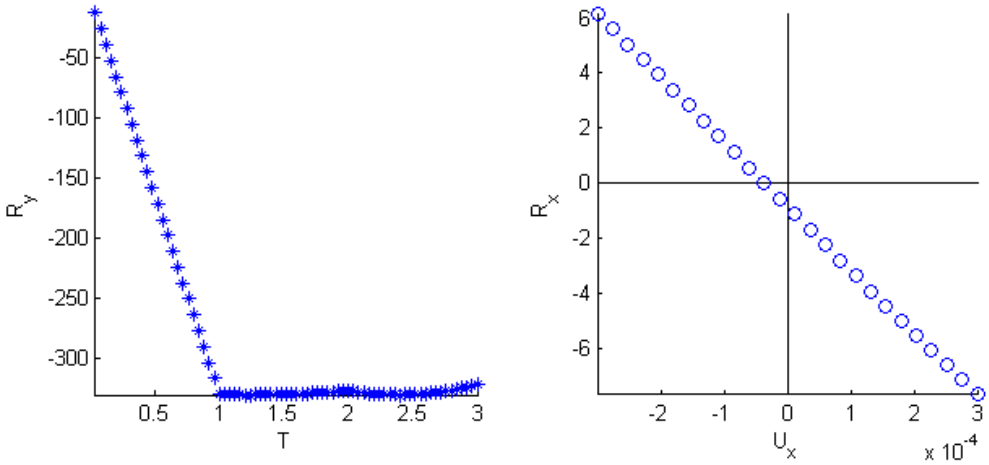

On the left the preload force is plotted against the displacement steps (in Ansys called time steps) during the 3 consecutive load cases. For each load case 25 steps are taken. On the right the force deflection graph is plotted of point 2 for load case 3 only.

Grasper

Boundary conditions are applied such that the blocks on the right are fixed. 2 consecutive load cases are applied on top of the all ready applied boundary conditions:

1. first load case: prescribing a half range displacement at point 1 in horizontal direction to fully open the grasper starting from rest position.
2. second load case: prescribing a full range displacement in horizontal direction at point 1 to fully close the grasper starting from fully open position.

Maximum stress occurs in at point 2, when the grasper is fully open.

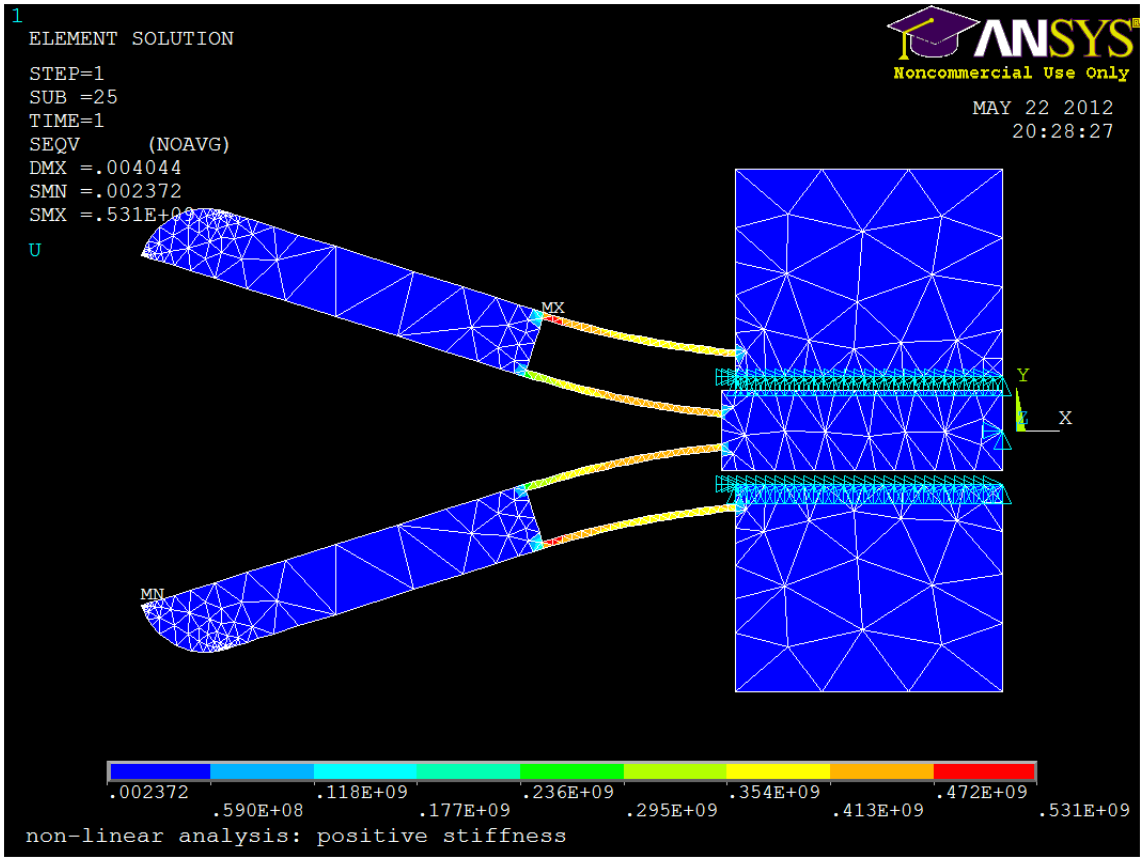

comment

The resulting force deflection graph is shown below (ref) for a displacement range of $[-0.3...0.3]$ [mm].

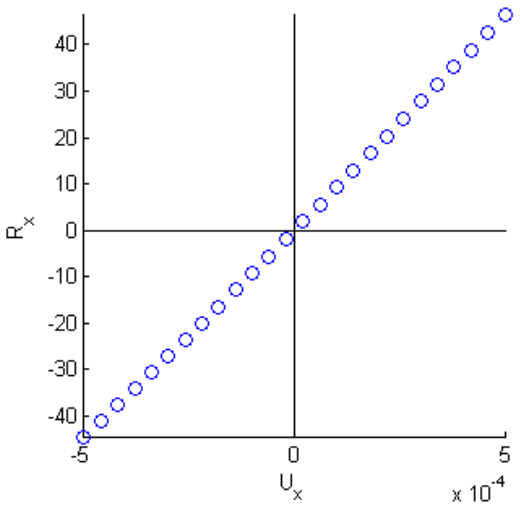

The force deflection graph is plotted of point 1 for load case 2 only.

Ansys code balancer

```
FINISH
/CLEAR

/FILENAME,optimum,1
/TITLE, non-linear symmetric analysis: negative stiffness
/UNITS, SI

/CWD,'D:\tlamers\tmp'

!*****************************************************************
! DEFINE PARAMETERS
!*****************************************************************
```

```
*SET,b,6e-3
*SET,E,113.9e9
*SET,v,0.3
*SET,nrsteps,25
*SET,range,0.5e-3
*SET,preload,0.2e-3

!*****************************************************************
! DEFINE GEOMETRY
!*****************************************************************
/PREP7

!KEYPOINTS
K, 1 , 0 , 0
K, 2 , 0 , 0.002
K, 3 , 0.0248 , 0.002
K, 4 , 0.0248 , 0.00575
K, 5 , 0.0295 , 0.00575
K, 6 , 0.0295 , 0.00225
K, 7 , 0.03 , 0.00225
K, 8 , 0.03 , 0.018
K, 9 , 0.0295 , 0.018
K, 10 , 0.0295 , 0.0092
K, 11 , 0 , 0.0092
K, 12 , 0 , 0.016
K, 13 , 0.0293 , 0.016
K, 14 , 0.0293 , 0.019
K, 15 , 0.034 , 0.019
K, 16 , 0.034 , 0.00125
K, 17 , 0.0293 , 0.00125
K, 18 , 0.0293 , 0.00425
K, 19 , 0.0288 , 0.00425
K, 20 , 0.0288 , 0.00075
K, 21 , 0.036 , 0.00075
K, 22 , 0.036 , 0

!LINES
LSTR, 1 , 2
LSTR, 2 , 3
LSTR, 3 , 4
LSTR, 4 , 5

LSTR, 5 , 6
LSTR, 6 , 7
LSTR, 7 , 8
LSTR, 8 , 9
LSTR, 9 , 10
LSTR, 10 , 11
LSTR, 11 , 12
LSTR, 12 , 13
LSTR, 13 , 14
LSTR, 14 , 15
LSTR, 15 , 16
LSTR, 16 , 17
LSTR, 17 , 18
LSTR, 18 , 19
LSTR, 19 , 20
LSTR, 20 , 21
LSTR, 21 , 22
LSTR, 22 , 1
```

```
!CREATE AREA
AL,ALL


!*****************************************************************
! DEFINE ELEMENT SETTINGS
!*****************************************************************

!DEFINE ELEMENT
ET,1,PLANE82
KEYOPT,1,3,3
R,1,b

!MATERIAL PROPERTIES
MP,EX,1,E
MP,PRXY,1,v

!*****************************************************************
! DOE DE MESH
!*****************************************************************

SMRT,6
MSHAPE,1,2D
MSHKEY,0
AMESH,1

FINISH

!*****************************************************************
! SOLUTION SETTINGS
!*****************************************************************
/SOLU

!STATIC ANALYSIS
ANTYPE,STATIC,NEW ! static analysis
NLGEOM,1 ! include large deflections
NSUBST,nrsteps,100,1 ! number of steps
OUTRES,ALL,ALL ! determine output write all results for all steps
AUTOTS,0 ! automatic timestep size

!*****************************************************************
! SET BOUNDARY CONDITIONS / LOADS
!*****************************************************************

!FIXED DOF
DL,11,1,UX
DL,22,1,UY
DK,22,UX

!*****************************************************************
! FIRST LOAD CASE: PRESCRIBED DISPLACEMENT
!*****************************************************************

!PRESCRIBED DISPLACEMENT
DK,12,UY,-preload

SOLVE

!*****************************************************************
! SECOND LOAD CASE: PRESCRIBED DISPLACEMENT
!*****************************************************************
```

```
! PRESCRIBED DISPLACEMENT
DK,22,UX,-range

SOLVE

!*****************************************************************
! THIRD LOAD CASE: PRESCRIBED DISPLACEMENT
!*****************************************************************

! PRESCRIBED DISPLACEMENT
DK,22,UX,range

SOLVE

!*****************************************************************
! POSTPROCES RESULTS
!*****************************************************************
/POST1

/DSCALE,1,1.0
PLESOL, S,EQV, 0,1.0
/REPLOT

FINISH

!*****************************************************************
! EXPORT RESULTS
!*****************************************************************

!stap 1: open de timehistory post processing

/POST26
FILE,'optimum','rst','.'
/UI,COLL,1
NUMVAR,200
SOLU,191,NCMIT
STORE,MERGE
FILLDATA,191,,,,1,1
REALVAR,191,191

!stap 2: selecteer verplaatsingen van knooppunt nrs X

KSEL,S,KP,,12
NSLK
*SET,node_nr,NDNEXT(0)
NSOL,2,node_nr,U,Y,U_y
STORE,MERGE
RFORCE,3,node_nr,F,Y,R_y
STORE,MERGE

KSEL,S,KP,,22
NSLK
*SET,node_nr,NDNEXT(0)
NSOL,4,node_nr,U,X,U_x
STORE,MERGE
RFORCE,5,node_nr,F,X,F_x
STORE,MERGE

!stap 4: exporteren geselecteerde knooppunt data naar text bestand

! Save time history variables to file exprot.txt
```

```
*CREATE,scratch,gui
*DEL,_P26_EXPORT
*DIM,_P26_EXPORT,TABLE,3*nrsteps,5
VGET,_P26_EXPORT(1,0),1
VGET,_P26_EXPORT(1,1),2
VGET,_P26_EXPORT(1,2),3
VGET,_P26_EXPORT(1,3),4
VGET,_P26_EXPORT(1,4),5
/OUTPUT,'exprot','txt'
*VWRITE,'LOAD/TIME','U_y','R_y','U_x','F_x'
%14C %14C %14C %14C %14C
*VWRITE,_P26_EXPORT(1,0),_P26_EXPORT(1,1),_P26_EXPORT(1,2),_P26_EXPORT(1,3),_P26_EXPORT(1,4)
%14.5G %14.5G %14.5G %14.5G %14.5G
/OUTPUT,TERM
*END
/INPUT,scratch,gui
! End of time history save

FINISH

!*****************************************************************
! ANIMATION
!*****************************************************************

/POST1
ANTIME,75,0.1, ,1,1,1,3

!*****************************************************************
! THE END
!*****************************************************************
```

Ansys code grasper

```
FINISH
/CLEAR

/FILENAME,optimum_grasper,1
/TITLE, non-linear analysis: positive stiffness
/UNITS, SI

/CWD,'D:\tmp'

!*****************************************************************
! DEFINE PARAMETERS
!*****************************************************************

*SET,b,6e-3
*SET,E,113.9e9
*SET,v,0.3
*SET,nrsteps,25
*SET,range,0.5e-3

!*****************************************************************
! DEFINE GEOMETRY
!*****************************************************************

/PREP7
!KEYPOINTS
K, 1 , 0 , 0
K, 2 , 0 , 0.0015
K, 3 , -0.0105 , 0.0015
K, 4 , -0.0105 , 0.00075
```

```
K, 5 , -0.01797 , 0.00142
K, 6 , -0.01779 , 0.00341
K, 7 , -0.0105 , 0.00276
K, 8 , -0.0105 , 0.002
K, 9 , -0.0005 , 0.002
K, 10 , -0.0005 , 0.00976
K, 11 , -0.0105 , 0.00976
K, 12 , -0.0105 , 0.00301
K, 13 , -0.03022 , 0.00477
K, 14 , -0.03271 , 0.00499
K, 15 , -0.03293 , 0.0025
K, 16 , -0.0105 , 0.0005
K, 17 , -0.0105 , 0


!LINES
LSTR, 1 , 2
LSTR, 2 , 3
LSTR, 3 , 4
LSTR, 4 , 5
LSTR, 5 , 6
LSTR, 6 , 7
LSTR, 7 , 8
LSTR, 8 , 9
LSTR, 9 , 10
LSTR, 10 , 11
LSTR, 11 , 12
LSTR, 12 , 13
LSTR, 13 , 14
LSTR, 14 , 15
LSTR, 15 , 16
LSTR, 16 , 17

LFILLT, 13 , 14 , 2.5e-3

!MIRROR OVER X-axis
LSYM,Y,ALL,,,,1,0

!GLUE LINES
LGLUE,ALL

!CREATE AREA
AL,ALL

!*****************************************************************
! DEFINE ELEMENT SETTINGS
!*****************************************************************

!DEFINE ELEMENT
ET,1,PLANE82
KEYOPT,1,3,3
R,1,b

!MATERIAL PROPERTIES
MP,EX,1,E
MP,PRXY,1,v

!*****************************************************************
! DOE DE MESH
!*****************************************************************

SMRT,6
```

```
MSHAPE,1,2D
MSHKEY,0
AMESH,1

FINISH

/SOLU
!*****************************************************************
! SOLUTION SETTINGS
!*****************************************************************

! STATIC ANALYSIS
ANTYPE,STATIC,NEW ! static analysis
NLGEOM,1 ! include large deflections
PSTRESS,1
NSUBST,nrsteps,100,1 ! number of steps
OUTRES,ALL,ALL ! determine output write all results for all steps
AUTOTS,0 ! automatic timestep size

!*****************************************************************
! SET BOUNDARY CONDITIONS / LOADS
!*****************************************************************

DL,8,1,ALL
DL,25,1,ALL
DK,1,UY

!*****************************************************************
! FIRST LOAD CASE: PRESCRIBED DISPLACEMENT
!*****************************************************************

DK,1,UX,-range

SOLVE

!*****************************************************************
! SECOND LOAD CASE: PRESCRIBED DISPLACEMENT
!*****************************************************************

DK,1,UX,range

SOLVE

!*****************************************************************
! EXPORT RESULTS
!*****************************************************************

!stap 1: open de timehistory post processing

/POST26
FILE,'optimum_grasper','rst','.'
/UI,COLL,1
NUMVAR,200
SOLU,191,NCMIT
STORE,MERGE
FILLDATA,191,,,,1,1
REALVAR,191,191

!stap 2: selecteer verplaatsingen van knooppunt nrs X

KSEL,S,KP,,1
NSLK
```

```
*SET,node_nr,NDNEXT(0)
NSOL,2,node_nr,U,X,U_x
STORE,MERGE
RFORCE,3,node_nr,F,X,R_x
STORE,MERGE

KSEL,S,KP,,15
NSLK
*SET,node_nr,NDNEXT(0)
NSOL,4,node_nr,U,Y,U_y
STORE,MERGE

!stap 4: exporteren geselecteerde knooppunt data naar text bestand

! Save time history variables to file exprot.txt
*CREATE,scratch,gui
*DEL,_P26_EXPORT
*DIM,_P26_EXPORT,TABLE,2*nrsteps,5
VGET,_P26_EXPORT(1,0),1
VGET,_P26_EXPORT(1,1),2
VGET,_P26_EXPORT(1,2),3
VGET,_P26_EXPORT(1,3),4
/OUTPUT,'exprot','txt'
*VWRITE,'LOAD/TIME','U_x','R_x','U_y'
%14C %14C %14C %14C
*VWRITE,_P26_EXPORT(1,0),_P26_EXPORT(1,1),_P26_EXPORT(1,2),_P26_EXPORT(1,3)
%14.5G %14.5G %14.5G %14.5G
/OUTPUT,TERM
*END
/INPUT,scratch,gui
! End of time history save

FINISH

!*****************************************************************
! ANIMATION STRESSES
!*****************************************************************

/POST1
PLESOL, S,EQV, 0,1.0
ANTIME,50,0.1, ,1,1,1,2

!*****************************************************************
! THE END
!*****************************************************************
```

link naar bron info

Appendix C

Stress stiffening effect of a clamped beam

This appendix presents the analytical solution of an elastic system transiting from stable to unstable behavior. This solution was adopted from Grootenboer (ref).

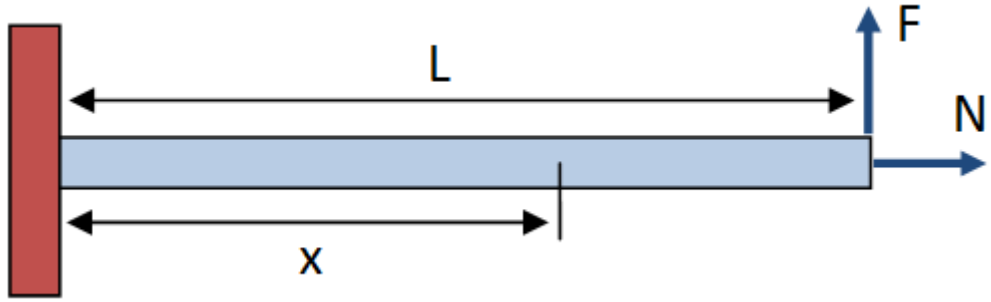

A clamped beam in transversal loading aswell as normal loading. Only transverse deflections are considered: $w(x)$.

The differential equation is obtained from linear beam theory, where the internal moment is related to the curvature of the beam, $M(x) = E \cdot I \cdot w''(x)$. The internal moment needs to equibrilate the external loads, in this case not only a transversal force but also a normal force. This leads to the following differential equation.

$$\frac{d^2w(x)}{dx^2} = F \cdot (L - x) - N \cdot (w(L) - w(x))$$

$$\frac{d^2w(x)}{dx^2} - N \cdot w(x) = -F \cdot x + F \cdot L - N \cdot w(L)$$

with the boundary conditions: $w(0) = 0$ and $w'(0) = 0$.

This is a non homogenous linear second order differential equation with constant coefficients. The non homogenuous part is linear. For this form of ordinary differential equation an analytical solution can be obtained. When this solution is evaluated at the tip of the beam the next formula follows according Grootenboer (ref):

$$w(L) = \frac{\beta - \tanh(\beta)}{\beta^3} \cdot \frac{F \cdot L^3}{E \cdot I} \text{ with } \beta = \sqrt{\frac{N \cdot L^2}{E \cdot I}}$$

This formula allows for an explicit solution of the stiffness being the ratio of $w(L)$ and F. This solutions depends on the axial load and shows how the stiffness value is influenced by the axial load.

Appendix D

Analytical solution of crank slider mechanism

In this appendix the derivation of the analytical force displacement relation of the crank slider mechanism is presented. First the equilibrium equations are solved for the unknown force, then naturally the next step is solving the kinematic relations. Both solutions exist analytically.

statics

Considering the crank slider mechanism in the figure below (ref). Two links connected by hinges A, B and C each having a torsion spring incorporated.

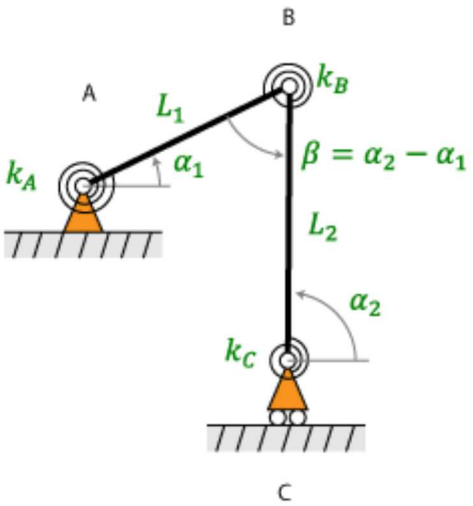

comment

Two free body diagrams can be drawn, of link 1 and link 2. For each the force and moment equilibira can be determined. See illustration below on the right.

The equilibrium equations for both links are:

link 1

$F_{Ax} + F_{Bx} = 0$ **(1)**
$F_{Ay} + F_{By} = 0$ **(2)**
$M_A + M_B + F_{By} \cdot L_1 \cdot \cos(\alpha_1) - F_{Bx} \cdot L_1 \cdot \sin(\alpha_1) = 0$ **(3)**

link 2

$-F_{By} + F_{Cy} = 0$ **(4)**
$-F_{Bx} + F_{Cx} = 0$ **(5)**
$-M_B + M_C + F_{Bx} \cdot L_2 \cdot \sin(\alpha_2) - F_{By} \cdot L_2 \cdot \cos(\alpha_2) = 0$ **(6)**

A solution for the unknown force F_{Cx} can be found in terms of the known moments M_A, M_B and M_C. The moments are known because they are fully determined by the kinematics, as will be derived below.

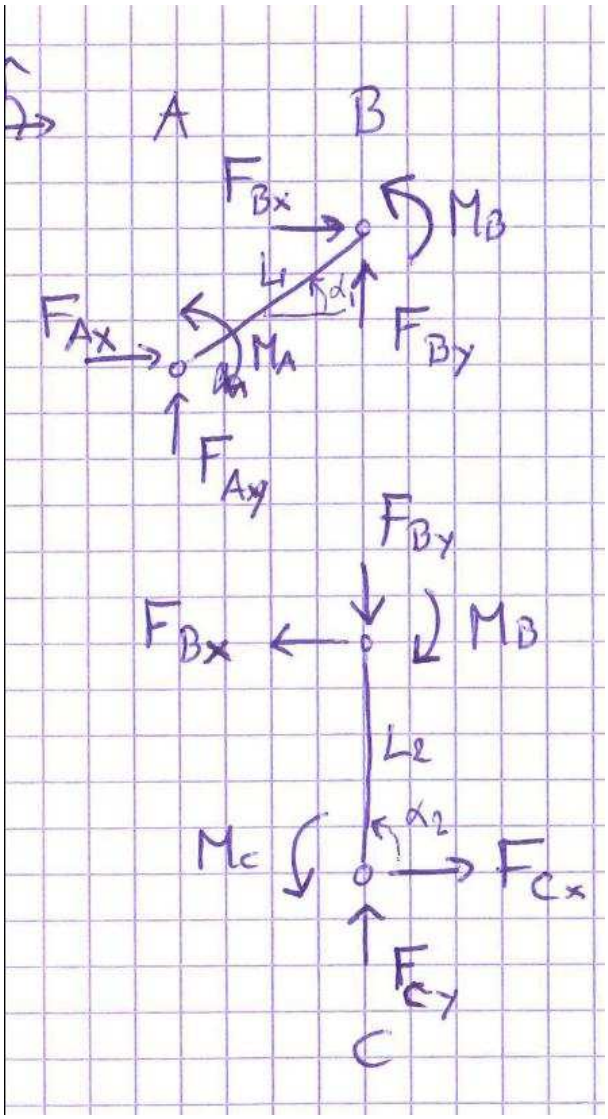

comment

The unknown force F_{Cx} can be solved from the system of equilibrium equations as follows. First solve equation (3) for F_{By} as a function of F_{Bx}. This result can be substituted into equation (6) to obtain a solution for F_{Bx}. This solution can be substituted in equation (5) which can be solved for F_{Cx}. See the detailed steps below.

solve (3) for F_{By}

$M_A + M_B + F_{By} \cdot L_1 \cdot \cos(\alpha_1) - F_{Bx} \cdot L_1 \cdot \sin(\alpha_1) = 0$ becomes

$$F_{By} = \frac{F_{Bx} \cdot L_1 \cdot \sin(\alpha_1) - M_A - M_B}{L_1 \cdot \cos(\alpha_1)} \quad \textbf{(7)}$$

substitute (7) in (6)

$-M_B + M_C + F_{Bx} \cdot L_2 \cdot \sin(\alpha_2) - F_{By} \cdot L_2 \cdot \cos(\alpha_2) = 0$ **(6)**
becomes:

$$-M_B + M_C + F_{Bx} \cdot L_2 \cdot \sin(\alpha_2) - \left[\frac{F_{Bx} \cdot L_1 \cdot \sin(\alpha_1) - M_A - M_B}{L_1 \cdot \cos(\alpha_1)}\right] \cdot L_2 \cdot \cos(\alpha_2) = 0$$

solve for F_{Bx}

$$-M_B + M_C + F_{Bx} \cdot L_2 \cdot \sin(\alpha_2) - \left[\frac{F_{Bx} \cdot L_1 \cdot \sin(\alpha_1)}{L_1 \cdot \cos(\alpha_1)} - \frac{M_A + M_B}{L_1 \cdot \cos(\alpha_1)}\right] \cdot L_2 \cdot \cos(\alpha_2) = 0$$

expand all terms:

$$-M_B + M_C + F_{Bx} \cdot L_2 \cdot \sin(\alpha_2) - \frac{F_{Bx} \cdot \sin(\alpha_1)}{\cos(\alpha_1)} \cdot L_2 \cdot \cos(\alpha_2) + \frac{M_A + M_B}{L_1 \cdot \cos(\alpha_1)} \cdot L_2 \cdot \cos(\alpha_2) = 0$$

reorder and group all terms containing F_{Bx} to the left side of the equation:

$$F_{Bx} \cdot L_2 \cdot \sin(\alpha_2) - \frac{F_{Bx} \cdot \sin(\alpha_1)}{\cos(\alpha_1)} \cdot L_2 \cdot \cos(\alpha_2) = M_B - M_C - \frac{M_A + M_B}{L_1 \cdot \cos(\alpha_1)} \cdot L_2 \cdot \cos(\alpha_2)$$

factorising F_{Bx}:

$$F_{Bx} \cdot L_2 \cdot \left[\sin(\alpha_2) - \frac{\sin(\alpha_1) \cdot \cos(\alpha_2)}{\cos(\alpha_1)}\right] = M_B - M_C - \frac{M_A + M_B}{L_1 \cdot \cos(\alpha_1)} \cdot L_2 \cdot \cos(\alpha_2)$$

solution for F_{Bx}:

$$F_{Bx} = \frac{M_B - M_C - \frac{M_A + M_B}{L_1 \cdot \cos(\alpha_1)} \cdot L_2 \cdot \cos(\alpha_2)}{L_2 \cdot \left[\sin(\alpha_2) - \frac{\sin(\alpha_1) \cdot \cos(\alpha_2)}{\cos(\alpha_1)}\right]}$$

simplify by multiplying with $\frac{\cos(\alpha_1)}{\cos(\alpha_1)}$

$$F_{Bx} = \frac{\cos(\alpha_1) \cdot (M_B - M_C) - \cos(\alpha_2) \cdot (M_A + M_B) \cdot \frac{L_2}{L_1}}{L_2 \cdot [\cos(\alpha_1) \cdot \sin(\alpha_2) - \sin(\alpha_1) \cdot \cos(\alpha_2)]}$$

simplify by multiplying with: $\frac{L_1}{L_1}$

$$F_{Bx} = \frac{L_1 \cdot \cos(\alpha_1) \cdot (M_B - M_C) - L_2 \cdot \cos(\alpha_2) \cdot (M_A + M_B)}{L_1 \cdot L_2 \cdot [\cos(\alpha_1) \cdot \sin(\alpha_2) - \sin(\alpha_1) \cdot \cos(\alpha_2)]}$$

And finally substitute the following trigonometric identity: $\sin(x - y) = \sin(x) \cdot \cos(y) - \cos(x) \cdot \sin(y)$

$$F_{Bx} = \frac{L_1 \cdot \cos(\alpha_1) \cdot (M_B - M_C) - L_2 \cdot \cos(\alpha_2) \cdot (M_A + M_B)}{L_1 \cdot L_2 \cdot \sin(\alpha_2 - \alpha_1)}$$

substitute into (5) and solve for F_{Cx}

$-F_{Bx} + F_{Cx} = 0$ **(5)**
will then become:

$$F_{Cx} = \frac{L_1 \cdot \cos(\alpha_1) \cdot (M_B - M_C) - L_2 \cdot \cos(\alpha_2) \cdot (M_A + M_B)}{L_1 \cdot L_2 \cdot \sin(\alpha_2 - \alpha_1)}$$

Now a solution is obtained for F_{Cx} as a function of the known moments. The magnitude of the moments at A, B and C depend on the relative rotational angle between links and fixed world and the initial preload angle of each spring as follows.

$$M_A = -k_A \cdot (\alpha_1 - \alpha_{p1})$$
$$M_B = k_B \cdot (\alpha_2 - \alpha_1 - \beta_p)$$
$$M_C = -k_C \cdot (\alpha_2 - \alpha_{p2})$$

So the moments are a function of the kinematic degrees of freedom α_1, α_2 and β. Then the next step is to find a solution for these variables as a function of the translational degree of freedom x_C. Then an explicit solution of F_{Cx} is obtained.

kinematics

The kinematics can be described by rotational coordinates (α_1, α_2 and β) or translational coordinates (x,y -coordinates of hinges A, B and C). So there are 6 translational coordinates, 2 constraining equations (loop closure equations) and 3 translational coordinates are constrained. This leaves one dynamic degree of freedom left ($6 - 2 - 3 = 1$) in this mechanism.

To get an insight in the kinematic relations, first the translational coordinates of all hinges are determined as function of the rotational coordinates. See table and illustration below.

$x_A = 0$	$x_B = L_1 \cdot \cos(\alpha_1)$	$x_C = x_B - L_2 \cdot \cos(\alpha_2)$
$y_A \neq 0$	$y_B = y_A + L_1 \cdot \sin(\alpha_1)$ en $y_B = L_2 \cdot \sin(\alpha_2)$	$y_C = 0$
translational coordinates		

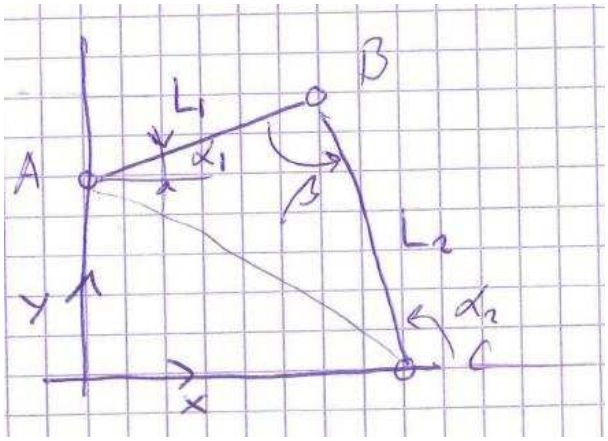

The table contains two expressions for the coordinate y_B. This relates α_1 to α_2 in an explicit and reversible way. If either one of the rotational coordinates is solved for x_C then the problem is fully solved. First a solution for α_1 is determined using the cosine rule. Secondly the solution for α_2 follows. Finally from the illustration it follows that $\beta = \alpha_2 - \alpha_1$.

solve α_1

From the illustration below it follows that:

$$\alpha_1 = A - \gamma$$

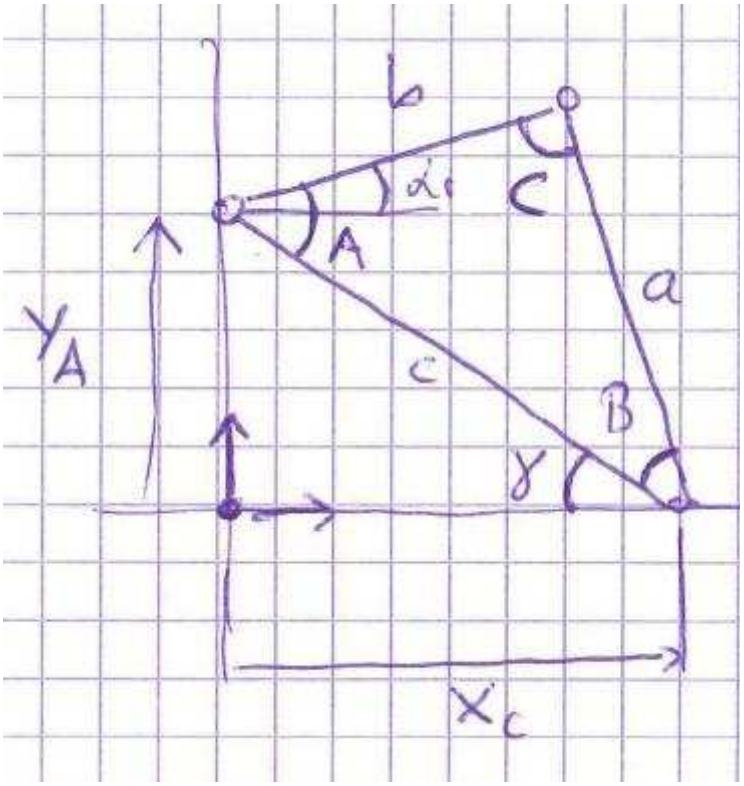

The angle γ can be determined using:

$$\gamma = \arctan\left(\frac{y_A}{x_C}\right)$$

with the condition:

$$-\frac{\pi}{2} \le \gamma \le \frac{\pi}{2}$$

The angle A can be determined using the cosine rule:

$$A = \arccos\left(\frac{-a^2 + b^2 + c^2}{2 \cdot b \cdot c}\right) \text{ and } c = \sqrt{y_A^2 + x_C^2}$$

with the condition:

$$0 \le A \le \pi$$

$$A = \arccos\left(\frac{-L_2^2 + L_1^2 + y_A^2 + x_C^2}{2 \cdot L_1 \cdot \sqrt{y_A^2 + x_C^2}}\right)$$

and for the argument of $\arccos(\text{arg})$

$$-1 \le \text{arg} \le 1$$

The angle α_1 becomes then:

$$\alpha_1 = \arccos\left(\frac{-L_2^2 + L_1^2 + y_A^2 + x_C^2}{2 \cdot L_1 \cdot \sqrt{y_A^2 + x_C^2}}\right) - \arctan\left(\frac{y_A}{x_C}\right)$$

with the condition:

$$-\frac{\pi}{2} \le \gamma \le \frac{\pi}{2}$$

$0 \le A \le \pi$ and $-1 \le \text{arg} \le 1$

solve α_2

Considering the relation between α_1 and α_2 it follows that:

$$y_A + L_1 \cdot \sin(\alpha_1) = L_2 \cdot \sin(\alpha_2)$$

$$\alpha_2 = \arcsin\left(\frac{y_A + L_1 \cdot \sin(\alpha_1)}{L_2}\right)$$

with the conditions:

$$-\frac{\pi}{2} \le \alpha_2 \le \frac{\pi}{2}$$

$$-1 \le \text{arg} \le 1$$

or

$$\alpha_2 = \pi - \arcsin\left(\frac{y_A + L_1 \cdot \sin(\alpha_1)}{L_2}\right)$$

with the conditions:

$$\frac{\pi}{2} < \alpha_2 \leq \frac{3}{2} \cdot \pi$$

$$-1 \leq \arg \leq 1$$

Explicit solutions have been found for the rotational coordinates as a function of x_C.

behavior preload force

As the crank slider model predicts, higher preload force at A means higher negative stiffness. This can be proven analytically by looking at the equilibrium equations of link 2. See the illustration below (ref) for the free body diagram.

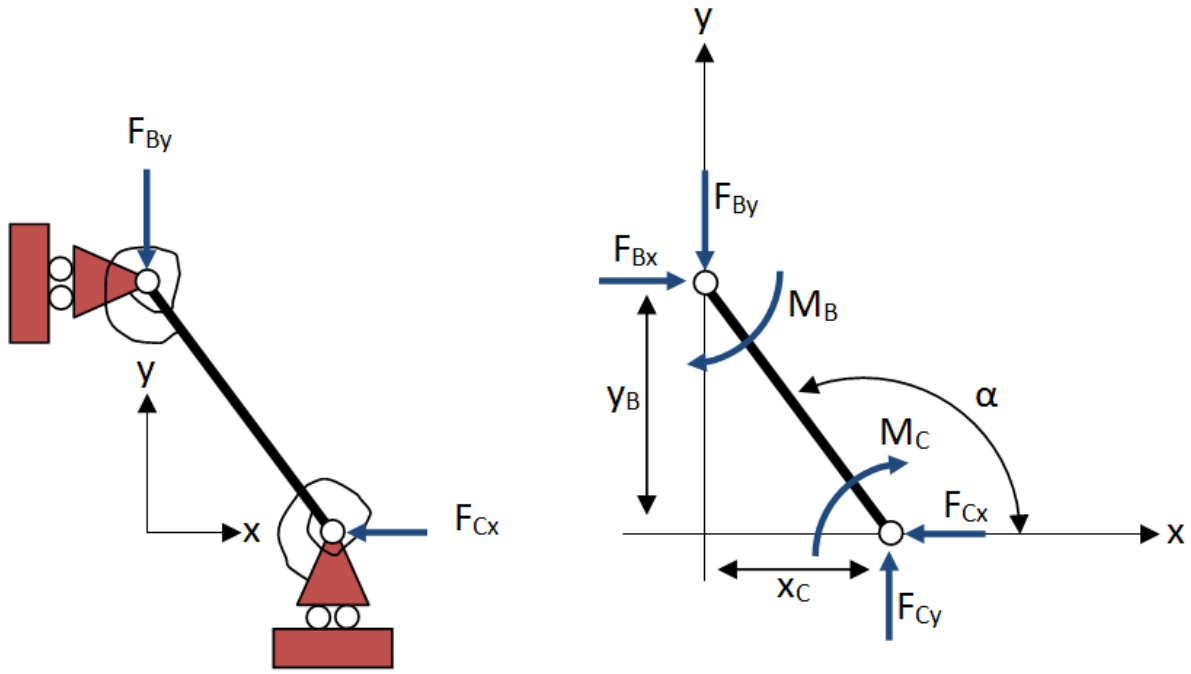

Illustration showing free body diagram of link 2.

Equilibrium equations are:

$$-F_{By} + F_{Cy} = 0$$
$$F_{Bx} - F_{Cx} = 0$$
$$F_{Cy} \cdot x_C - M_C - M_B - F_{Cx} \cdot y_B = 0$$

From the equilibrium equations F_{Cx} can be solved:

$$F_{Cx} = \frac{F_{By} \cdot x_C - M_C - M_B}{y_B}$$

The internal moments are defined by the rotational coordinate α and the preload angles α_{pB} and α_{pC} :

$$M_B = (\alpha - \alpha_{pB}) \cdot k_B$$
$$M_C = (\alpha - \alpha_{pC}) \cdot k_C$$

Now α and y_B are expressed as functions of x_C and may be substituted in the equation for F_{Cx}.

For α follows:

$$L_2 \cdot \cos(\pi - \alpha) = x_C$$

$$\alpha = \pi - \arccos\left(\frac{x_C}{L}\right)$$

For y_B follows:

$$y_B = \sqrt{L_2^2 - x_C^2}$$

$$F_{Cx} = F_{By} \cdot \frac{x_C}{y_B} - \frac{\alpha}{y_B} \cdot (k_B + k_C) + \frac{\alpha_{pB} \cdot k_B + \alpha_{pC} \cdot k_C}{y_B}$$

Now we have the analytical expression for F_{Cx} as a function of x_C we can consider its behavior around the angle $\alpha = \frac{\pi}{2}$ where x_C is close to zero. For that purpose the following factors are considered for small values of x_C:

$$\frac{x_C}{y_B} = \frac{x_C}{\sqrt{L_2^2 - x_C^2}} \cong \frac{x_C}{L_2}$$

$$\frac{\alpha}{y_B} = \frac{\pi - \arccos\left(\frac{x_C}{L_2}\right)}{\sqrt{L_2^2 - x_C^2}} \cong \frac{\pi}{2 \cdot L_2}$$

$$\frac{1}{y_B} = \frac{1}{\sqrt{L_2^2 - x_C^2}} \cong \frac{1}{L_2}$$

The solution then becomes:

$$F_{Cx} = F_{By} \cdot \frac{x_C}{L_2} - \frac{\pi}{2 \cdot L_2} \cdot (k_B + k_C) + \frac{\alpha_{pB} \cdot k_B + \alpha_{pC} \cdot k_C}{L_2}$$

From this expression it can be seen that F_{Cx} (and thus the negative stiffness) when neglecting the torsion stiffness :

- increases when F_{By} increases

Appendix E

Numerical scheme for crank slider mechanism and GUI

In this appendix the numerical scheme is explained used for studying the behavior of the crank slider mechanism. The goal is to see how model parameters affect the behavior to finally select the design variables that boost the negative stiffness. The numerical scheme is combined with a graphical user interface in which the model parameters are coupled to sliders that influence their values. The resulting change of behavior is instantaneously numerically calculated and visualized in a force deflection graph. The preload force versus displacement and the intial as well as the actual configuration are plotted.

A preview of the GUI can be found in the first section of this appendix. There after a section is devoted to the calculation steps in the numerical scheme. Then the derivation of equations is given and the last section contains the Matlab programming code used.

Graphical user interface

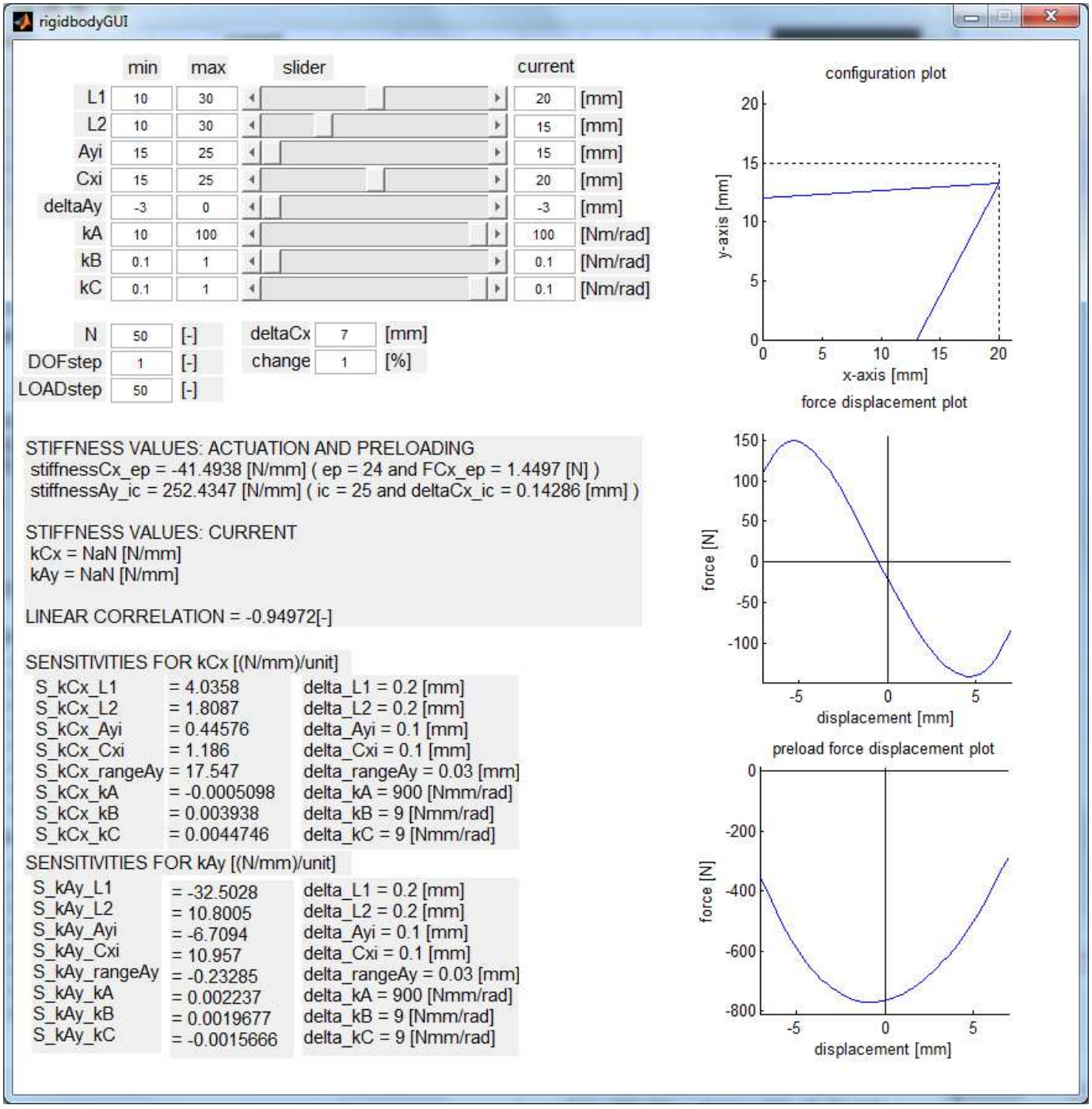

Calculation steps

There are 13 steps in the scheme to be divided in three main parts.

1. solve forces and displacements, steps 1 to 4
2. analyse stiffness, steps 5 to 7
3. analyse sensitivity, steps 8 to 12

In part one statics and kinematics are solved. Then Force displacement relations are known and in part 2 stiffness values can be calculated at several points of interest. In this case the stiffness along the displacents x_C and y_A are considered. In part 3 the sensitivity values are calculated. This means the change of the stiffness values to changes in any model parameter. All equations used are derived in the section "Equations" of this appendix.

For each calculation step the related variables are mentioned, and the custom made Matlab functions are named, which can be looked up in the last section of this appendix, starting with the main script. All the steps are (in)directly addressed from the main script.

part 1: solve forces and displacements

1. *"main script"*: set initial values for all system parameters.

   geometric: L_1, L_2, A_{xi}, A_{yi}, C_{xi}, C_{yi}

   static: k_A, k_B, k_C

2. *"main script"*: set displacement ranges and number of steps for preloading and the range of motion. Both ranges are discretized using the same number of steps. In order to calculate current stiffness and sensitivity values also an actual degree of freedom step and a preload step need to be specied.

   range of motion: ΔC_x

   preload displacement: ΔA_y

   number of steps: N

   actual degree of freedom step (used in part 2 and 3): DOF_{step}

   actual load step (used in part 2 and 3): LOAD_{step}

   Defining two ranges means defining two independent variables. Thus all variables depending on both ranges become matrices.
3. *"kinematics2DOF"*: solve all variables which are independent of the ranges given the set of system parameters.

   preload angles: α_{p1},α_{p2},β_p

   initial configuration: A_{xi},A_{yi},B_{xi},B_{yi},C_{xi},C_{yi}
4. *"kinematics2DOF"* / *"statics2DOF"*: solve all configurations and forces/moments for the specified ranges given the set of system parameters.

   angles: α_1,α_2,β_p

   configurations: A_x,A_y,B_x,B_y,C_x,C_y

   moments: M_A,M_B,M_C

   forces: F_{Ax},F_{Ay},F_{Bx},F_{By},F_{Cx},F_{Cy}

part 2: analyse stiffness

5. *"stiffnesskCx2DOF"* / *"stiffnesskAy2DOF"*: calculate stiffness values for all DOF/LOAD steps given the model parameters

   DOF stiffness: $[k_{Cx}]$

   preload stiffness: $[k_{Ay}]$

6. *"analyse_stiffness"*: determine stiffness values at equilibrium point and at initial preload step

   equilibrium point stiffness: $k_{Cx\text{-}ep}$

   initial configuration preload stiffness: $k_{Ay\text{-}ic}$

7. *"analyse_stiffness"*: determine stiffness values for current degree of freedom/load step

   current DOF step stiffness: k_{Cx}

current preload step stiffness: k_{Ay}

8. *"main script"*: determine linear correlaction coefficient of force displacement function for F_{Cx}.

part 3: analyse sensitivity

9. *"main script"*: set minimal and maximal values for system parameters and a percentage of change in order to determine the absolute parameter changes.

   minimal values:
   $L_{1\text{-min}}$, $L_{2\text{-min}}$, $A_{xi\text{-min}}$, $A_{yi\text{-min}}$, $C_{xi\text{-min}}$, $C_{yi\text{-min}}$
   $k_{A\text{-min}}$, $k_{B\text{-min}}$, $k_{C\text{-min}}$

   maximal values:
   $L_{1\text{-max}}$, $L_{2\text{-max}}$, $A_{xi\text{-max}}$, $A_{yi\text{-max}}$, $C_{xi\text{-max}}$, $C_{yi\text{-max}}$
   $k_{A\text{-max}}$, $k_{B\text{-max}}$, $k_{C\text{-max}}$

   change value: Δ [%]

10. *"analyse_sensitivity"*: set the current design vector using the given system paramters

    design vector: $\{L_1, L_2, A_{yi}, C_{xi}, \Delta A_y, k_A, k_B, k_C\}^T$

11. *"sensitivitykCx"* / *"sensitivitykAy"*: calculate parameter change for each system parameter given the minima, maxima and change value.

    change vector: $\{\delta L_1, \delta L_2, \delta A_{yi}, \delta C_{xi}, \delta \Delta A_y, \delta k_A, \delta k_B, \delta k_C\}^T$

12. *"sensitivitykCx"*: for each parameter change independently calculate the sensitivity vector for the stiffness k_{Cx} at the equilibrium point for the given design and change vectors

    sensitivity vector: $\{S_{kCx\text{-}L1}, S_{kCx\text{-}L2}, S_{kCx\text{-}Ayi}, S_{kCx\text{-}Cxi}, S_{kCx\text{-}\Delta Ay}, S_{kCx\text{-}kA}, S_{kCx\text{-}kB}, S_{kCx\text{-}kC}\}^T$

13. *"sensitivitykAy"*: for each parameter change independently calculate the sensitivity vector for the stiffness k_{Ay} at the initial preload step for the given design and change vectors

    sensitivity vector: $\{S_{kAy\text{-}L1}, S_{kAy\text{-}L2}, S_{kAy\text{-}Ayi}, S_{kAy\text{-}Cxi}, S_{kAy\text{-}\Delta Ay}, S_{kAy\text{-}kA}, S_{kAy\text{-}kB}, S_{kAy\text{-}kC}\}^T$

Equations

Kinematic equations

Kinematics are solved using the exact same equatoins as presented in appendix 2 (ref) - section "kinematics". These equations (and their conditions) are evaluated in the function "*kinematics2DOF*".

Static equations

The set of equilibrium equations is rearranged as follows before implemented into the numerical scheme. The equilibrium equations as derived in appendix 2 (ref) are:

element 1

$$F_{Ax} + F_{Bx} = 0$$
$$F_{Ay} + F_{By} = 0$$
$$M_A + M_B + F_{By} \cdot L_1 \cdot \cos(\alpha_1) - F_{Bx} \cdot L_1 \cdot \sin(\alpha_1) = 0$$

element 2

$$-F_{By} + F_{Cy} = 0$$
$$-F_{Bx} + F_{Cx} = 0$$
$$-M_B + M_C + F_{Bx} \cdot L_2 \cdot \sin(\alpha_2) - F_{By} \cdot L_2 \cdot \cos(\alpha_2) = 0$$

This set of equations can be factorized as a linear set, namely the product of a vector $\underline{F}$ containing all forces and moments, and a matrix $[M]$ containing geometrical and kinematical dependent coefficients.

$$[M] \cdot \underline{F} = \underline{0}$$

The force vector

This vector contains all forces and moments appearing in the free body diagrams (see appendix 2 (ref)) and is organized as follows:

$$\underline{F} = \langle F_{Ax} \quad F_{Ay} \quad M_A \quad F_{Bx} \quad F_{By} \quad M_B \quad F_{Cx} \quad F_{Cy} \quad M_C \rangle^T$$

It is possible to partition the force vector into known $\underline{F}_k$ and unknown $\underline{F}_u$ forces:

$$\underline{F} = \langle \underline{F}_k \quad \underline{F}_u \rangle^T$$

The moments are considered to be known, and the forces unknown.

$$\underline{F}_k = \begin{pmatrix} M_A \\ M_B \\ M_C \end{pmatrix} = \begin{pmatrix} -k_A \cdot (\alpha_1 - \alpha_{p1}) \\ k_B \cdot (\alpha_2 - \alpha_1 - \beta_p) \\ -k_C \cdot (\alpha_2 - \alpha_{p2}) \end{pmatrix}$$

$$\underline{F}_u = \langle F_{Ax} \quad F_{Ay} \quad F_{Bx} \quad F_{By} \quad F_{Cx} \quad F_{Cy} \rangle^T$$

The matrix

The matrix contains all kinematic and geometric dependent coefficients, the partition applied to the vector can be extended to the matrix.

$$[M] = [M_k \quad M_u]$$

Linear set of equations

Considering the proposed partioning the next linear set of equations can be derived.

$$[M_k \quad M_u] \cdot \begin{pmatrix} \underline{F}_k \\ \underline{F}_u \end{pmatrix} = \underline{0} \quad \textbf{(1)}$$

Keeping the same order as in the list above we get:

$$[M_k] = \begin{bmatrix} 0 & 0 & 0 \\ 0 & 0 & 0 \\ 1 & 1 & 0 \\ 0 & 0 & 0 \\ 0 & 0 & 0 \\ 0 & -1 & 1 \end{bmatrix} \text{ and } [M_u] = \begin{bmatrix} 1 & 0 & 1 & 0 & 0 & 0 \\ 0 & 1 & 0 & 1 & 0 & 0 \\ 0 & 0 & -L_1 \cdot \sin(\alpha_1) & L_1 \cdot \cos(\alpha_1) & 0 & 0 \\ 0 & 0 & 0 & -1 & 0 & 1 \\ 0 & 0 & -1 & 0 & 1 & 0 \\ 0 & 0 & L_2 \cdot \sin(\alpha_2) & -L_2 \cdot \cos(\alpha_2) & 0 & 0 \end{bmatrix}$$

Equation (1) can be solved for the unknown forces:

$$[M_k] \cdot \underline{F}_k + [M_u] \cdot \underline{F}_u = \underline{0}$$
$$[M_u] \cdot \underline{F}_u = -[M_k] \cdot \underline{F}_k$$
$$\underline{F}_u = -[M_u]^{-1} \cdot [M_k] \cdot \underline{F}_k \quad \textbf{(2)}$$

When the kinematics are solved, matrix $[M_u]$ becomes known. By that equation (2) gives the solution for the unknown forces. Numerically speaking this means that first a solution to the kinematics need to be obtained. In this case the solution is analytically known, but for more complex mechanism newton raphson scheme can be implemented. Then matrix $[M_u]$needs to be inverted. Since this matrices is not very big and sparse only low computational effort is demanded. Equation (2) is used in function *"statics2DOF"*.

Stiffness equations

The stiffness is determined on pure numerical basis. The force displacement solution is known from the *"statics2DOF"* function. The stiffness is then determined by using the central differences method:

$$k_{Cx}(n) = \frac{F_{Cx}(n+1) - F_{Cx}(n-1)}{2 \cdot \delta C_x}$$

For which the step size is determined by

$$\delta C_x = \frac{2 \cdot \Delta C_x}{N}$$

This explains why the GUI gives NaN values for solutions at first/last load step or degree of freedom step.

Sensitivity equations

The sensitivity values are calculated based on the following thought. If one of the model parameters changes a bit in magnitude, then most likely the behavior (the force displacement graph) will change too. Since stiffness is all ready determined using the central differences method one only has to keep track of the amount of change of the stiffness value divided by the change of parameter value. This is called the sensitivity in this work.

In order to do that, first a set of design parameters need to be appointed.

$$\underline{D} = \left\{L_1, L_2, A_{\mathrm{yi}}, C_{\mathrm{xi}}, \Delta A_y, k_A, k_B, k_C\right\}^T$$

Then the change in parameter value needs to be set. This is done by predefining a range for each parameter value. The range sizes are all set to values that are realistic and achievable for the design problem considered. Then a specific percentage of this range determines the size of the parameter change. This percentage is taken equal for all parameters for simplicity and a typical value is 1 [%].

$$\delta\underline{D} = \left\{\delta L_1, \delta L_2, \delta A_{\mathrm{yi}}, \delta C_{\mathrm{xi}}, \delta\Delta A_y, \delta k_A, \delta k_B, \delta k_C\right\}^T$$

Now an initial value and a change is known, stiffness values can be calculated. To determine a change in stiffness two points need to be evaluated. For this it is necessary to determine how the two points are positioned relative to the initial value. In this case a central difference approach is taken:

$$\underline{D}_1 = \underline{D} - \frac{1}{2} \cdot \delta\underline{D}$$

$$\underline{D}_2 = \underline{D} + \frac{1}{2} \cdot \delta\underline{D}$$

Having a parameter change defined, then the way of obtaining the stiffness change must be determined. Two approaches can be considered

1. orthogonal: change only one parameter at a time and calculate the sensitivity. The change vector has only one non-zero element.
2. non orthogonal: change multiple parameters at once and calculate the sensitivity. The change vector has multiple non-zero elements.

For simplicity approach number one is used. If the numerical scheme becomes part of some optimization algorithm then approach two will probably be taken. This also depends on the design problem, because model parameters might be related to each other when they are considered to approximately model an elastic continuum of some geometry. Finally the next formula is used to determine the sensitivity value.

$$S_i = \frac{k(\underline{D}_2) - k(\underline{D}_1)}{\delta D_i} \text{ for } i = 1...n$$

Where n is the number of parameters in the design vector $\underline{D}$ and k the stiffness value according equation 3454(ref) (see stiffness section). The sensitivity values are determined in the functions *"sensitivitykCx"* and *"sensitivitykAy"*.

Programming code

The programmed scripts and functions are listed in this section, they are related via the following structure.

calling structure of functions	list of scripts and functions

• main2DOF
  ◦ solve_csm
  ▪ kinematics2DOF
  ▪ statics2DOF
  ◦ analyse_stiffness
  ▪ stiffnesskCx2DOF
  ▪ stiffnesskAy2DOF
  ◦ analyse_sensitivity
  ▪ sensitivitykCx
  ▪ kinematics2DOF
  ▪ statics2DOF
  ▪ stiffnesskCx2DOF
	1. main2DOF
	2. solve_csm
	3. kinematics2DOF
	4. statics2DOF
	5. analyse_stiffness
	6. analyse_sensitivity
	7. stiffnesskCx2DOF
	8. stiffnesskAy2DOF
	9. sensitivitykCx
	10. sensitivitykAy

▪ sensitivitykAy ▪ kinematics2DOF ▪ statics2DOF ▪ stiffnesskAy2DOF	

```
% this script calculates sensitivities of stiffnesses in directions Ay and
% all 2DOF named functions accept meshgrid variables for ranges of deltaCx
% and deltaAy
% Cx for design variables
clear
clc
close all

% STEP 1
L1 = 0.020;
L2 = 0.015;
Axi = 0;
Ayi = 0.015;
Cxi = 0.020;
Cyi = 0;
kA = 100;
kB = 1;
kC = 1;
% END STEP 1

% STEP 2
rangeCx = 0.007; % range of motion actuation
rangeAy = -0.003; % range of motion preloading
N = 50; % number of DOF steps
DOFstep = 1; % set actuation step
LOADstep = 50; % set preload step
% END STEP 2

% STEP 3 and 4
[U P F C] = solve_csm(L1,L2,Ayi,Cxi,N,rangeCx,rangeAy,kA,kB,kC,DOFstep,LOADstep,1);
% END STEP 3 and 4

% STEP 5, 6 and 7
[kCx_ep ep kAy_ic ic kCx kAy C] = analyse_stiffness(C,1);
% END STEP 5,6 and 7

% STEP 8
LC = corrcoef(U,F);
disp(['LINEAR CORRELATION = ', num2str(LC(1,2)), '[-]']);
disp(' ');
% END STEP 8

% STEP 9
C.sensitivity.L1_min = 0.010;
C.sensitivity.L1_max = 0.030;
C.sensitivity.L2_min = 0.010;
C.sensitivity.L2_max = 0.030;
C.sensitivity.Ayi_min = 0.015;
C.sensitivity.Ayi_max = 0.025;
C.sensitivity.Cxi_min = 0.015;
C.sensitivity.Cxi_max = 0.025;
C.sensitivity.rangeAy_min = -0.003;
C.sensitivity.rangeAy_max = 0;
C.sensitivity.kA_min = 10;
C.sensitivity.kA_max = 100;
```

```
C.sensitivity.kB_min = 0.1;
C.sensitivity.kB_max = 1;
C.sensitivity.kC_min = 0.1;
C.sensitivity.kC_max = 1;

change = 0.01;
% END STEP 9

% STEP 10,11,12 and 13
[S_kCx change_vector_kCx S_kAy change_vector_kAy C] = analyse_sensitivity(change,C,1);
% END STEP 10,11,12 and 13
```

```
function [U P F CONTAINER] = solve_csm(L1,L2,Ayi,Cxi,N,rangeCx,rangeAy,kA,kB,kC,↙
DOFstep,LOADstep,plotON)

    % KINEMATICS: INITIALIZE VARIABLES
    Axi = 0;
    Cyi = 0;

    % STEP 3 - KINEMATICS: SOLVE STRESS FREE CONFIGURATION
    [alphap1 alphap2 betap] = kinematics2DOF(L1,L2,Ayi,0,Cxi,0);
    Bxi = L1*cos(alphap1);
    Byi = L2*sin(alphap2);
    % END STEP 3

    % STEP 4 - KINEMATICS: SOLVE STRESSED CONFIGURATIONS
    deltaCx = linspace(-rangeCx,rangeCx,N)';
    deltaAy = linspace(0,rangeAy,N)';
    [deltaCx deltaAy] = meshgrid(deltaCx,deltaAy);
    [alpha1 alpha2 beta] = kinematics2DOF(L1,L2,Ayi,deltaAy,Cxi,deltaCx);
    Ax = zeros(N,N);
    Ay = Ayi + deltaAy;
    Bx = L1*cos(alpha1);
    By = L2*sin(alpha2);
    Cx = Cxi + deltaCx;
    Cy = zeros(N,N);
    % STATICS: SOLVE FORCES AND MOMENTS
    [MA MB MC FAx FAy FBx FBy FCx FCy] = statics2DOF(alpha1,alpha2,beta,alphap1,↙
alphap2,betap,kA,kB,kC,L1,L2);
    F = FCx(LOADstep,:)';
    P = FAy(LOADstep,:)';
    U = deltaCx(LOADstep,:)';
    % END STEP 4

    CONTAINER.L1 = L1;
    CONTAINER.L2 = L2;
    CONTAINER.N = N;
    CONTAINER.rangeCx = rangeCx;
    CONTAINER.rangeAy = rangeAy;
    CONTAINER.stiffness = [kA kB kC];
    CONTAINER.DOFstep = DOFstep;
    CONTAINER.LOADstep = LOADstep;
    CONTAINER.preloadangles = [alphap1 alphap2 betap];
    CONTAINER.initialconfiguration = [Axi Ayi Bxi Byi Cxi Cyi];
    CONTAINER.rotations.alpha1 = alpha1;
    CONTAINER.rotations.alpha2 =  alpha2;
    CONTAINER.rotations.beta = beta;
    CONTAINER.translations.Ax = Ax;
    CONTAINER.translations.Ay = Ay;
    CONTAINER.translations.Bx = Bx;
    CONTAINER.translations.By = By;
    CONTAINER.translations.Cx = Cx;
    CONTAINER.translations.Cy = Cy;
    CONTAINER.displacements.deltaCx = deltaCx;
    CONTAINER.displacements.deltaAy = deltaAy;
    CONTAINER.moments.MA = MA;
    CONTAINER.moments.MB = MB;
```

```
    CONTAINER.moments.MC = MC;
    CONTAINER.forces.FAx = FAx;
    CONTAINER.forces.FAy = FAy;
    CONTAINER.forces.FBx = FBx;
    CONTAINER.forces.FBy = FBy;
    CONTAINER.forces.FCx = FCx;
    CONTAINER.forces.FCy = FCy;

    if plotON == 1
        % PLOT CONFIGURATION AND FORCE DISPLACEMENT GRAPH
        figure('Position',[10 50 1200 400])

        subplot(1,3,1)
        plot_config(CONTAINER,0)

        subplot(1,3,2)
        plot_force(CONTAINER,0,0,0,0);

        subplot(1,3,3)
        plot_load(CONTAINER,'Cx',0)
    end

end
```

```
% solves kinematics for 2 dimensional domain (deltaAy and deltaCx)
function [alpha1 alpha2 beta] = kinematics2DOF(L1,L2,Ayi,deltaAy,Cxi,deltaCx)
    [tmp cols] = size(deltaCx);
    [rows tmp] = size(deltaAy);

    Cx = Cxi + deltaCx;
    Ay = Ayi + deltaAy;

    alpha1 = acos((-L2^2+L1^2+Cx.^2+Ay.^2)./(2*L1*sqrt(Cx.^2+Ay.^2)))-atan(Ay./Cx);

    Bx = L1*cos(alpha1);

    alpha2 = NaN(rows,cols); % create empty vector

    for r = 1:rows
        for c = 1:cols;
            % check in which range alpha2 is, by looking at sign of Bx-Cx (inner
            % product), then use correct function to determine alpha2.

            % range1: alpha2 < pi/2
            % border: alpha2 = pi/2
            % range2: alpha2 > pi/2

            if Bx(r,c)-Cx(r,c)<0 % RANGE 2
                arg = (Ay(r,c) + L1*sin(alpha1(r,c)))/L2;
                if (arg>1) % check for complex solution
                    poscomplex = [r c] % step for which solution becomes complex
                    arg = 1;
                elseif (arg<-1) % check for complex solution
                    negcomplex = [r c] % step for which solution becomes complex
                    arg = -1;
                end
                alpha2(r,c) = pi - asin(arg);
            elseif Bx(r,c)==Cx(r,c) % BORDER
                alpha2(r,c) = pi/2;
            else % RANGE 1
                arg = (Ay(r,c) + L1*sin(alpha1(r,c)))/L2;
                if (arg>1)
                    poscomplex = [r c]
                    arg = 1;
                elseif (arg<-1)
                    negcomplex = [r c]
                    arg = -1;
                end
                alpha2(r,c) = asin(arg);
            end
        end
    end
    beta = alpha2 - alpha1;
end
```

```
function [MA MB MC FAx FAy FBx FBy FCx FCy] = statics2DOF(alpha1,alpha2,beta,alphap1,↙
alphap2,betap,kA,kB,kC,L1,L2)
    [rows cols] = size(alpha1);
    % determine moments from torsion stiffnesses
    MA = -kA*(alpha1-alphap1);
    MB = kB*(beta-betap);
    MC = -kC*(alpha2-alphap2);
    % determine all free body diagram translational forces of the 2 links (according↙
notes id = 4223)

    % global matrix partion for vector known forces/moments
    M_k = [0 0  0,
           0 0  0,
           1 1  0,
           0 0  0,
           0 0  0,
           0 -1 1];
    F_u = NaN(rows,cols,6); % create empty global vector for unknown forces
    for r = 1:rows
        for c = 1:cols
            % vector with known forces/moments
            F_k = [MA(r,c) MB(r,c) MC(r,c)]';
            % matrix partition for vector with unknown forces/moments
            M_u = [1 0 1                 0                0 0,
                   0 1 0                 1                0 0,
                   0 0 -L1*sin(alpha1(r,c))  L1*cos(alpha1(r,c))  0 0,
                   0 0 0                 -1               0 1,
                   0 0 -1                0                1 0,
                   0 0 L2*sin(alpha2(r,c))   -L2*cos(alpha2(r,c)) 0 0];
            % vector with unknown forces/moments
            F_u(r,c,:) =  -inv(M_u)*M_k*F_k;
        end
    end

    % define nodal forces of free body diagram of the 2 links
    FAx = F_u(:,:,1);
    FAy = F_u(:,:,2); % the preload force
    FBx = F_u(:,:,3);
    FBy = F_u(:,:,4);
    FCx = F_u(:,:,5); % the negative stiffness force
    FCy = F_u(:,:,6);
end
```

```
function [kCx_ep ep kAy_ic ic kCx kAy CONTAINER] = analyse_stiffness(CONTAINER,dispON)

    DOFstep = CONTAINER.DOFstep;
    LOADstep = CONTAINER.LOADstep;
    N = CONTAINER.N;

    Cx = CONTAINER.translations.Cx;
    FCx = CONTAINER.forces.FCx;
    Ay = CONTAINER.translations.Ay;
    FAy = CONTAINER.forces.FAy;
    deltaCx = CONTAINER.displacements.deltaCx;

    % STEP 5
    kCx = stiffnesskCx2DOF(Cx,FCx);
    kAy = stiffnesskAy2DOF(Ay,FAy);
    % END STEP 5

    % STEP 6
    % ACTUATION STIFFNESS
    [FCx_ep ep] = min(abs(FCx(LOADstep,:))); % force value closest to zero
    kCx_ep = kCx(N-1,ep); % determine stiffness near equilibrium point
    % PRELAOD STIFFNESS
    [deltaCx_ic ic] = min(abs(deltaCx(1,:))); % determine actuation step most close to↙
initial configuration
    kAy_ic = kAy(2,ic); % determine stiffness of preloading near initial position↙
deltaCx
    % END STEP 6

    % STEP 7
    % determine current stiffnesses
    kCx = kCx(LOADstep,DOFstep);
    kAy = kAy(LOADstep,DOFstep);
    % END STEP 7

    CONTAINER.kCx_ep = kCx_ep;
    CONTAINER.ep = ep;
    CONTAINER.kAy_ic = kAy_ic;
    CONTAINER.ic = ic;
    CONTAINER.kCx = kCx;
    CONTAINER.kAy = kAy;


    if dispON == 1
        disp(['STIFFNESS VALUES: ACTUATION AND PRELOADING']);
        disp(['stiffnessCx_ep = ',num2str(kCx_ep*1e-3), ' [N/mm] ( ep = ',num2str(ep),'↙
and FCx_ep = ',num2str(FCx_ep),' [N] )']);
        disp(['stiffnessAy_ic = ',num2str(kAy_ic*1e-3),' [N/mm] ( ic = ',num2str(ic),'↙
and deltaCx_ic = ',num2str(deltaCx_ic*1e3),' [mm] )']);
        % ACTUAL STIFFNESSES
        disp(' ');
        disp('STIFFNESS VALUES: ACTUAL');

        disp(['kCx = ',num2str(kCx*1e-3),' [N/mm]']);
        disp(['kAy = ',num2str(kAy*1e-3),' [N/mm]']);
        disp(' ');
```

```
    end

end
```

```
function [S_kCx change_vector_kCx S_kAy change_vector_kAy CONTAINER] =↙
analyse_sensitivity(change,CONTAINER,dispON)

    % ANALYSIS: SENSITIVITIES
    % determine ranges of independend variables for sensitivity calculation

    L1_min = CONTAINER.sensitivity.L1_min;
    L1_max = CONTAINER.sensitivity.L1_max;
    L2_min = CONTAINER.sensitivity.L2_min;
    L2_max = CONTAINER.sensitivity.L2_max;
    Ayi_min = CONTAINER.sensitivity.Ayi_min;
    Ayi_max = CONTAINER.sensitivity.Ayi_max;
    Cxi_min = CONTAINER.sensitivity.Cxi_min;
    Cxi_max = CONTAINER.sensitivity.Cxi_max;
    rangeAy_min = CONTAINER.sensitivity.rangeAy_min;
    rangeAy_max = CONTAINER.sensitivity.rangeAy_max;
    kA_min = CONTAINER.sensitivity.kA_min;
    kA_max = CONTAINER.sensitivity.kA_max;
    kB_min = CONTAINER.sensitivity.kB_min;
    kB_max = CONTAINER.sensitivity.kB_max;
    kC_min = CONTAINER.sensitivity.kC_min;
    kC_max = CONTAINER.sensitivity.kC_max;

    range_matrix = [    L1_min L1_max;
                    L2_min L2_max;
                    Ayi_min Ayi_max;
                    Cxi_min Cxi_max;
                    rangeAy_min rangeAy_max;
                    kA_min kA_max;
                    kB_min kB_max;
                    kC_min kC_max  ];

    L1 = CONTAINER.L1;
    L2 = CONTAINER.L2;
    Ayi = CONTAINER.initialconfiguration(1,2);
    Cxi = CONTAINER.initialconfiguration(1,5);
    rangeAy = CONTAINER.rangeAy;
    kA = CONTAINER.stiffness(1,1);
    kB = CONTAINER.stiffness(1,2);
    kC = CONTAINER.stiffness(1,3);

    % STEP 10
    design_vector = [L1; L2; Ayi; Cxi; rangeAy; kA; kB; kC];
    % END STEP 10

    deltaCx = CONTAINER.displacements.deltaCx;
    ep = CONTAINER.ep;
    ic = CONTAINER.ic;
    N = CONTAINER.N;

    % STEP 11 and 12 - calculate sensitivity vectors
    [S_kCx change_vector_kCx] = sensitivitykCx(deltaCx,ep,N,range_matrix,design_vector,↙
change);
    % END STEP 11,12
```

```
    % STEP 11 and 13
    [S_kAy change_vector_kAy] = sensitivitykAy(deltaCx,ic,2,range_matrix,design_vector,↙
change);
    % END STEP 11,13

    CONTAINER.S_kCx = S_kCx;
    CONTAINER.change_vector_kCx = change_vector_kCx;
    CONTAINER.S_kAy = S_kAy;
    CONTAINER.change_vector_kAy = change_vector_kAy;

    if dispON == 1
        S_kCx_L1 = S_kCx(1,1);
        S_kCx_L2 = S_kCx(2,1);
        S_kCx_Ayi = S_kCx(3,1);
        S_kCx_Cxi = S_kCx(4,1);
        S_kCx_rangeAy = S_kCx(5,1);
        S_kCx_kA = S_kCx(6,1);
        S_kCx_kB = S_kCx(7,1);
        S_kCx_kC = S_kCx(8,1);
        disp(['SENSITIVITIES FOR kCx [(N/mm)/unit]']);
        disp(['S_kCx_L1      = ',num2str(S_kCx_L1*1e-6),'       delta_L1 = ',num2str↙
(change_vector_kCx(1)*1e3),' [mm]']);
        disp(['S_kCx_L2      = ',num2str(S_kCx_L2*1e-6),'       delta_L2 = ',num2str↙
(change_vector_kCx(2)*1e3),' [mm]']);
        disp(['S_kCx_Ayi     = ',num2str(S_kCx_Ayi*1e-6),'       delta_Ayi = ',num2str↙
(change_vector_kCx(3)*1e3),' [mm]']);
        disp(['S_kCx_Cxi     = ',num2str(S_kCx_Cxi*1e-6),'       delta_Cxi = ',num2str↙
(change_vector_kCx(4)*1e3),' [mm]']);
        disp(['S_kCx_rangeAy = ',num2str(S_kCx_rangeAy*1e-6),'       delta_rangeAy = ',↙
num2str(change_vector_kCx(5)*1e3),' [mm]']);
        disp(['S_kCx_kA      = ',num2str(S_kCx_kA*1e-6),'       delta_kA = ',num2str↙
(change_vector_kCx(6)*1e3),' [Nmm/rad]']);
        disp(['S_kCx_kB      = ',num2str(S_kCx_kB*1e-6),'       delta_kB = ',num2str↙
(change_vector_kCx(7)*1e3),' [Nmm/rad]']);
        disp(['S_kCx_kC      = ',num2str(S_kCx_kC*1e-6),'       delta_kC = ',num2str↙
(change_vector_kCx(8)*1e3),' [Nmm/rad]']);

        S_kAy_L1 = S_kAy(1,1);
        S_kAy_L2 = S_kAy(2,1);
        S_kAy_Ayi = S_kAy(3,1);
        S_kAy_Cxi = S_kAy(4,1);
        S_kAy_rangeAy = S_kAy(5,1);
        S_kAy_kA = S_kAy(6,1);
        S_kAy_kB = S_kAy(7,1);
        S_kAy_kC = S_kAy(8,1);
        disp(['SENSITIVITIES FOR kAy [(N/mm)/unit]']);
        disp(['S_kAy_L1      = ',num2str(S_kAy_L1*1e-6),'       delta_L1 = ',num2str↙
(change_vector_kAy(1)*1e3),' [mm]']);
        disp(['S_kAy_L2      = ',num2str(S_kAy_L2*1e-6),'       delta_L2 = ',num2str↙
(change_vector_kAy(2)*1e3),' [mm]']);
        disp(['S_kAy_Ayi     = ',num2str(S_kAy_Ayi*1e-6),'       delta_Ayi = ',num2str↙
(change_vector_kAy(3)*1e3),' [mm]']);
        disp(['S_kAy_Cxi     = ',num2str(S_kAy_Cxi*1e-6),'       delta_Cxi = ',num2str↙
(change_vector_kAy(4)*1e3),' [mm]']);
        disp(['S_kAy_rangeAy = ',num2str(S_kAy_rangeAy*1e-6),'       delta_rangeAy = ',↙
```

```
num2str(change_vector_kAy(5)*1e3),' [mm]']);
        disp(['S_kAy_kA      = ',num2str(S_kAy_kA*1e-6),'       delta_kA = ',num2str↙
(change_vector_kAy(6)*1e3),' [Nmm/rad]']);
        disp(['S_kAy_kB      = ',num2str(S_kAy_kB*1e-6),'       delta_kB = ',num2str↙
(change_vector_kAy(7)*1e3),' [Nmm/rad]']);
        disp(['S_kAy_kC      = ',num2str(S_kAy_kC*1e-6),'       delta_kC = ',num2str↙
(change_vector_kAy(8)*1e3),' [Nmm/rad]']);
    end
end
```

```
function kCx = stiffnesskCx2DOF(Cx,FCx)
    [rows cols] = size(FCx);
    % determine stepsize, having correct sign
    Cx_step = Cx(1,cols)-Cx(1,cols-1);
    % create NaN matrix to store stiffness values for kCx
    kCx = NaN(rows,cols);
    % calculate stiffness matrix
    for r = 1:rows
        for c = 2:cols-1
            kCx(r,c) = (FCx(r,c+1) - FCx(r,c-1))/2/Cx_step;
        end
    end
end
```

```
function kAy = stiffnesskAy2DOF(Ay,FAy)
    [rows cols] = size(FAy);
    % determine stepsize, having correct sign
    Ay_step = Ay(rows,1)-Ay(rows-1,1);
    % create NaN matrices to store stiffness values for kAy and kCx
    kAy = NaN(rows,cols);
    % calculate stiffness matrices
    for c = 1:cols
        for r = 2:rows-1
            kAy(r,c) = (FAy(r+1,c) - FAy(r-1,c))/2/Ay_step;
        end
    end
end
```

```
function [S_kCx change_vector] = sensitivitykCx(deltaCx,DOFstep,LOADstep,range_matrix,↙
design_vector,change)
    label_array = { 'L1'; 'L2'; 'Ayi'; 'Cxi'; 'rangeAy'; 'kA'; 'kB'; 'kC' };
    N = length(deltaCx);

    % STEP 11
    change_vector = change*(range_matrix(:,2) - range_matrix(:,1));
    % END STEP 11


    % CHECK INPUT DATA
    % check ranges, all positive (minimum is lower than maximum ?)
    k = 1;
    while k <= length(change_vector)
        if change_vector(k) > 0
            k = k+1;
        else
            msg = strcat(label_array{k},' has negative or zero range')
            error('error');
        end
    end
    % check ranges, is design_vector value inside range ?
    n = 1;
    while n <= length(change_vector)
        if design_vector(n) >= range_matrix(n,1) && design_vector(n) <= range_matrix(n,↙
2)
            n = n+1;
        else
            msg = strcat(label_array{n},' out of range')
            error('error');
        end
    end

    % COMPUTE SENSITIVITIES
    % create DOF range / initialize variables
    ND = length(design_vector); % number of design variables
    deltaCx = deltaCx(1,DOFstep-1:DOFstep+1);
    S_kCx = NaN(ND,1); % empty vector for sensitivity values
    % compute for each design variable seperately its effect on the
    % stiffness matrix.

    % STEP 12
    for n=1:ND
        CV = zeros(ND,1);
        CV(n) = change_vector(n)/2;
        DV1 = design_vector - CV;
        DV2 = design_vector + CV;
        %{ 'L1'; 'L2'; 'Ayi'; 'Cxi'; 'rangeAy'; 'kA'; 'kB'; 'kC' };
        L1_1 = DV1(1); L1_2 = DV2(1);
        L2_1 = DV1(2); L2_2 = DV2(2);
        Ayi_1 = DV1(3); Ayi_2 = DV2(3);
        Cxi_1 = DV1(4); Cxi_2 = DV2(4);
        rangeAy_1 = DV1(5); rangeAy_2 = DV2(5);
        kA_1 = DV1(6); kA_2 = DV2(6);
        kB_1 = DV1(7); kB_2 = DV2(7);
```

```
        kC_1 = DV1(8); kC_2 = DV2(8);
        % solve kinematics: preload angles
        [alphap1_1 alphap2_1 betap_1] = kinematics2DOF(L1_1,L2_1,Ayi_1,0,Cxi_1,0);
        [alphap1_2 alphap2_2 betap_2] = kinematics2DOF(L1_2,L2_2,Ayi_2,0,Cxi_2,0);
        % solve kinematics: for actual DOFstep range
        deltaAy_1 = linspace(0,rangeAy_1,N)'; % create preload range
        [deltaCx deltaAy_1] = meshgrid(deltaCx,deltaAy_1(LOADstep));
        [alpha1_1 alpha2_1 beta_1] = kinematics2DOF(L1_1,L2_1,Ayi_1,deltaAy_1,Cxi_1,↙
deltaCx);
        Cx_1 = Cxi_1 + deltaCx;
        deltaAy_2 = linspace(0,rangeAy_2,N)';
        [deltaCx deltaAy_2] = meshgrid(deltaCx,deltaAy_2(LOADstep));
        [alpha1_2 alpha2_2 beta_2] = kinematics2DOF(L1_2,L2_2,Ayi_2,deltaAy_2,Cxi_2,↙
deltaCx);
        Cx_2 = Cxi_2 + deltaCx;
        % solve statics
        [~, ~, ~, ~, ~, ~, ~, FCx_1, ~,] = statics2DOF(alpha1_1,alpha2_1,beta_1,↙
alphap1_1,alphap2_1,betap_1,kA_1,kB_1,kC_1,L1_1,L2_1);
        [~, ~, ~, ~, ~, ~, ~, FCx_2, ~,] = statics2DOF(alpha1_2,alpha2_2,beta_2,↙
alphap1_2,alphap2_2,betap_2,kA_2,kB_2,kC_2,L1_2,L2_2);
        % determine stiffness
        kCx_1 = stiffnesskCx2DOF(Cx_1,FCx_1);
        kCx_2 = stiffnesskCx2DOF(Cx_2,FCx_2);
        % determine sensitivities
        S_kCx(n,1) = (kCx_2(2) - kCx_1(2))/change_vector(n);
    end
    % END STEP 12
end
```

```
function [S_kAy change_vector] = sensitivitykAy(deltaCx,DOFstep,LOADstep,range_matrix,↙
design_vector,change)
    label_array = { 'L1'; 'L2'; 'Ayi'; 'Cxi'; 'rangeAy'; 'kA'; 'kB'; 'kC' };
    N = length(deltaCx);

    % STEP 11
    change_vector = change*(range_matrix(:,2) - range_matrix(:,1));
    % END STEP 11

    % CHECK INPUT DATA
    % check ranges, all positive (minimum is lower than maximum ?)
    k = 1;
    while k <= length(change_vector)
        if change_vector(k) > 0
            k = k+1;
        else
            msg = strcat(label_array{k},' has negative or zero range')
            error('error');
        end
    end
    % check ranges, is design_vector value inside range ?
    n = 1;
    while n <= length(change_vector)
        if design_vector(n) >= range_matrix(n,1) && design_vector(n) <= range_matrix(n,↙
2)
            n = n+1;
        else
            msg = strcat(label_array{n},' out of range')
            error('error');
        end
    end

    % COMPUTE SENSITIVITIES
    % compute for each design variable seperately its effect on the
    % stiffness matrices.
    ND = length(design_vector); % number of design variables
    deltaCx_step = deltaCx(DOFstep);
    S_kAy = NaN(ND,1);

    % STEP 13
    for n=1:ND
        CV = zeros(ND,1);
        CV(n) = change_vector(n)/2;
        DV1 = design_vector - CV;
        DV2 = design_vector + CV;
        %{ 'L1'; 'L2'; 'Ayi'; 'Cxi'; 'rangeAy'; 'kA'; 'kB'; 'kC' };
        L1_1 = DV1(1); L1_2 = DV2(1);
        L2_1 = DV1(2); L2_2 = DV2(2);
        Ayi_1 = DV1(3); Ayi_2 = DV2(3);
        Cxi_1 = DV1(4); Cxi_2 = DV2(4);
        rangeAy_1 = DV1(5); rangeAy_2 = DV2(5);
        kA_1 = DV1(6); kA_2 = DV2(6);
        kB_1 = DV1(7); kB_2 = DV2(7);
        kC_1 = DV1(8); kC_2 = DV2(8);
        % solve kinematics: preload angles
```

```
        [alphap1_1 alphap2_1 betap_1] = kinematics2DOF(L1_1,L2_1,Ayi_1,0,Cxi_1,0);
        [alphap1_2 alphap2_2 betap_2] = kinematics2DOF(L1_2,L2_2,Ayi_2,0,Cxi_2,0);
        % solve kinematics: range of motion
        deltaAy_1 = linspace(0,rangeAy_1,N)';
        [deltaCx deltaAy_1] = meshgrid(deltaCx_step,deltaAy_1(LOADstep-1:LOADstep+1));
        [alpha1_1 alpha2_1 beta_1] = kinematics2DOF(L1_1,L2_1,Ayi_1,deltaAy_1,Cxi_1,↙
deltaCx);
        Ay_1 = Ayi_1 + deltaAy_1;
        deltaAy_2 = linspace(0,rangeAy_2,N)';
        [deltaCx, deltaAy_2] = meshgrid(deltaCx_step,deltaAy_2(LOADstep-1:LOADstep+1));
        [alpha1_2 alpha2_2 beta_2] = kinematics2DOF(L1_2,L2_2,Ayi_2,deltaAy_2,Cxi_2,↙
deltaCx);
        Ay_2 = Ayi_2 + deltaAy_2;
        % solve statics
        [~, ~, ~, ~, FAy_1, ~, ~, ~, ~] = statics2DOF(alpha1_1,alpha2_1,beta_1,↙
alphap1_1,alphap2_1,betap_1,kA_1,kB_1,kC_1,L1_1,L2_1);
        [~, ~, ~, ~, FAy_2, ~, ~, ~, ~] = statics2DOF(alpha1_2,alpha2_2,beta_2,↙
alphap1_2,alphap2_2,betap_2,kA_2,kB_2,kC_2,L1_2,L2_2);
        % determine stiffness
        kAy_1 = stiffnesskAy2DOF(Ay_1,FAy_1);
        kAy_2 = stiffnesskAy2DOF(Ay_2,FAy_2);
        % determine sensitivities
        S_kAy(n,1) = (kAy_2(2) - kAy_1(2))/change_vector(n);
    end
    % END STEP 13
end
```

Appendix F

Behavioral study of crank slider mechanism

This appendix contains a detailed report of change in behavior due to changes in model parameters. The behaviors are calculated using the numerical scheme presented in appendix 3 (ref). After gaining some knowledge and experience with the model through the GUI the next typical behavioral changes have been observed. All discussed behavioral changes are with respect to the initial configuration in which link 1 is horizontal and link 2 vertical, and thus perpendicular to each other. Some orthogonal parameter changes are considered and some non orthogonal.

The initial configuration is given by the nominal values in the next table (ref).

parameter	value
ΔA_y [m]	-0.001
A_{yi} [m]	0.015
C_{xi} [m]	0.020
L_1 [m]	0.020
L_2 [m]	0.015
k_A [Nm/rad]	100
k_B [Nm/rad]	1
k_C [Nm/rad]	1

In all cases below those values are true unless specified otherwise. In each situation the corresponding configuration is shown. The continuous lines show the current configuration of the mechanism in either one of the two extreme positions, to illustrate the range of motion. The dotted lines show the initial configuration corresponding to the stress free state. Also the force displacement graphs are plotted. The line having the circles belongs to the nominal value of the corresponding parameter, the line having the squares belongs to the final value. Dotted lines in between are calculations for intermediate values.

orthogonal changes

Orthogonal changes are those changes in which only one model parameter is changed, all others are left unchanged.

preloading $\Delta Ay = 0$

Increasing the preload displacement downwards clearly tunes the stiffness value from positive to negative. The graph of the stress free system (the line having circles) intersects the point <0,0>, the equilibrium. When preloading is applied (either positive or negative) a small shift occurs to the left (the line having squares). For all other cases described below this line having squares is the nominal situation.

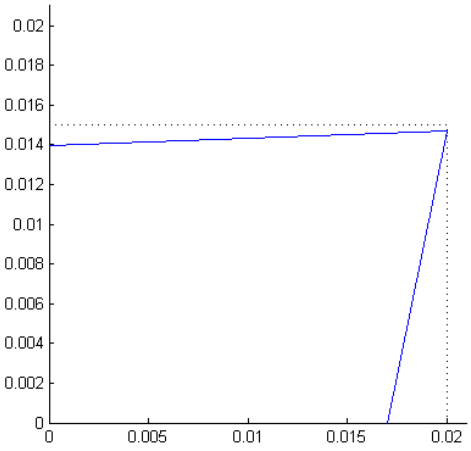

$\Delta Ay = -0.001$

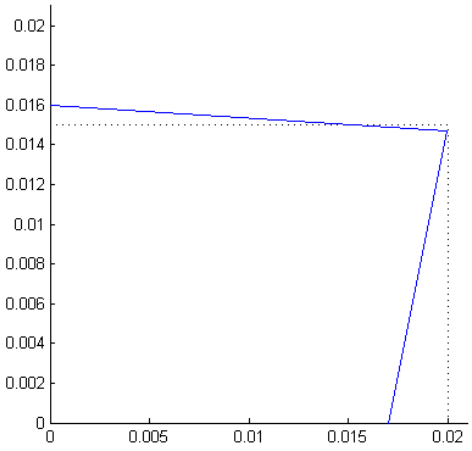

$\Delta Ay = 0.001$

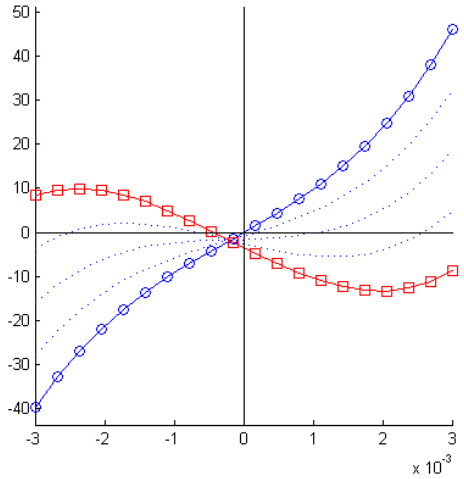

$\Delta Ay = -0.001$

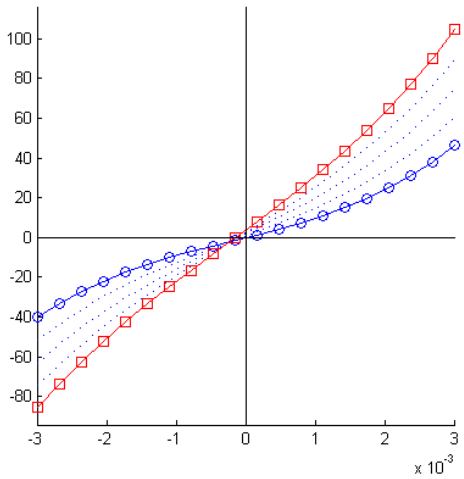

$\Delta Ay = 0.001$

rotate link 1: $A_{yi} = 0.015$

The graph does not rotate. It shifts in both cases in roughly equal manner to the lower left corner, moving perpendicular to the slope. Thereby shifting the equilibrium further away from the origin.

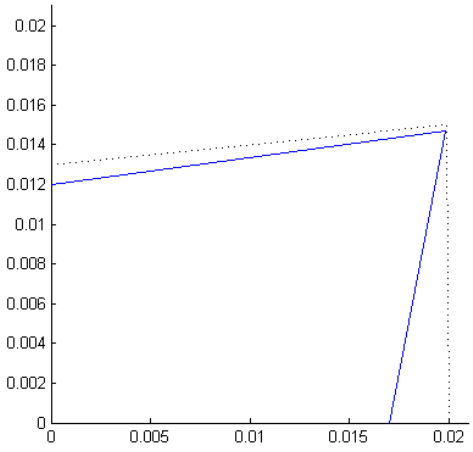

$A_{yi} = 0.013$

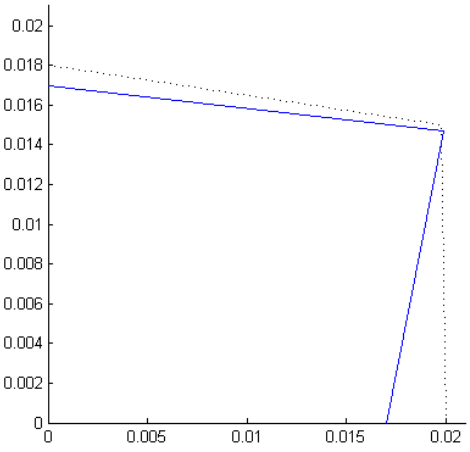

$A_{yi} = 0.018$

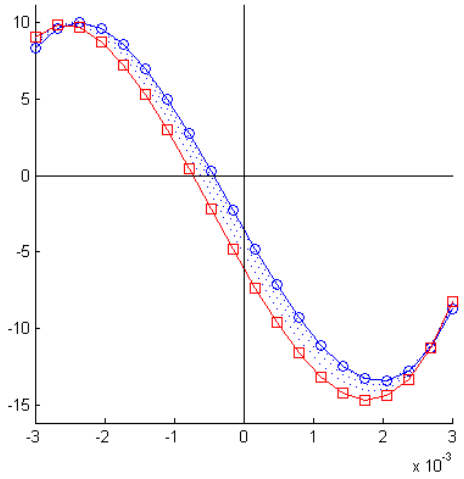

$A_{yi} = 0.013$

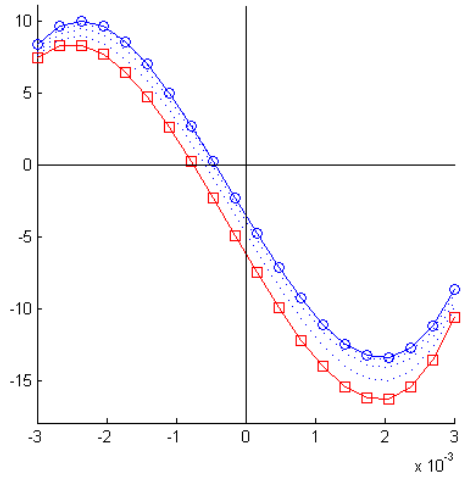

$A_{yi} = 0.018$

rotate link 2: $C_{xi} = 0.020$

A large shift of the graph perpendicular to the slope without rotation. The equilibrium can be shifted towards or away from the origin. This effect is much stronger than rotating link 1.

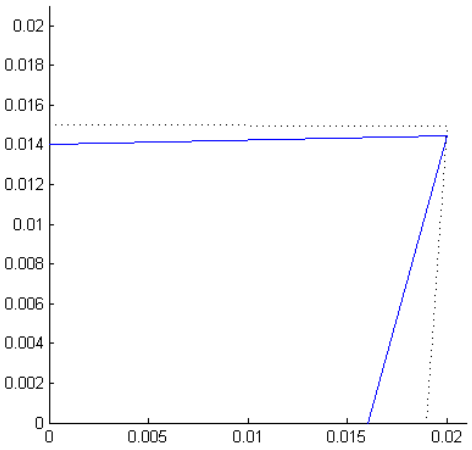

C_{xi} = 0.019

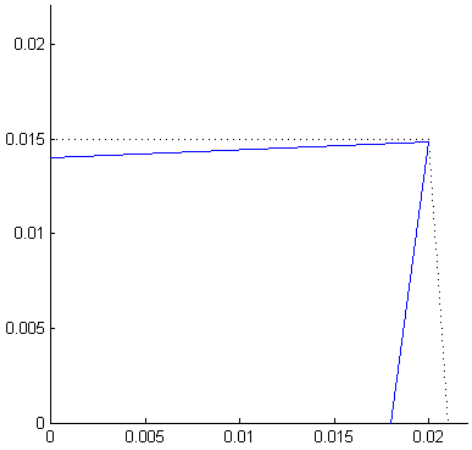

C_{xi} = 0.021

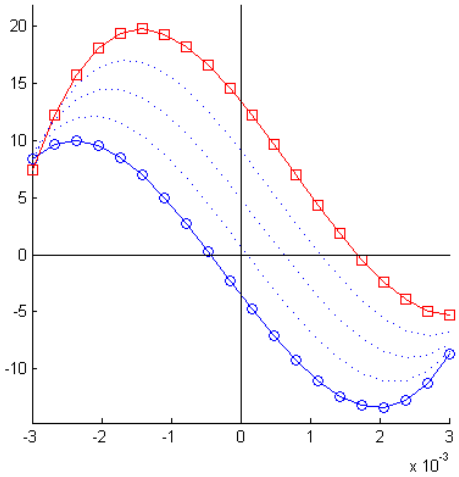

C_{xi} = 0.019

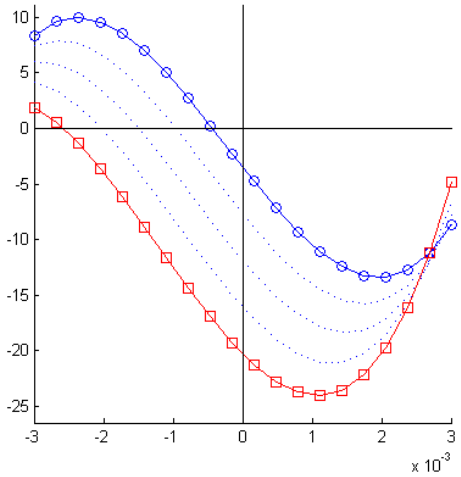

C_{xi} = 0.021

change torsion stiffness A: k_A = 100

A clear effect on the slope of the graph, it tends to rotate. The configuration remains the same of course. The rotation point of the graph lies close to y-coordinate axis and below the x-coordinate axis. Causing a shift of the equilibrium. Magnifying 2 times changes the slope more then a division by 2. In creasing the value makes the equilibrium move to the origin.

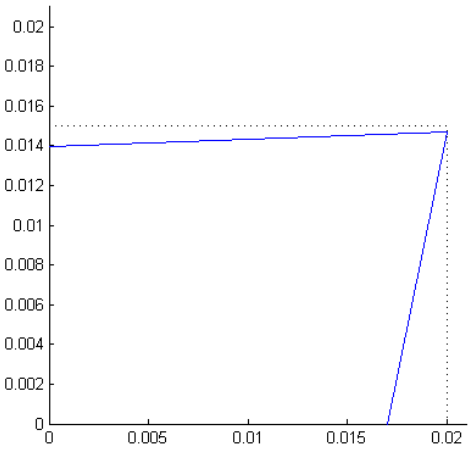

k_A = 50

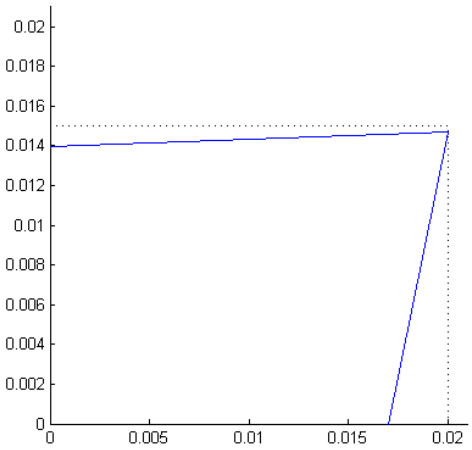

k_A = 200

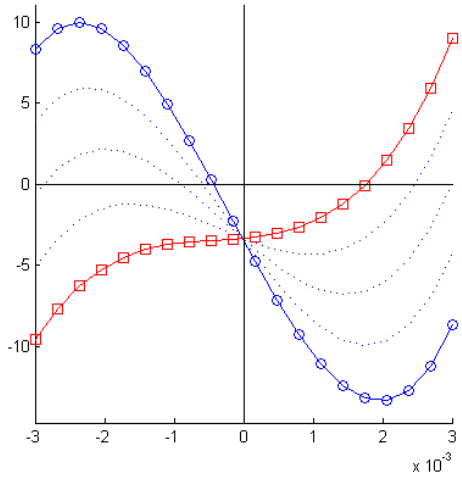

$k_A = 50$

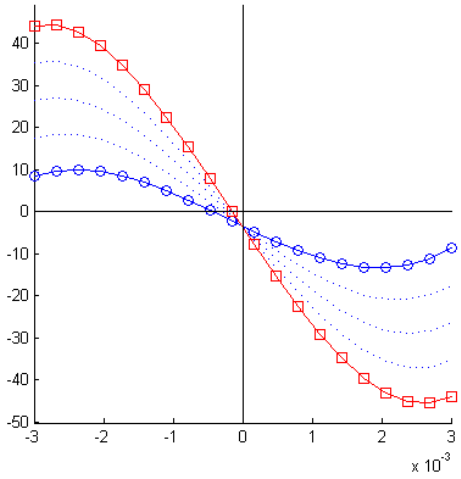

$k_A = 200$

change torsion stiffness B: $k_B = 1$

The slope is effected. No shift of the graph. The rotation point lies in the lower left quadrant of the coordinate axis. Multiplication by 5 has roughly the same effect (but opposes in sign) on the slope than division by 5. Equilibrium shifts to the origin when value is lowered.

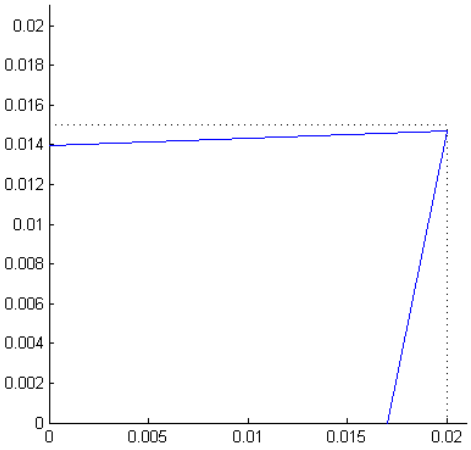

$k_B = 0.2$

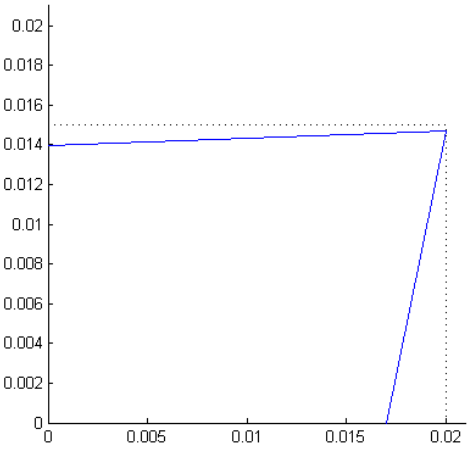

$k_B = 5$

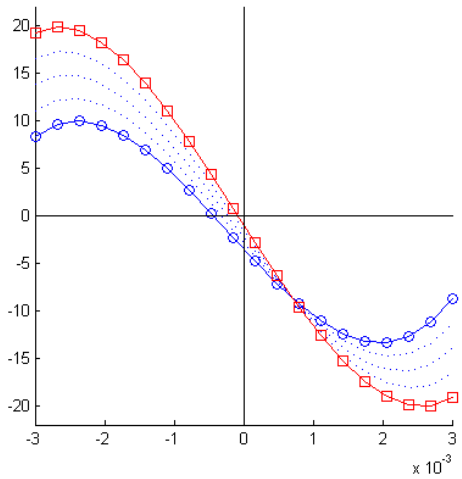

$k_B = 0.2$

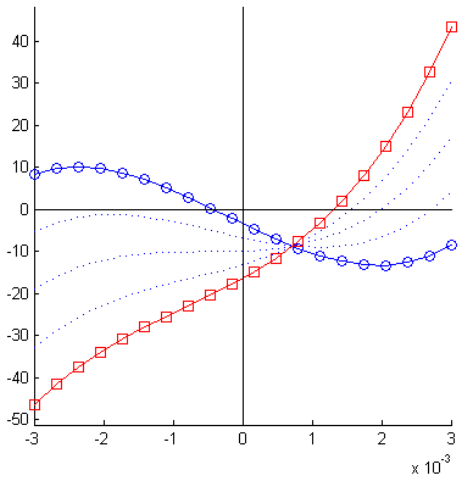

$k_B = 5$

change torsion stiffness C: $k_C = 1$

Same effect as for k_B with the difference that in this case the rotation point of the graph lies on the y-coordinate axis en below the x-coordinate axis. Decrease of value shifts the equilibrium closer to the origin.

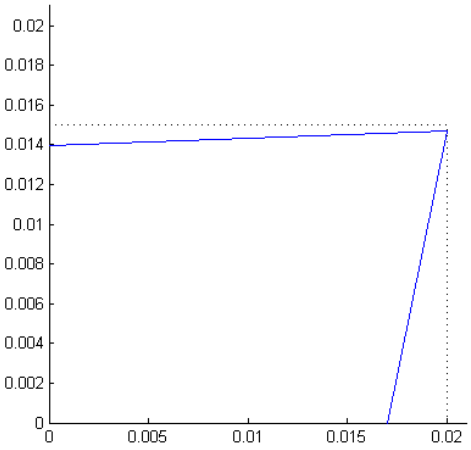

k_C = 0.2

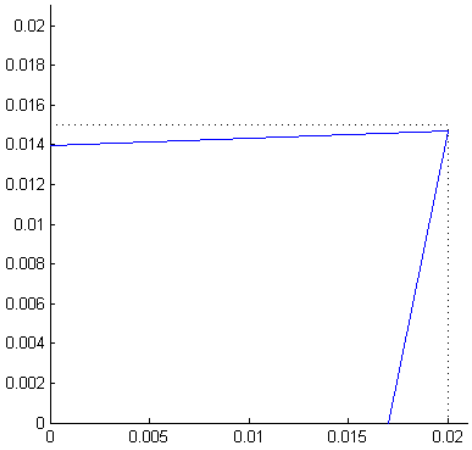

k_C = 5

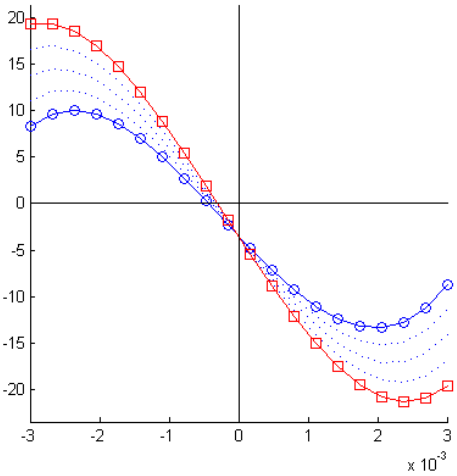

k_C = 0.2

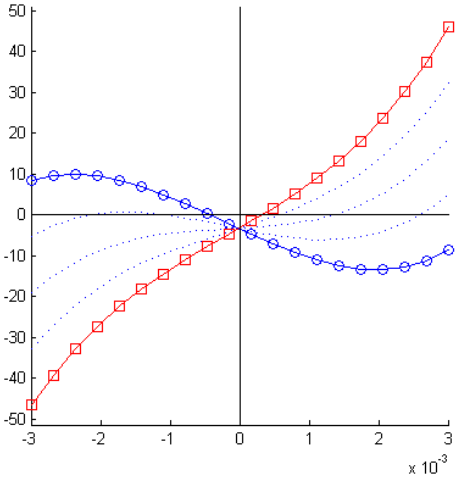

k_C = 5

non orthogonal changes

Non orthogonal changes regard those changes in which multiple parameters are changed sequentially.

change link length 1: $L_1 = C_{xi} = 0.020$

The length of link 1 is changed while both links are kept perpendicular. No shift of the graph, but clear effect on the slope. The rotation point lies in the lower left quadrant of the coordinate axis. The shorter link length 2 is the higher the negative stiffness.

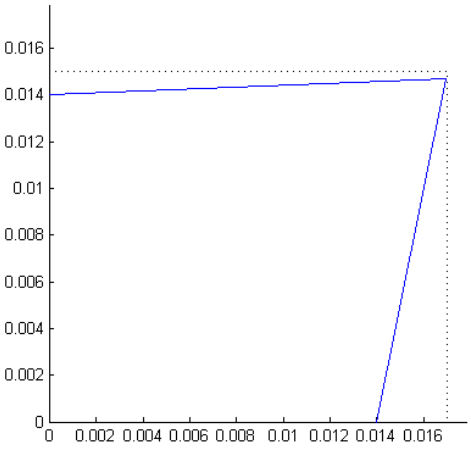

$L_1 = C_{xi} = 0.017$

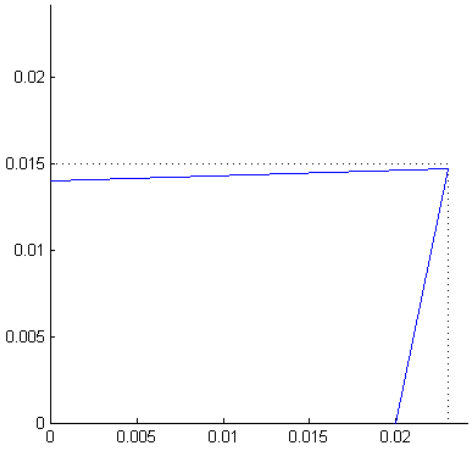

$L_1 = C_{xi} = 0.023$

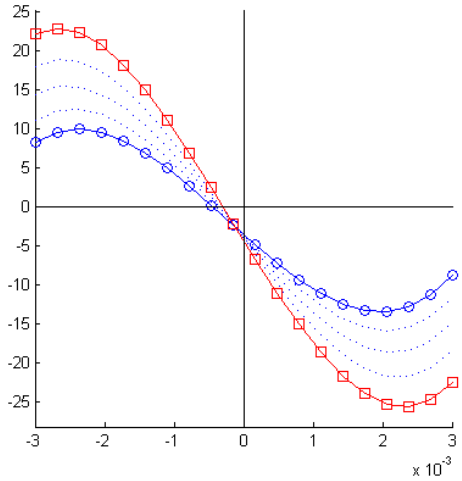

$L_1 = C_{xi} = 0.017$

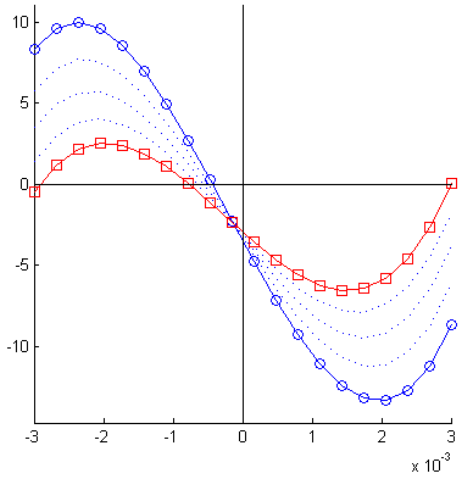

$L_1 = C_{xi} = 0.023$

change link length 2: $L_2 = A_{yi} = 0.015$

Link length 2 is changed while both links keep perpendicular. No clear shift or rotation of the graph occurs. It seems that it is scaled up in the direction roughly equal to the tangent of the curve around equilibrium. This effect increases the (linear) range of motion of the system. Although it also transforms the shape of the behavior a bit.

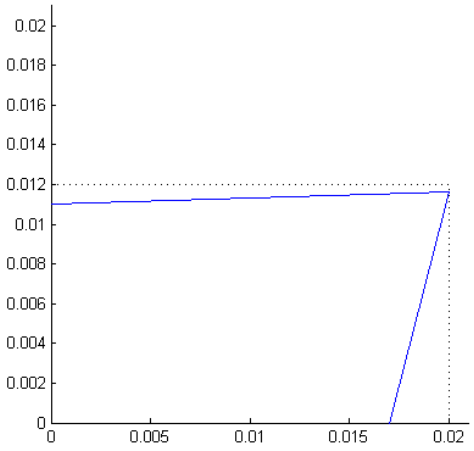

$L_2 = A_{yi} = 0.012$

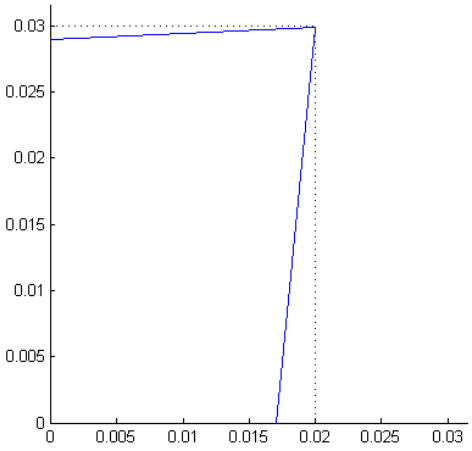

$L_2 = A_{yi} = 0.030$

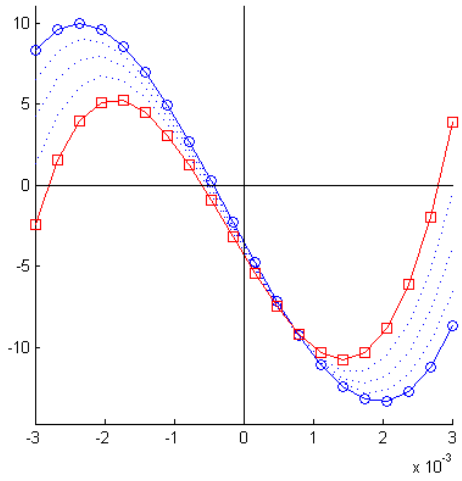

$L_2 = A_{yi} = 0.012$

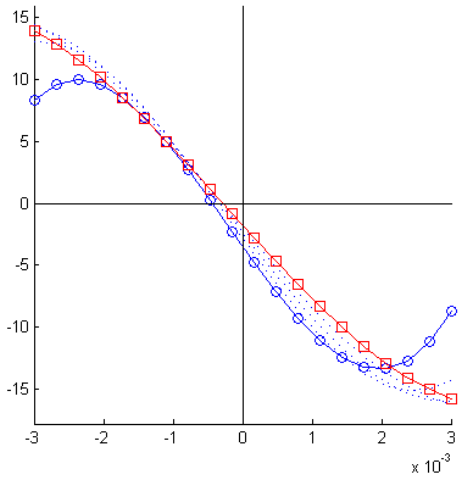

$L_2 = A_{yi} = 0.030$

change ratio torsion stiffnesses at A and B,C: $k_A = 100$, $k_B = k_C = 1$

A combined effect of increasing stiffness A and decreasing stiffness B and C sequentially. Of course negative stiffness increases. There is no shift of the graph, its rotation point lies in the lower right quadrant of the coordinate axis.

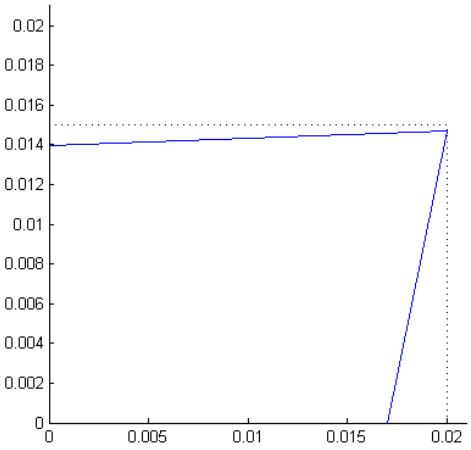

$k_A = 100$, $k_B = k_C = 1$

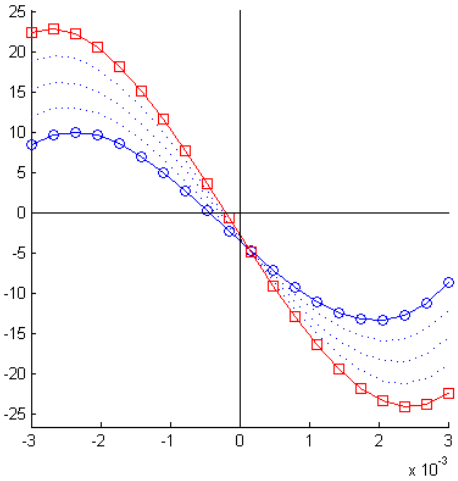

$k_A = 120$, $k_B = k_C = 0.75$

Appendix G

Effects of mirroring

This appendix explains the main effects of mirroring as applied in the design method described in the paper. The mechanism is mirrored over axis y-y' and x-x' as illustrated below (ref).

mirroring over y-y'

The crank slider model predicts an offset of the equilibrium from the origin when the mechanism is preloaded. By mirroring the mechanism over the y-y' axis any offset will vanish. Consider situation 1, a mechanism having offset due to any reason. The mirrored version is shown in situation 2, it has an equal graph but then rotated 180 degrees around the origin. When both mechanism are connected situation 3 will result with a perfect rotational symmetric (rotated 180 degrees with respect to the origin) force displacement graph.

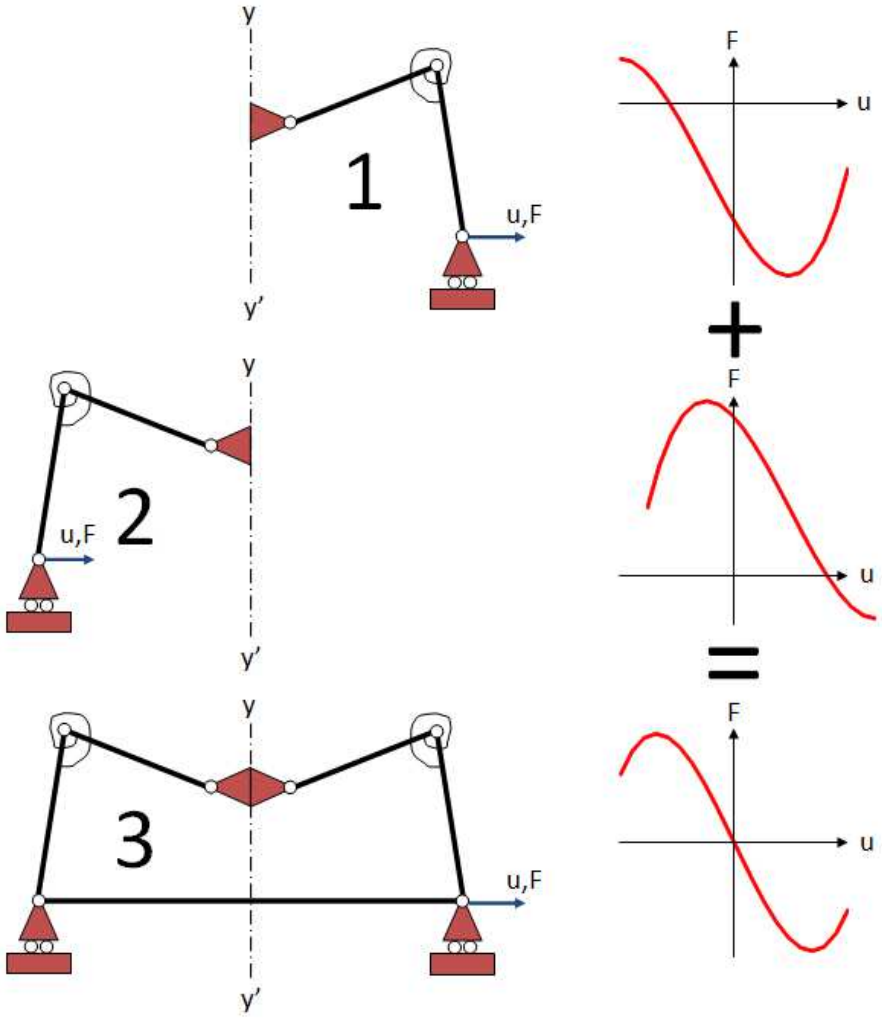

mirroring over x-x'

Mirroring over the horizontal axis is equal to multiplying the graph by 2, as can be seen in situation 4 in the illustration below (ref). The dotted line is the non mirrored version and the continuous line belongs to the mirrored version. So negative stiffness is raised two times.

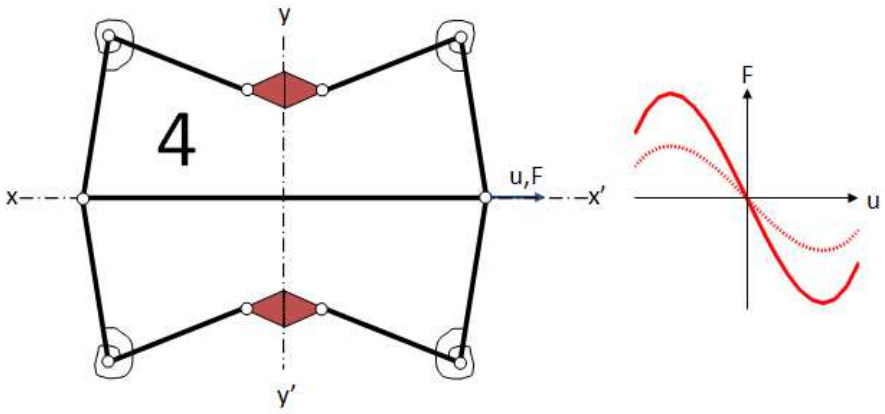

link naar bron data

Appendix H

Linear pre-buckling analysis

It can not be excluded on before hand that low stiffness occurs in some other direction then intended due to the chosen combination of geometry and loading. To investigate this a linear buckling analysis is performed. The (Ansys) FEM code used can be found at the end of this section. The resulting buckling modes can be seen as modes of deformation that occur when the corresponding critical load is reached. So in this case the lowest buckling mode should be similar to the deformation producing the range of motion for which the geometry was designed to do given the preload force. Additionally the buckling load should be in the same range of magnitude as the preload force, but they can not be equal. Since the buckling load is only valid for the transition point of the elastic mechanism from stable to unstable behavior. Exactly at that transition point the stiffness of the structure is zero for infinitesimal motions corresponding with the buckling mode. The preload force is supposed to be larger than the buckling load because it must be beyond the transition point in order to generate negative stiffness in stead of zero stiffness.

The following buckling analysis is performed using Ansys. See illustration below (ref). The full geometry is used and constraint to the fixed world at point 1. At point 2 a unit force in downward vertical direction is applied. The linear buckling problem is solved. Meaning that the linear stiffness matrix of this structure is summed together with a stress stiffening matrix. The stress stiffening matrix depends on the stress distribution of the linear solution to the unitary load case. This stress distribution is scaled by a load factor and thus the load factor scales the stress stiffening matrix. In case of buckling the stress stiffening matrix is scaled to a point where it makes the linear stiffness matrix singular. Stiffness of the elastic structure becomes zero. This is the eigenvalue problem, where the eigenvalues are the critical load factors and the eigenvectors correspond with the deformation mode.

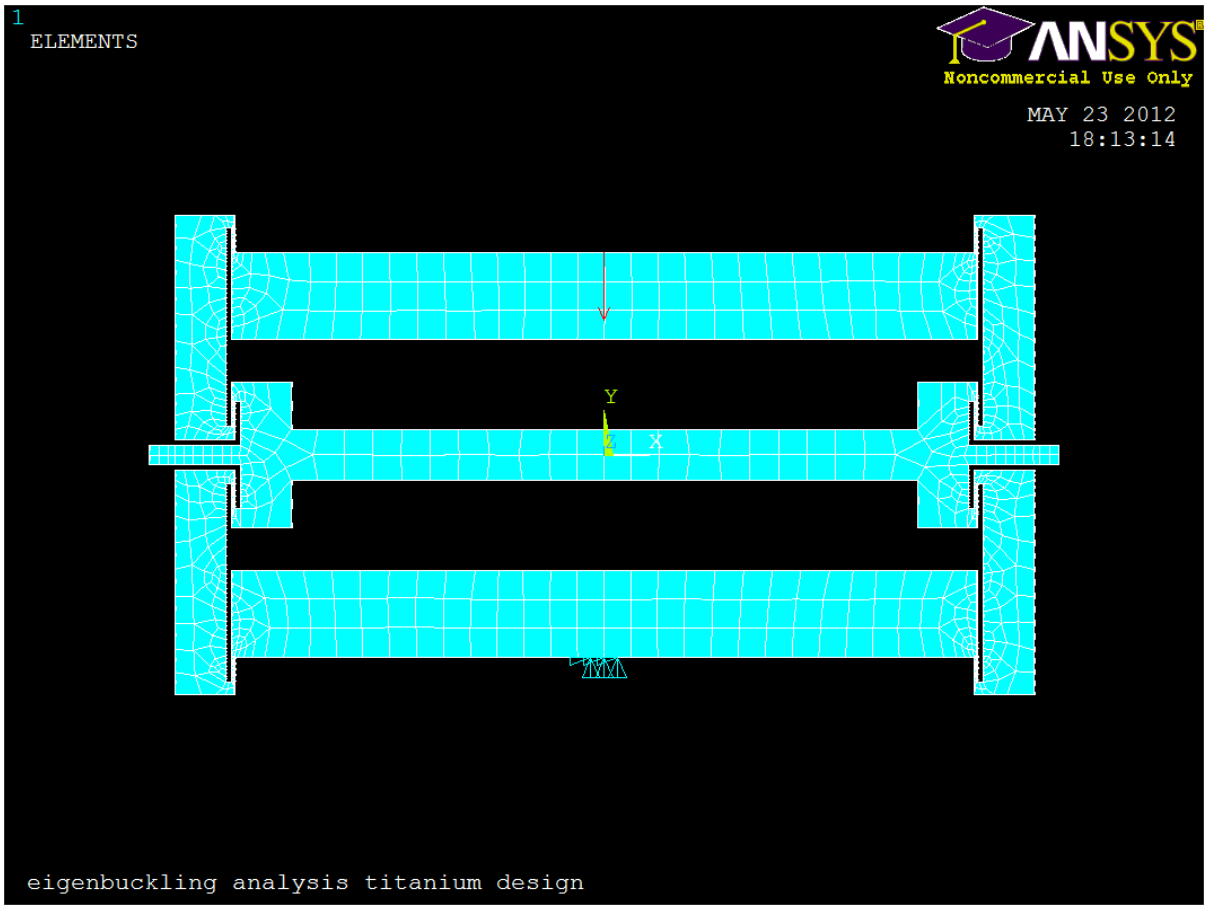

The maximum number of possible buckling modes is equal to the number of degrees of freedom in the finite element model. Since only the buckling modes in the range of the preload force are of interest only the first 4 modes are considered. The first mode at 57.005 [N] is all ready differing from the desired mode of motion. This shows that the design needs extra contraints to prevent this motion, those contraints are applied in the

manufactured prototype. See the straight line guidance for the preload displacements. The second mode is nearly occuring at equal critical load 57.128 [N]. This mode corresponds with the desired mode of motion. Buckling modes 3 and 4 are occurring at much higher critical loads, ranging from 23 to 48 [kN]. While prelaoding it is expected that the load stays below 800 to 1000 [N]. So only first to buckling modes are of interest. Eventhough the critical load of mode 4 is about 1000 times higher then the lowest mode, it may be of interest. Mode 4 shows rotational motion of the shutle. Suppose one is capable of lowering the critical load for this mode and constraining the other lower modes. Then a design for a fully compliant rotational balanced joint might evolve. Lowering the critical load for mode 4 might be achieved by shortening the horizontal distance between the elastic hinges. Also the geometry might be produced such that it's rest configuration has a deviation towards mode 4.

MODE 1: 57.005 [N]

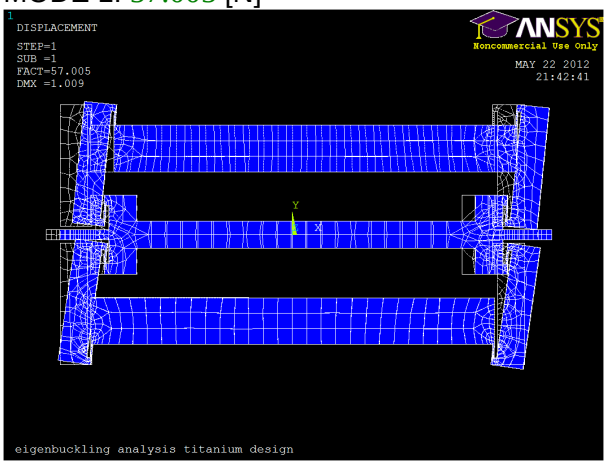

MODE 2: 57.128 [N]

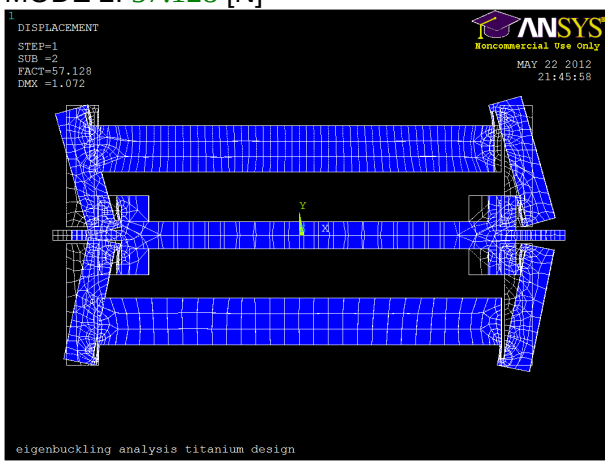

MODE 3: 23934 [N]

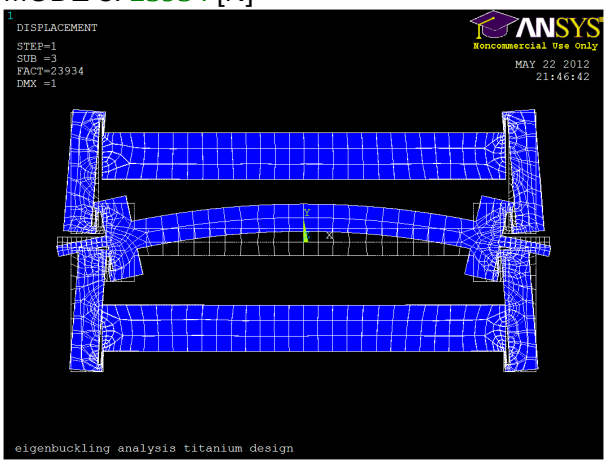

MODE 4: 48520 [N]

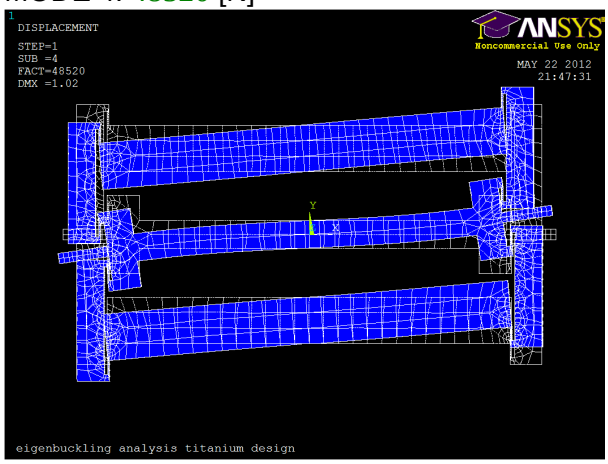

Ansys FEM code for linear buckling analysis

```
FINISH
/CLEAR
/ESHAPE,1

/FILENAME,leafspringdesign,0
/TITLE, eigenbuckling analysis titanium design
/UNITS, SI

!*************************************************************
! DEFINE PARAMETERS
!*************************************************************
b = 6e-3
E = 113.9e9
v = 0.3
```

```
!*****************************************************************
! DEFINE GEOMETRY AND ELEMENT MESH
!*****************************************************************
/PREP7

!KEYPOINTS
K, 1 , 0 , 0
K, 2 , 0 , 0.002
K, 3 , 0.0248 , 0.002
K, 4 , 0.0248 , 0.00575
K, 5 , 0.0295 , 0.00575
K, 6 , 0.0295 , 0.00225
K, 7 , 0.03 , 0.00225
K, 8 , 0.03 , 0.018
K, 9 , 0.0295 , 0.018
K, 10 , 0.0295 , 0.0092
K, 11 , 0 , 0.0092
K, 12 , 0 , 0.016
K, 13 , 0.0293 , 0.016
K, 14 , 0.0293 , 0.019
K, 15 , 0.034 , 0.019
K, 16 , 0.034 , 0.00125
K, 17 , 0.0293 , 0.00125
K, 18 , 0.0293 , 0.00425
K, 19 , 0.0288 , 0.00425
K, 20 , 0.0288 , 0.00075
K, 21 , 0.036 , 0.00075
K, 22 , 0.036 , 0

!LINES
LSTR, 2 , 3
LSTR, 3 , 4
LSTR, 4 , 5
LSTR, 5 , 6
LSTR, 6 , 7
LSTR, 7 , 8
LSTR, 8 , 9
LSTR, 9 , 10
LSTR, 10 , 11
LSTR, 12 , 13
LSTR, 13 , 14
LSTR, 14 , 15
LSTR, 15 , 16
LSTR, 16 , 17
LSTR, 17 , 18
LSTR, 18 , 19
LSTR, 19 , 20
LSTR, 20 , 21
LSTR, 21 , 22


! Mirror the second half of the grasper
LSYM,Y,ALL,,,,1,0
LSYM,x,ALL,,,,1,0

! Glue the two parts together
LGLUE,ALL

! Make an area
```

```
AL,ALL


/PREP7
! DEFINE ELEMENT
ET,1,PLANE82
KEYOPT,1,3,3
R,1,b

! MATERIAL PROPERTIES
MP,EX,1,E
MP,PRXY,1,v

! mesh Area
TYPE,1
REAL,1

!mesh size
SMRTSIZE,4
AMESH,1

!*****************************************************************
! SET BOUNDARY CONDITIONS STATIC SOLUTION
!*****************************************************************

/SOLU


! fixed DOF
D,1232,ALL
D,32,ALL
D,534,ALL

! unitary load case
F,11,FY,-1


!*****************************************************************
! SOLVE PROBLEM
!*****************************************************************

! STATIC ANALYSIS
ANTYPE,STATIC,NEW
PSTRES,ON
SOLVE
FINISH


! EIGENBUCKLING ANALYSIS
/SOLU
ANTYPE,1,NEW
BUCOPT,LANB,10,0,0
SOLVE
FINISH
! EXPANDING BUCKLING MODES
/SOLU
EXPASS,1
MXPAND,10,0,0,0,0.001,
SOLVE
```

FINISH

link to source info buckling analysis

Appendix I

Non linear FEM analysis of strain energy

Since the design was based on the behavior exposed by the crank slider model one expects that there is an equivalince in working principle for the monolithic version and the rigid body linkage version, as explained in the following. To investigate the monolithic design the elastic energy is determined using Ansys (the used FEM code can be found at the end of this section).
For the crank slider mechanism: the elastic energy is stored in the mechanism is equal to the work done by the prelaod force over the preload displacement. As long as point C is fixed in translation, the work done is mainly stored in the torsion spring at hinge A and a little bit of energy is stored in the much softer torsion springs in point B and C. This stored elastic energy can be released by moving point C in horizontal direction. The torsion spring in point A relaxes, the springs in B and C wind up, but because of their low stiffness they consume not to much energy and leave a remainder of energy to be released via negative work done by the reaction force at point C.

For the monolithic mechanism: the same story holds, but in this case the preload beam corresponds to the torsion spring in hinge A and the compliant hinges correspond to the torsion springs in hinge B and C. The energy release happens at the same point and same direction.

Since the monolithic design is fully elastic, the elastic energy provided by the work done by the preload force does not necessarily have to be stored in the preload beam only. Other parts of the structure might store a significant part of the elastic energy too. For example the thin elastic hinges under tension, or the stiff links under compression. To check the share of each functional part of the elastic mechanism the total strain energy per part is calculated as is illustrated in the figure below.

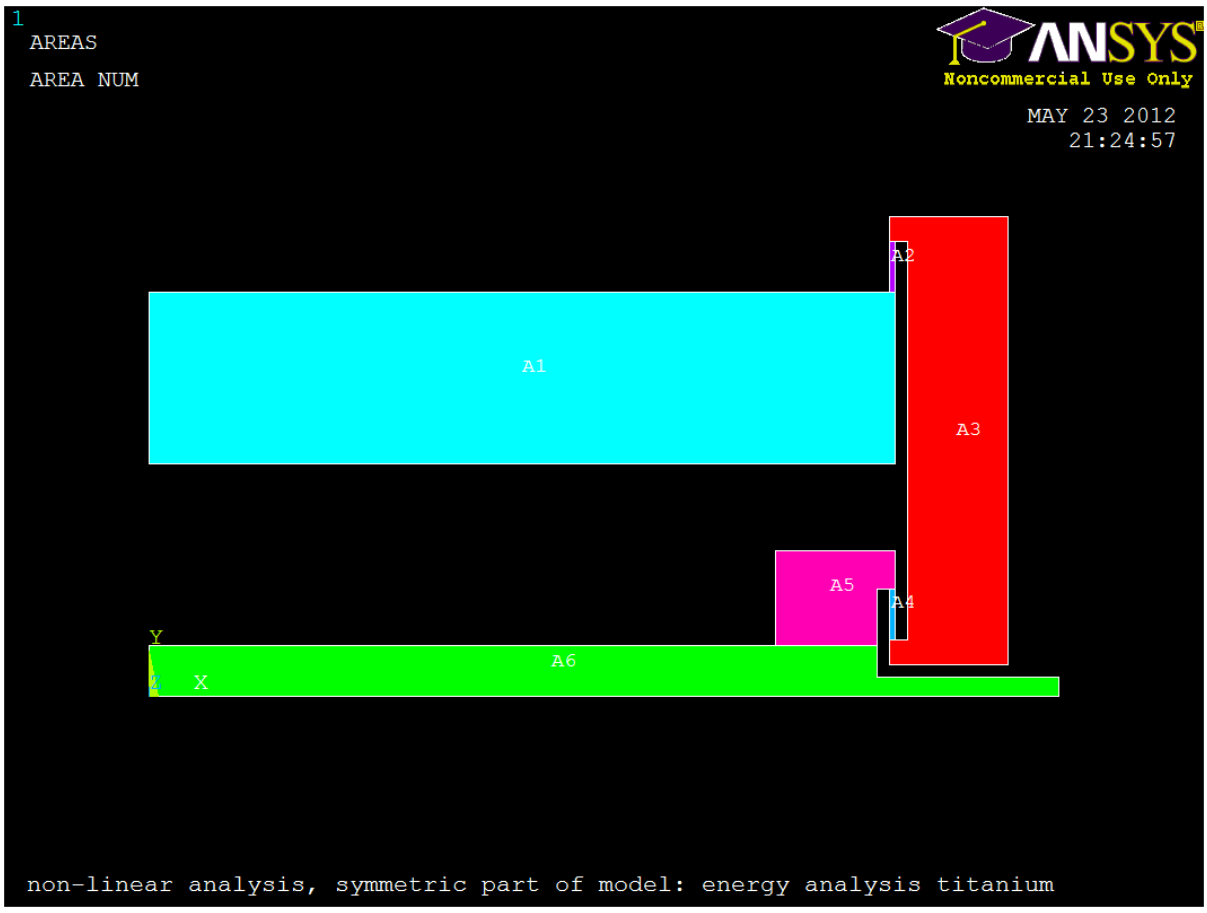

comment

The areas are devided based on functionality. By functionality is meant that the part of the structure should transmit or store elastic energy. The storing part is covered by area 1. Transmitting without any deformation is covered by areas 3,5 and 6. And transmitting energy while allowing for bending deformations is covered by

area 2 and 4. The loading and constraining is exactly the same as in the non linear force deflection analysis. In the table below the results are presented.

	strainenergy [mJ]					
	preload		**actuation**		**delta (a - p)**	
	[mJ]	%	[mJ]	%	[mJ]	%
area1	27.0658	82.04	25.9994	78.81	-1.0664	-3.23
area2	0.8041	2.44	0.8046	2.44	0.0005	0.00
area3	3.3641	10.20	3.1993	9.70	-0.1648	-0.50
area4	0.8038	2.44	0.8206	2.49	0.0169	0.05
area5+6	0.9525	2.89	0.8708	2.64	-0.0817	-0.25
sum	32.9903	100	31.6948	96.07	-1.2955	-3.93
work	33.0180	100.08			-1.2807	-3.88

comment

In the table one can see how much elastic energy is present in each area (and the total sum for all areas) for two different load cases. The difference in energy is shown to.

1. After preloading. Meaning after the preload force is applied while the shutle remains at its initial rest position from before prelaoding.
2. After actuation. Meaning after the preload force is applied the shuttle has moved to its end position in the range of motion.

To clearly indicate the proportions the percentages are calculated. The total sum of elastic energy after load case 1 is referenced as 100%. Looking at the percentages one can see that the efficiency in the sense of preloading and compensating is very low. In this design, only 3.93 % of the preloading energy is released and can be used for compensating a positive stiffness. When the range of motion is extended to the next stable equilibrium (to approximately 2.2 [mm]) a much higher efficiency can be achieved (up to 83 %), but then maximum stresses are exceeded (977 [MPa], see figure below (ref)) and nonlinear behavior shows up in the force deflection graph as pictured below (ref).

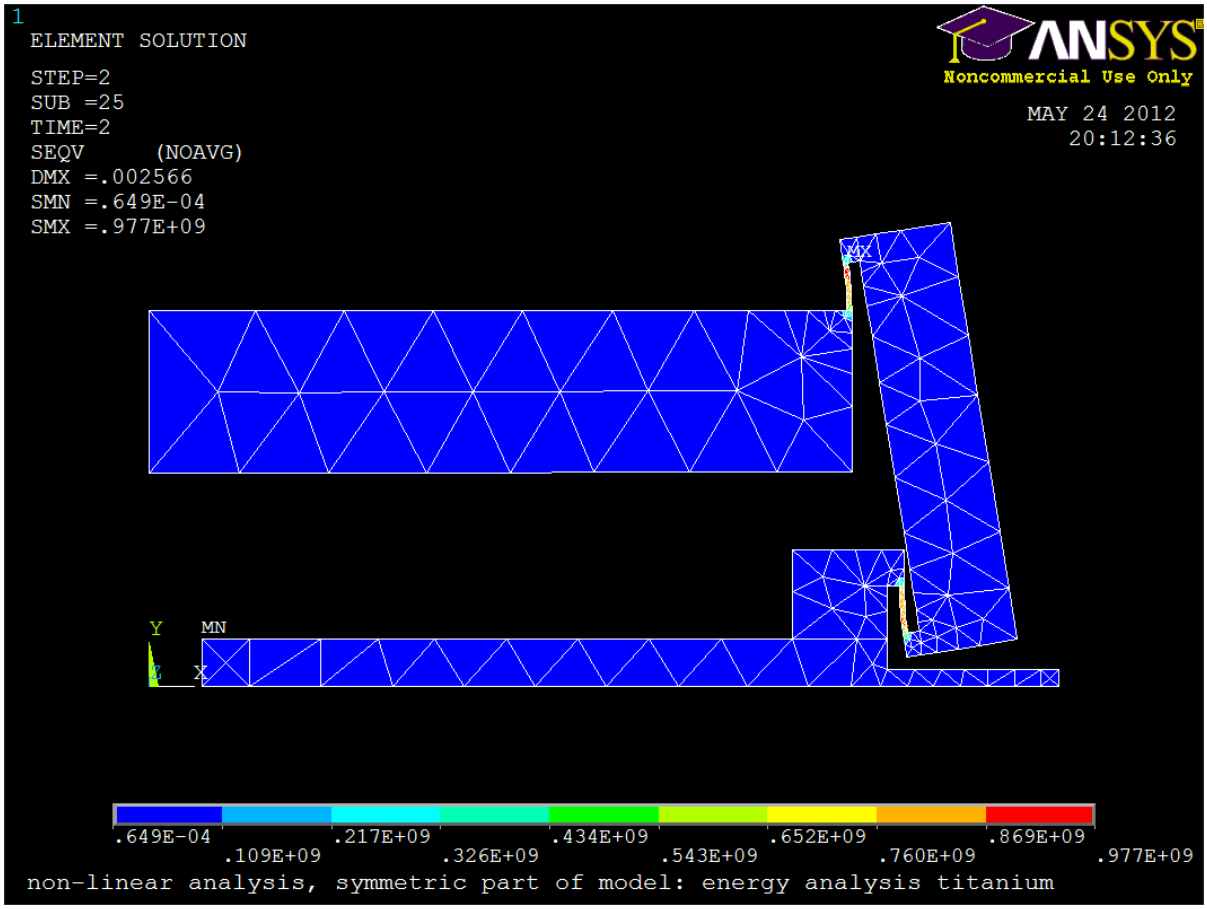

comment

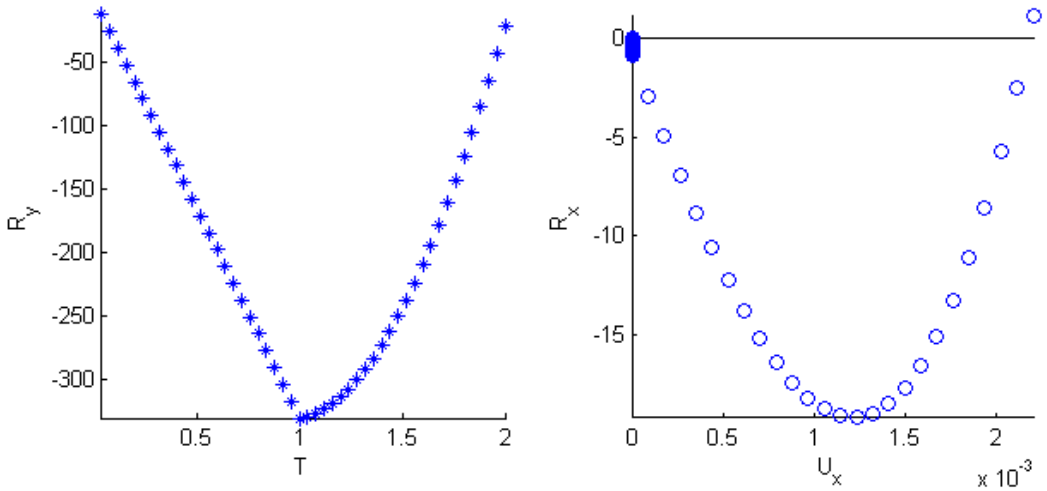

comment

ANSYS code for energy analysis

```
!*****************************************************************
! STRAIN ENERGY AFTER ACTUATION
!*****************************************************************
/POST1

!DETERMINE ENERGY OF AREA 1
ASEL,S, , ,1
ALLSEL,BELOW,AREA
```

```
AVPRIN,0,0
ETABLE,energie,SENE
SSUM
*GET,TotaleEnergie1A,SSUM, ,ITEM,energie

!DETERMINE ENERGY OF AREA 2
ASEL,S, , ,2
ALLSEL,BELOW,AREA
AVPRIN,0,0
ETABLE,energie,SENE
SSUM
*GET,TotaleEnergie2A,SSUM, ,ITEM,energie

!DETERMINE ENERGY OF AREA 3
ASEL,S, , ,3
ALLSEL,BELOW,AREA
AVPRIN,0,0
ETABLE,energie,SENE
SSUM
*GET,TotaleEnergie3A,SSUM, ,ITEM,energie

!DETERMINE ENERGY OF AREA 4
ASEL,S, , ,4
ALLSEL,BELOW,AREA
AVPRIN,0,0
ETABLE,energie,SENE
SSUM
*GET,TotaleEnergie4A,SSUM, ,ITEM,energie

!DETERMINE ENERGY OF AREA 5
ASEL,S, , ,5
ASEL,A, , ,6
ALLSEL,BELOW,AREA
AVPRIN,0,0
ETABLE,energie,SENE
SSUM
*GET,TotaleEnergie5A,SSUM, ,ITEM,energie
```

link to source info

Appendix J

Pseudo rigid body model of crank slider mechanism

Links connected by hinges having torsion springs are used to model the behavior of the negative stiffness building block. In the thereafter applied rigid body replacement method beam like shapes having constant cross section are used to define the compliant segments, see figure below (ref). This might allow for using the formula for equivalent torsion stiffness values and hinge locations accompanied by the pseudo rigid body model as presented in (ref) (boek howell).

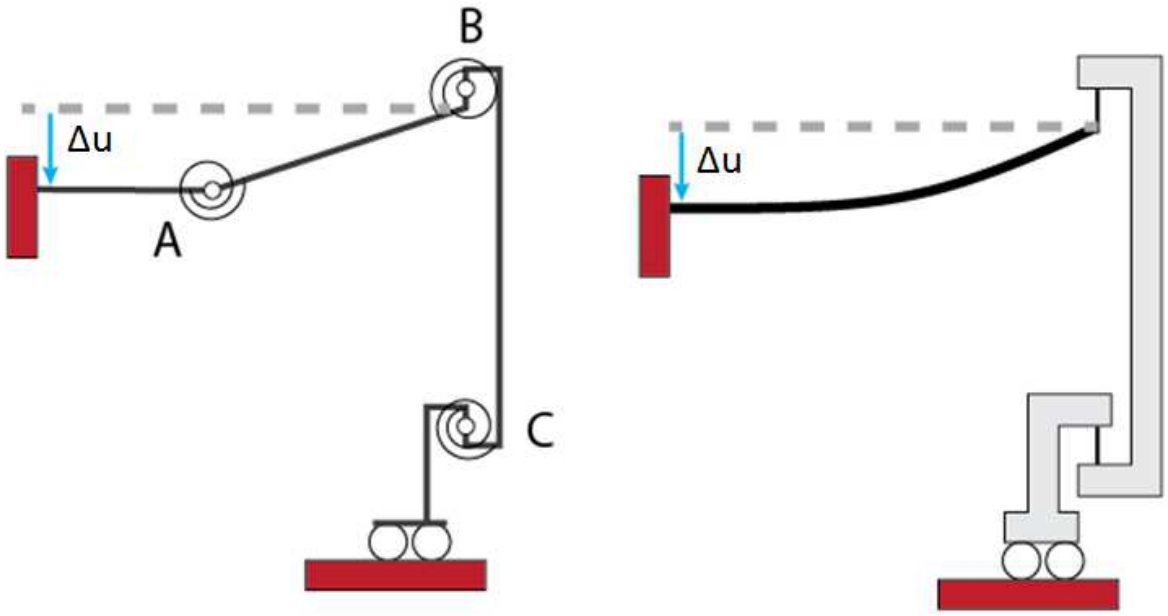

distributed compliance: preload beam

The preload beam is modeled using the pseudo rigid body model for distributed compliance. This modeling method is not entirely valid for the crank slider mechanism but it applies satisfactory, as explained below. The first figure below shows how a rigid body mechanism can model an elastic beam loaded at the tip.

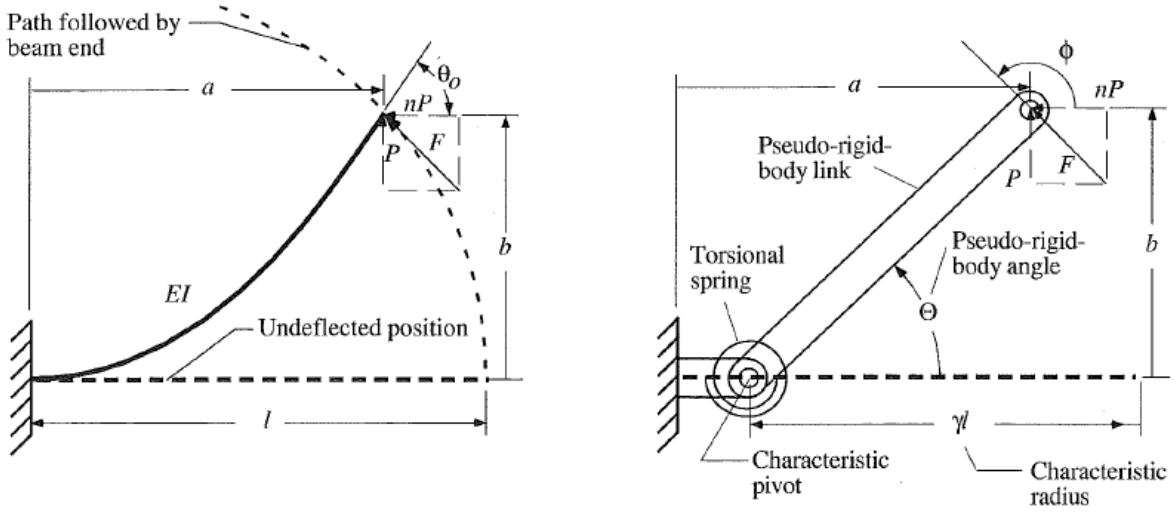

Figure showing the method of pseudo rigid body modelling for distributed compliance. Source book: Compliant Mechanisms, Larry L. Howell, Brigham Young University.

On the right is the replacing compliant segment for the link between A and B illustrated. This situation has strong equivalence with the PRB modeling method shown above (ref). Still there is a difference. The load case is not equal. The crank slider mechanism also introduces a moment at the tip, which is not incorporated in the PRB modeling method. But considering that this moment is very small compared to the moment induced by the force at the tip it may be neglected. Then the next formulas can be used:

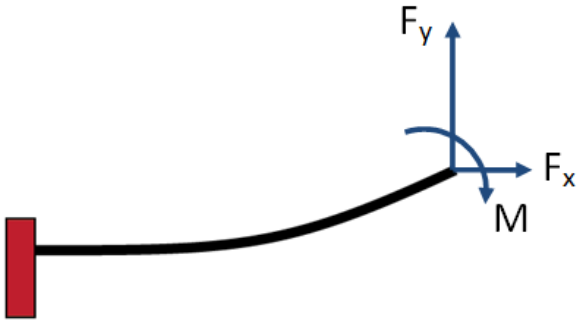

$$L_1 = \gamma \cdot l \text{ and } k_A = \gamma \cdot K_\Theta \cdot \frac{E \cdot I_b}{l}$$

The values for γ and K_Θ depend on the orientation of the composed force at the tip during deflection. In this design the angle is dependent on the ratio of F_x and F_y: $F_y = n \cdot F_x$. Since the deflections of the preload beam are very small it is assumed that this will not influence the ratio. The horizontal force F_x will change magnitude during deflection and thus influence n. However for a rough approximation it is assumed that $n = 0$, justification of this choice will follow in appendix 9 (ref), then:

$\gamma = 0.852144$
$K_\Theta = 1.967647$

Assuming the nominal values for geometry the next value for the equivalent stiffness is found:

$k_A = 1017.8$ [Nm/rad]

lunped compliance: elastic hinge

The elastic tensional joint is modeled by a pseudo rigid body modeling method for a lumped compliance. In this case the modeling method is also not entirely valid but for a rough approximation good enough. The figure below shows how a lumped compliance is modeled.

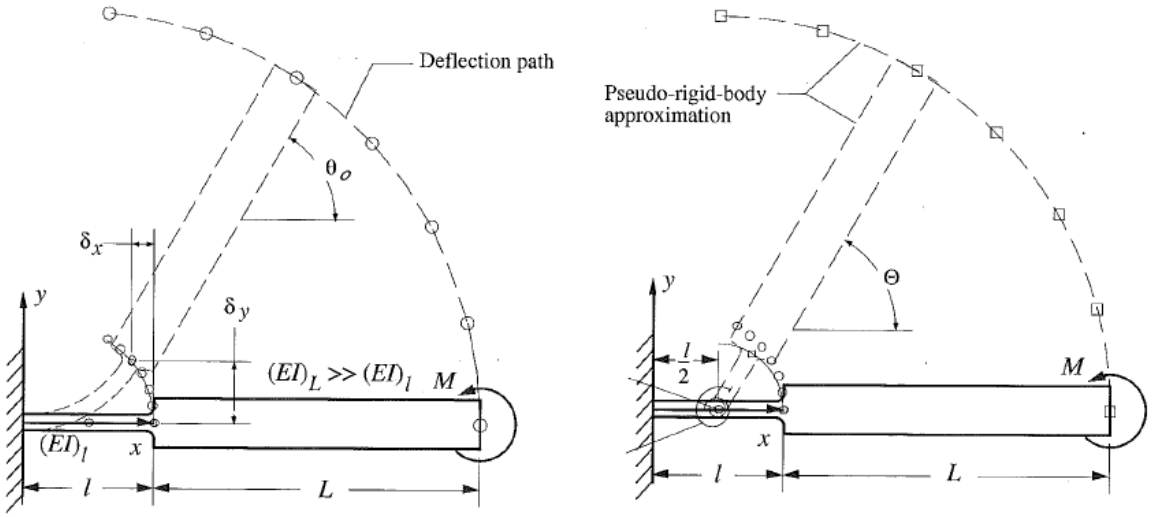

Figure showing the method of pseudo rigid body modelling (ref) for lumped compliance. Source book: Compliant Mechanisms, Larry L. Howell, Brigham Young University.

Two replacing compliant segments are illustrated on the right (ref). One for the lumped compliance at point B and on for point C. Both load cases are similar, so only one has to be considered. A few differences can be noticed compared to the PRB model. The geometry differs in location of the hinge. The PRB modeling method assumes that the hinge is in between the clamped end and the application point of the moment. While the replacing compliant segment has a tensional joint which places the hinge somewhere behind the clamped end. Besides that the load cases differ, only a moment is assumed at the tip in the PRB modeling method while the replacing compliant segment is apart from a moment also loaded by forces.
Both differences may be neglected when the ratio between rigid link length and compliant joint length is large enough. A minimal value of 10 is recommended. In this case the link length is estimated to be:

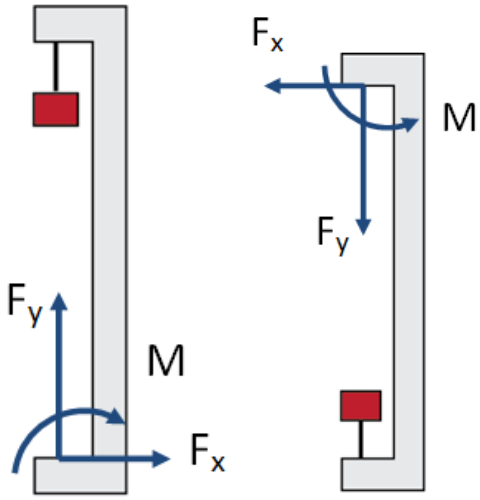

$$L_2 = r + l - j_l = 15.75 - 2 = 13.75 \text{ [mm]}$$

This makes the ratio rather small: $\frac{15.75 - 2}{2} = 6.88$, however this value is justified in the validation, appendix (9). Finally the next formula may be used to find an equivalent torsional stiffness value for the elastic joints in point B and C, considering the nominal values for the geometry:

$$k_B = k_C = \frac{E \cdot I_j}{l} = 0.2278 \text{ [Nm/rad]}$$

behavior of PRB model

Knowing the link lengths and the torsional stiffnesses it becomes possible to calculate a force deflection graph using the crank slider mechanism. The stiffness ratio between point A and B or C is 4468 [-]. The following curve was plotted:

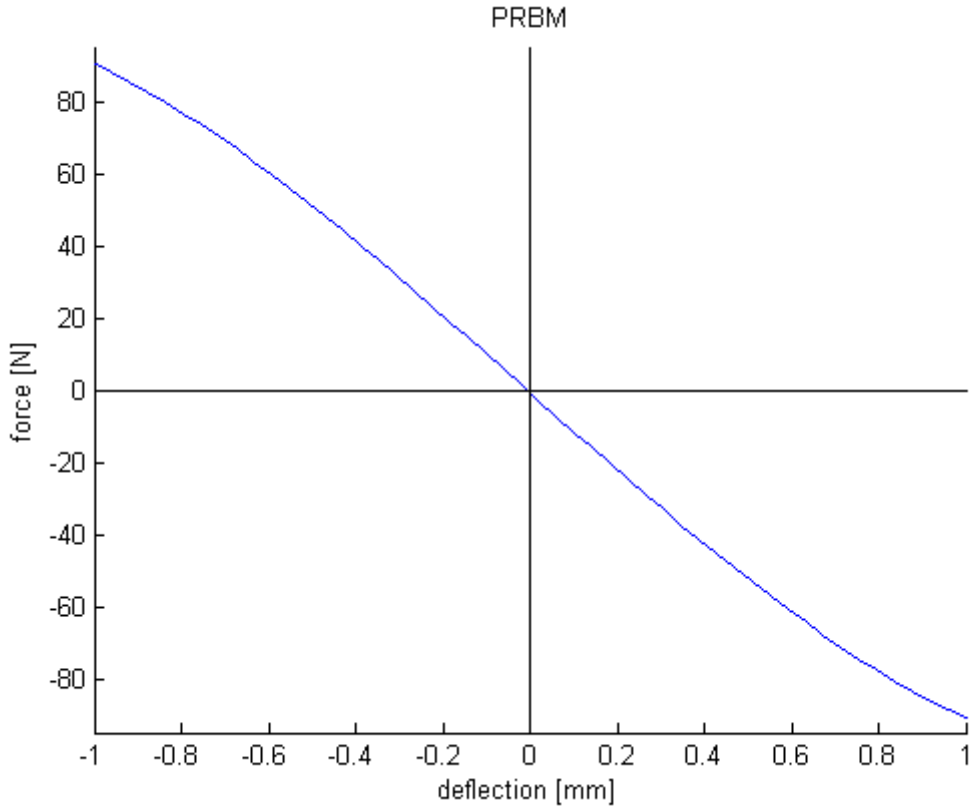

A plot of the pseudo rigid body model applied to the crank slider mechanism.

Over the intended range of motion (about $-0.4...0.4$ [mm]) the behavior looks quite linear. In appendix 9 this model is evaluated compared to the measurement results of the manufactured prototype and the finite element model.

Appendix K

Sensitivity analysis of FE model and PRB model

This appendix discusses the sensitivity of the behavior of the finite element model and the pseudo rigid body model to changes in the preload displacement, material properties or geometry. For a list of parameters (see table (ref)) the change of behavior of is plotted. In the figure below (ref) the geometric parameters are illustrated. The sensitivity results are compared for both models for each parameter.

parameter	minimal	nominal	maximal
preload displacement Δu [mm]	−0.20	−0.25	−0.30
young's modulus E [GPa]	100	113.9	120
poisson's ratio v [-]	0.28	0.30	0.36
preload beam thickness b_{th} [mm]	6.7	6.8	6.9
preload beam length b_l[mm]	28.5	29.5	30.5
elastic joint tickness j_{th} [mm]	0.15	0.20	0.25
elastic joint length j_l[mm]	1.5	2.0	2.5
rigid link length r_l [mm]	14.75	15.75	16.75

The change in parameter value is chosen such that it complies with the worst case scenario regarding fabrication tolerances (for the geometry), experimental inaccuracy (for the preload displacement) and lack of knowledge (material properties). The conclusion is that for both models the preload displacement has the largest influence on the negative stiffness compared with the other parameters. All parameter deviations individually seem not to be capable of causing the big difference in behavior between the nominal case and the measurement result as discussed in appendix 9 (ref).

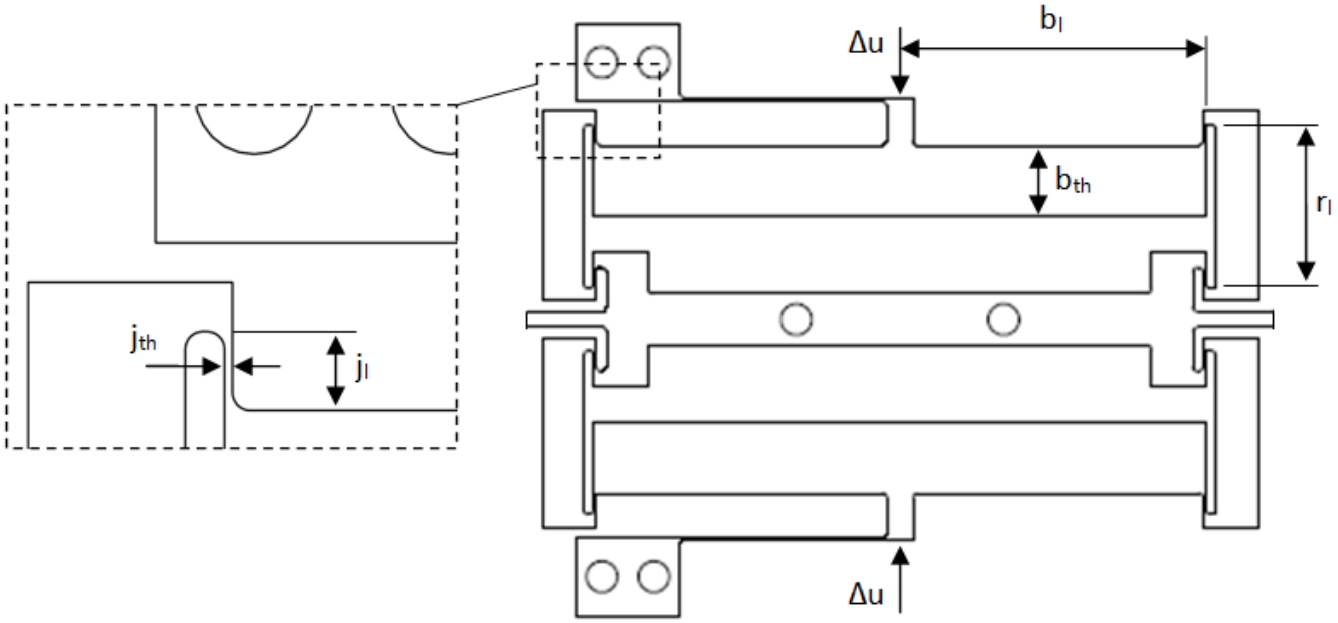

The geometric parameters that change value and affect the behavior.

Another conclusion is that at least for this specific design the sensitivities of the FE model and the PRB model are highly equal.

Sensitivities

In each graph the measurement result is plotted in order to see if the change in each model parameter individually might be held responsible for the big difference between the nominal behaviors of both models and the measurement (as discussed in appendix 9 (ref)). Graphs on the left belong to the pseudo rigid body model, graphs on the right to the finite element model.

nominal case

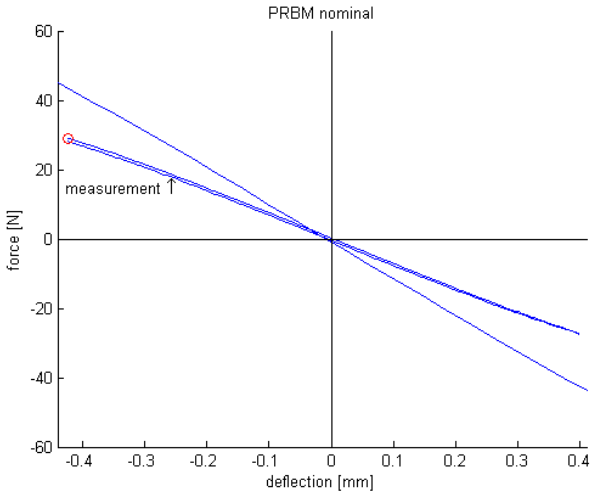

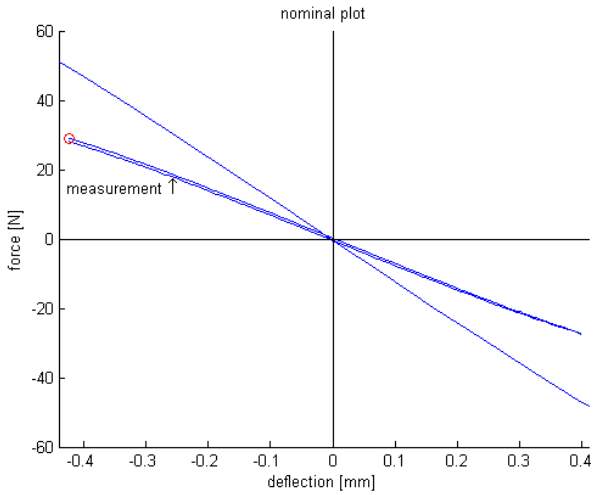

The nominal case over predicts the negative stiffness with large amount for both models. The PRB model is some what closer to the measurement than the FE model.

preload displacement: Δu [mm]

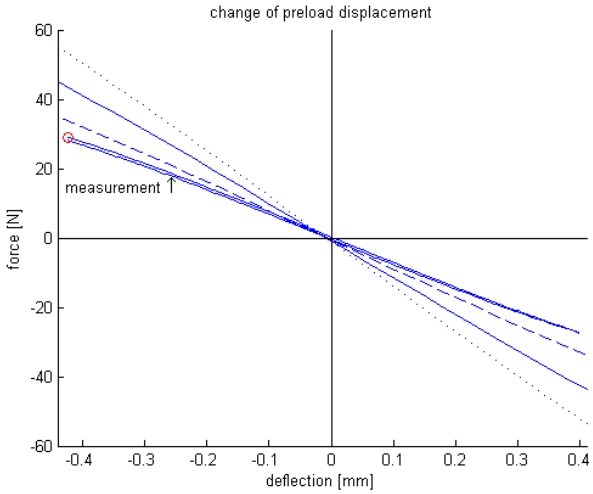

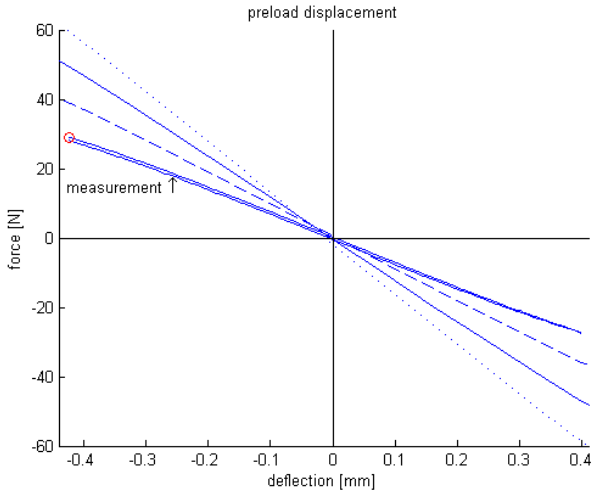

minimal (striped): -0.20 *nominal (continuous):* -0.25 *maximal (dotted):* -0.30

A small change with respect to the overall size of the mechanism (0.05 [mm]) in preloading affects the behavior significantly. Increasing preload increases negative stiffness. For both models the deviations are of the same order of magnitude.

young's modulus: E [GPa]

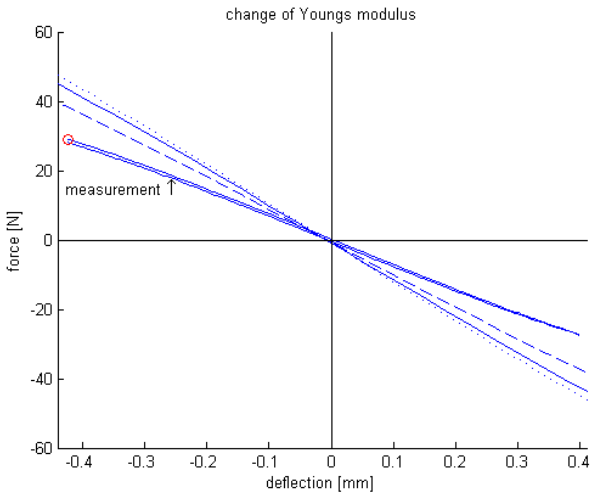

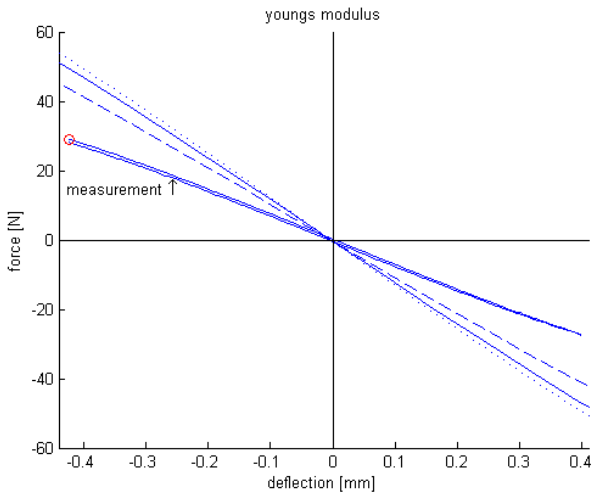

minimal (striped): 100 *nominal (continuous):* 113.9 *maximal (dotted):* 120

Changing Young's modulus has an significant effect too, but it is assumed that the real value lies close to 113.9 [GPa]. Increasing the elasticity modulus increases the negative stiffness. For both models the deviations are of the same order of magnitude.

poission's ratio: v [-]

-

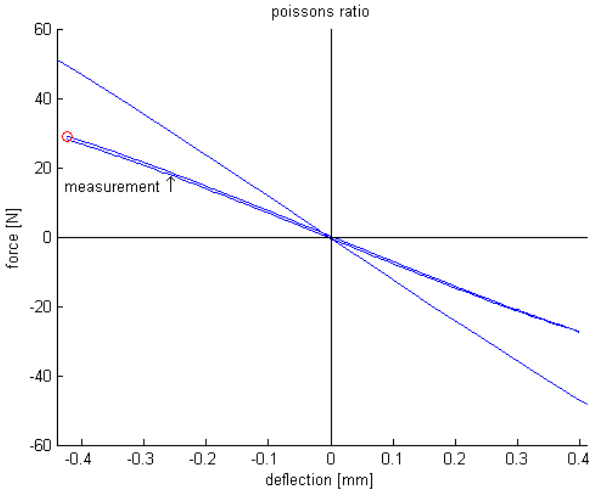

minimal (striped): 0.28 *nominal (continuous):* 0.30 *maximal (dotted):* 0.36

Altering the poisson's ratio for the FE model has no effect. The minimal and maximal values result in behavior equal to the nominal case. No plot is made for the PRB model because dependence of the behavior to possion's ratio can only be due to the relation between shear modulus and Young's modulus ($G = \frac{E}{2 \cdot (1 + v)}$). This is equal to changing the young's modulus itself.

This is a consequence of the assumption of beam theory in the PRB model, where shear stresses and strains are neglected.

preload beam tickness: b_{th} [mm]

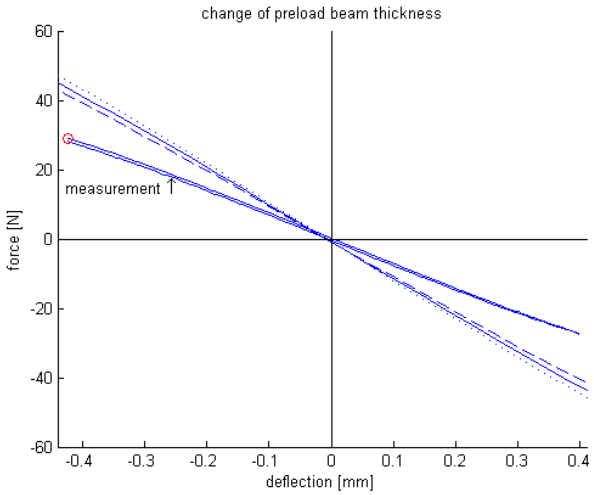

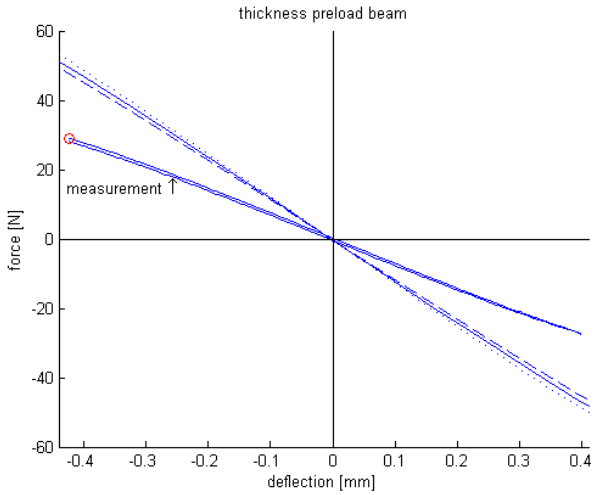

minimal (striped): 6.7 *nominal (continuous):* 6.8 *maximal (dotted):* 6.9

Changing the thickness of the beam by 0.1 [mm] has some effect. The thicker the beam the higher the negative stiffness. Increasing beam thickness means increasing torsion stiffness in the PRB model. For both models the deviations are of the same order of magnitude.

preload beam length: b_l [mm]

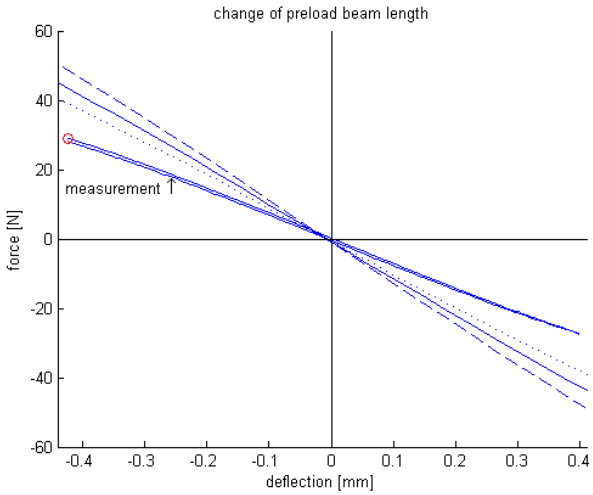

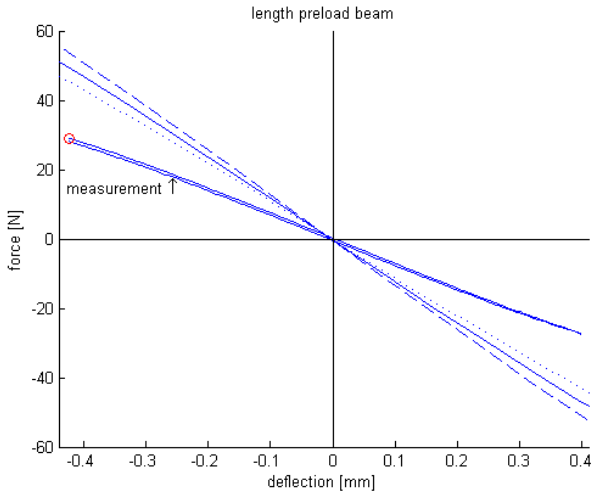

minimal (striped): 28.5 *nominal (continuous):* 29.5 *maximal (dotted):* 30.5

The shorter the beam is the higher the negative stiffness becomes. Shortening the beam is equal to increasing torsion stiffness of spring A in the PRB model. For both models the deviations are of the same order of magnitude.

elastic joint thickness: j_{th} **[mm]**

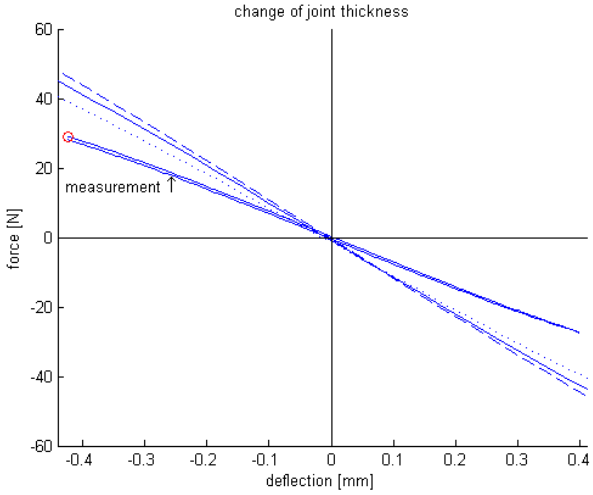

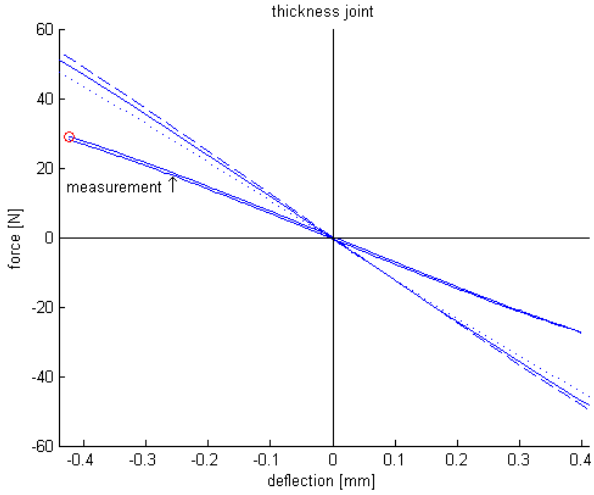

minimal (striped): 0.15 *nominal (continuous):* 0.20 *maximal (dotted):* 0.25

Making the elastic joint thinner increases the negative stiffness. Equal to lowering the torsion stiffness in hinge B and C of the PRB model. For both models the deviations are of the same order of magnitude.

elastic joint length: j_l **[mm]**

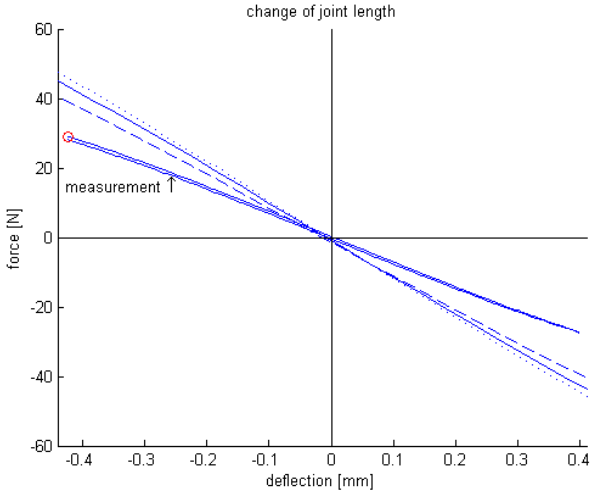

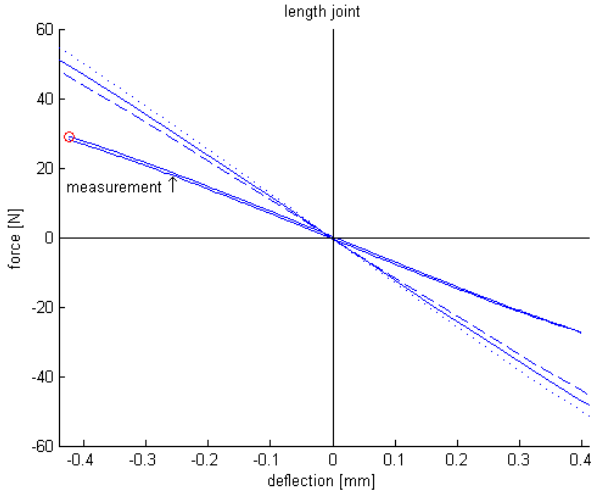

minimal (striped): 1.5 *nominal (continuous):* 2.0 *maximal (dotted):* 2.5

Increasing the length of the elastic joint increases the negative stiffness. For the PRB model the nominal case does not seem to be in the center of the limit cases, for the FE model it does. The difference may be explained by the effect of changing the location of the high which is modeled by the FE model but not by the PRB model. However for both models the deviations are of the same order of magnitude.

rigid link length: r_1 **[mm]**

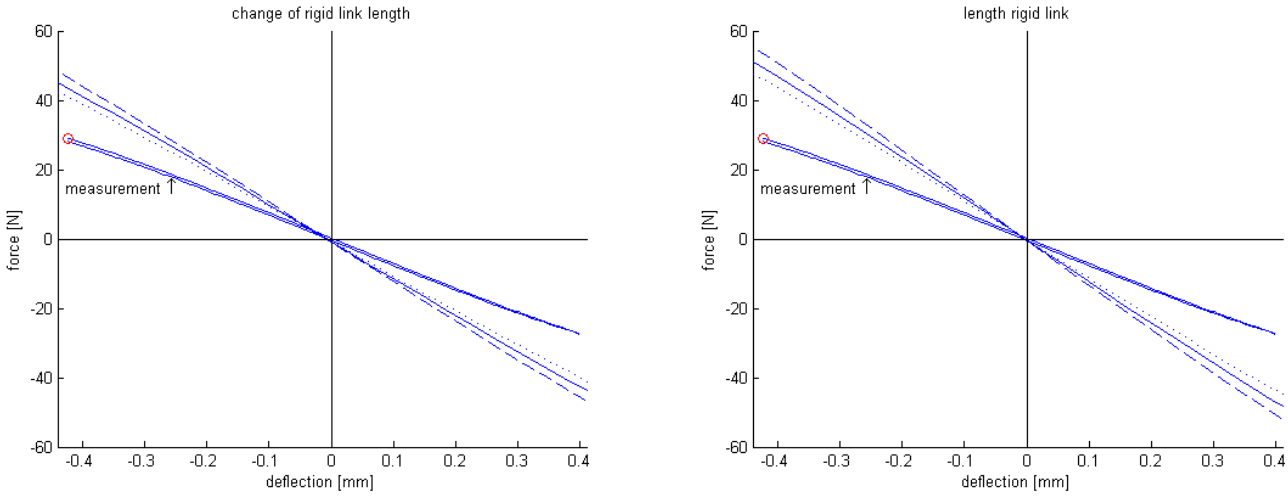

minimal (striped): 14.75 *nominal (continuous):* 15.75 *maximal (dotted):* 16.75

Shortening the rigid link will increase the negative stiffness. For both models the deviations are of the same order of magnitude.

link naar bron data

Appendix L

Measurement report of titanium prototype

In this appendix the measurement results are discussed and two effects are explained, out of plane motion of the shuttle and shifting of the equilibrium point. The discussion is structured as follows. First results of load case 1,2 and 3 are described consecutively. The load cases are defined in the "Evaluation method" section. Then the negative stiffness of the balancer is measured independently from the grasper. Each measurement is a record of the force over the distance traveled back and forth through the range of motion, so hysteris effects can be observed. The red circle in the measurement graphs indicates the starting point of the measurement.

loadcase 1

In this loadcase only the behavior of the grasper is measured. See graph below (ref).

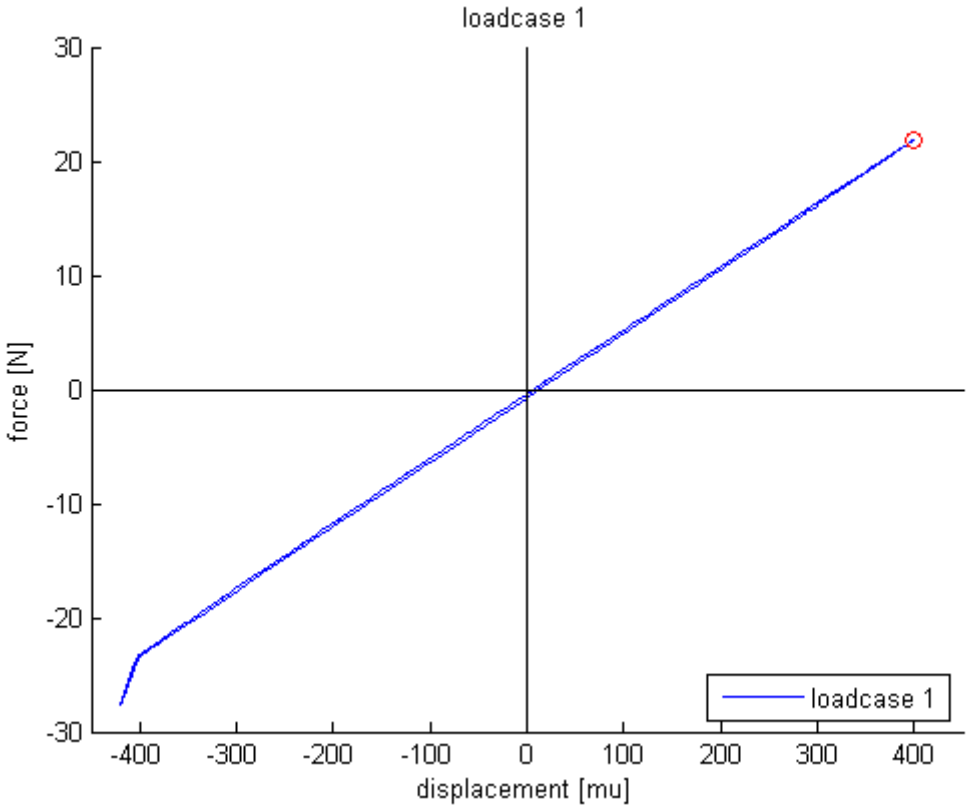

loadcase 1: force deflection graph of grasper

The behavior is quite linear, the positive stiffness can be approximated by the formula $k = \frac{\Delta F}{\Delta U} \cong 56$ [N/mm].

The hysteresis is very low compared to the work done and is estimated to be maximal 2 [%]. On the lower left side an sudden change in slope can be seen, this is the point where the grasper is fully closed and both sides touch each other such that stiffness raises suddenly.

loadcase 2

The positive stiffness of the grasper + balancer without any preload is measured according to loadcase 2. See graph below (ref).

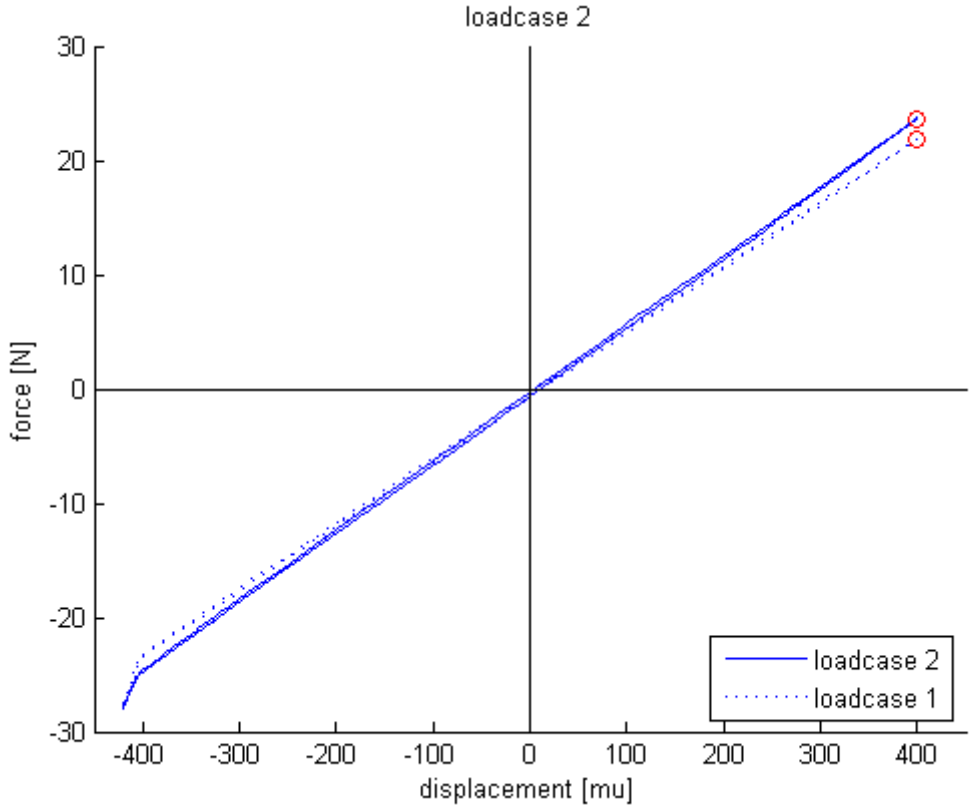

loadcase 2: force deflection graph of grasper and balancer in non-preloaded state.

The stiffness is a little bit increased compared to loadcase 1, approximating the value of 60 [N/mm]. The difference can be seen when plotted next to the graph of loadcase 1, which is depicted with a dotted line. This means that the positive stiffness of the non-preloaded balancer is about the value 4 [N/mm].

Zooming in to the equilibrium points of loadcase one and two, a small offset is visible. See figure below (ref). The zero displacement axis corresponds with the initial configuration when the monolithic structure is unmounted. A shifting effect on the equilibrium points shows up after clamping of the structure to the base plate. The shift is rather small.

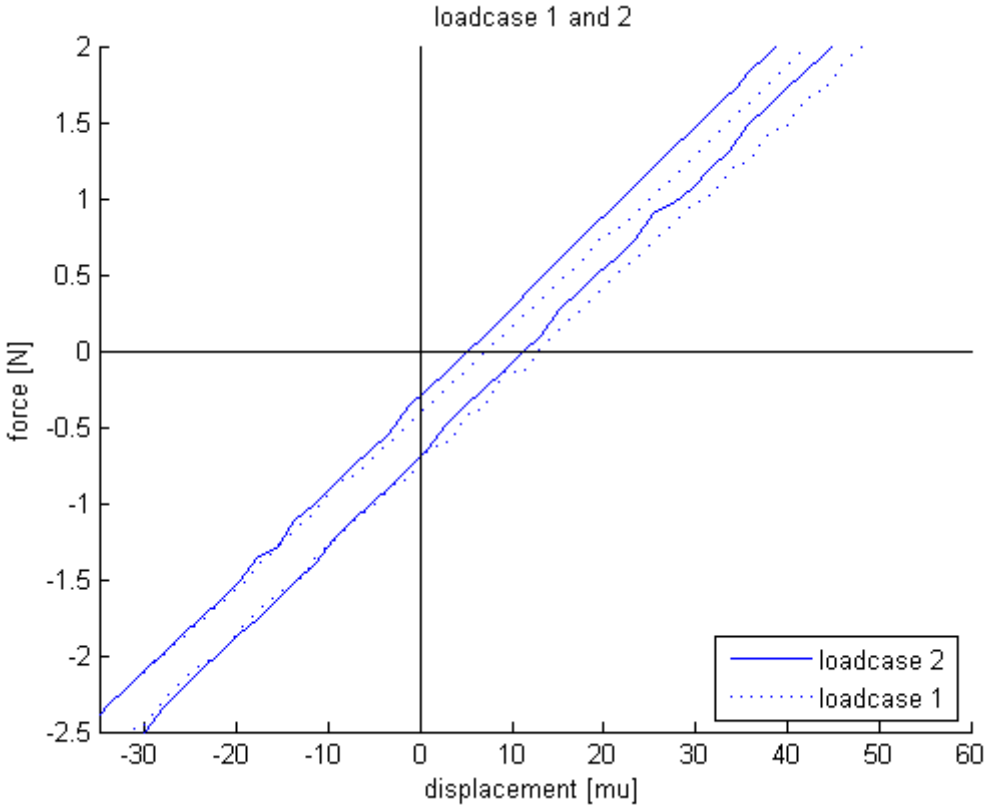

loadcase 1 and 2: shift effect due to clamping.

loadcase 3

The balancer and grasper are fixed according to loadcase 3 and preloading is incrementally applied. See graph below.

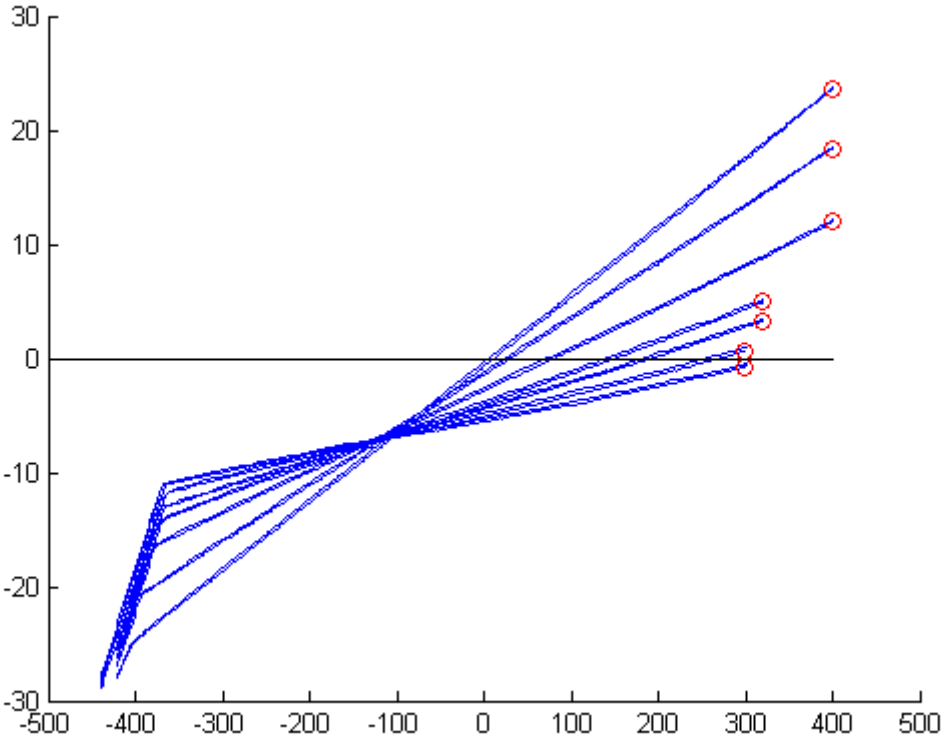

loadcase 3: preloading the balancer.

The slope is clearly effected by preloading, stiffness decreases gradually. In the mean time the graph is dropping below the zero force line, going towards a negative constant force behavior. The graph rotates around a point below the zero force line, see point A. The consequence is that the stable equilibrium point is moving to the right while preloading is incremented. In the mean time point A does not move much when preload is gradually increased. This means that if this rotation point is on the zero force line, near zero force behavior will be exposed once preloading is increased enhough. The fact that the rotation point is not on the zero line may be a consequence of initial stresses, caused for example by (the heat involved in the) fabrication proces, clamping of the elastic mechanism to the fixed world or plastic deformation. The initial stresses cause a relative shift of the equibrilium points of the positive and negative stiffness. As soon as they do not intersect, a constant force behavior will result, as illustrated in the graph below.

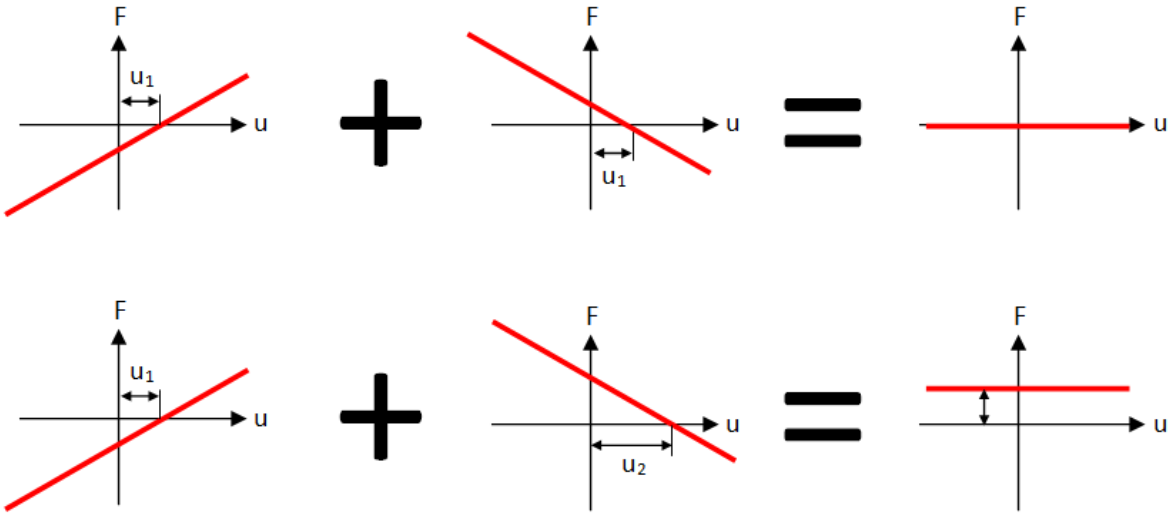

Two linear functions with equal slope but with opposite sign will add up to a constant value. The constant value is zero if both intersection points (equilibrium points) on the u axis coincide at u_1. When there is a relative shift (u_1 and u_2) the constant value will be non zero.

Another remarkable effect is that that the closing point in the graph (the point of sudden change in slope) of the grasper is shifting to the right. This is due to out of plane motion of the shutle. Both sides of the grasper rotate a bit as illustrated in the picture below.

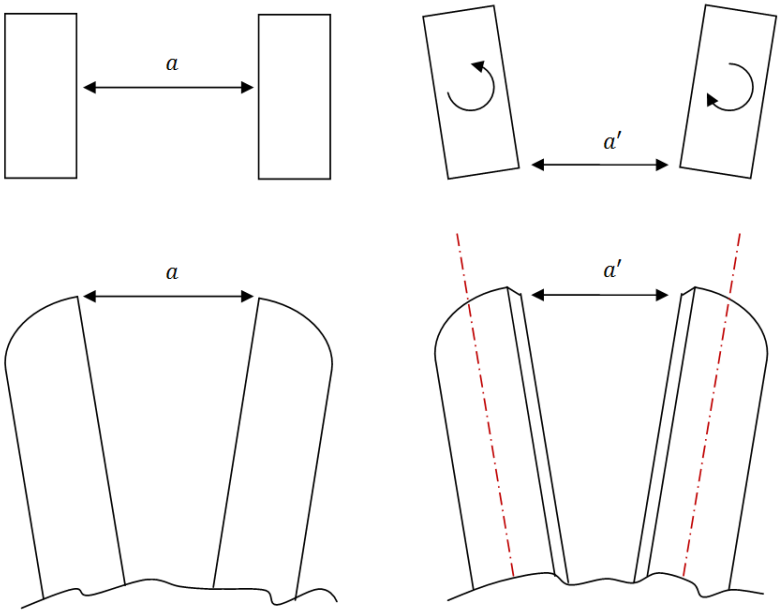

rotation of both sides of grasper around the dotted axis due to very small out of plane motion of shutle: $a > a'$.

The out of plane deformation is probably due to the high preload forces which also form a bending moment reaction on the base plate. The bending moment is accompanied by a bending deformation which results in

preload forces oriented a bit out of plane.

negative stiffness

In loadcase 3 a large shift of equilibrium occurred while only little shifts are introduced by clamping in loadcase 1 and 2. To determine the cause of the large shift the negative stiffness is measured alone. The grasper is unfixed, the balancer is fixed and gradually preloaded. The next graph results.

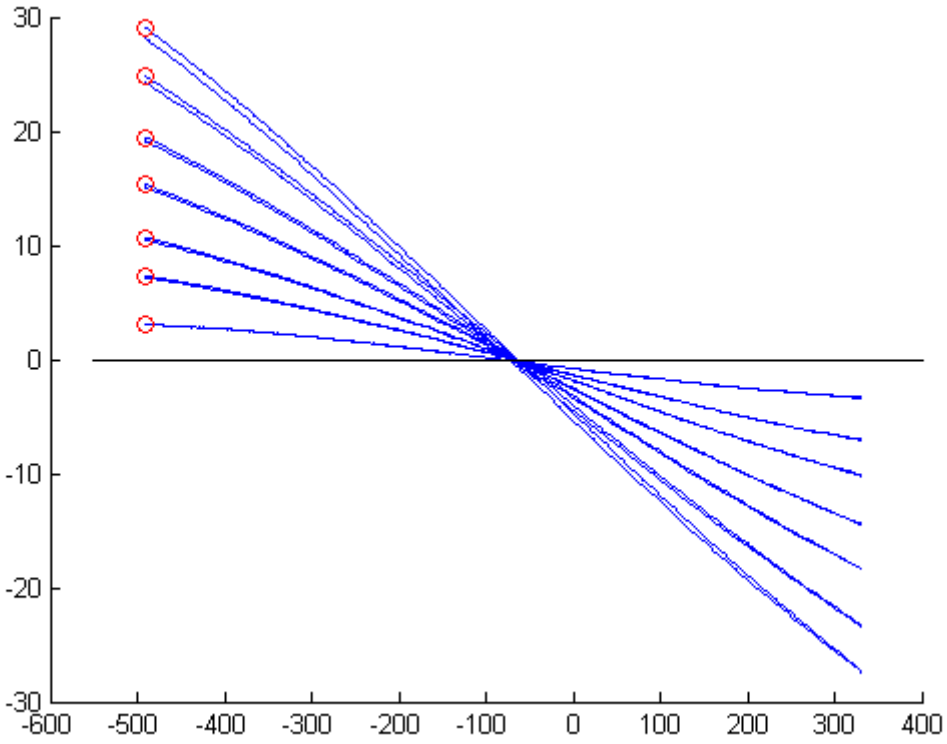

Negative stiffness with non shifting equilibrium point.

The point of rotation (point B) of the graph lies close to the zero force line. This means that the balancer itself is not responsible for the equibrilium shift. It then is likely to be a consequence of initial stresses induced by clamping the elastic mechanism to the base plate.

negative stiffness after plastic deformation

After the measurement results where obtained for the negative stiffness probably a small plastic deformation occurred in the elastic hinges, due to overloading of the balancer, introducing initial stresses. The effect of this can be seen in the graph below where the negative stiffness is measured again.

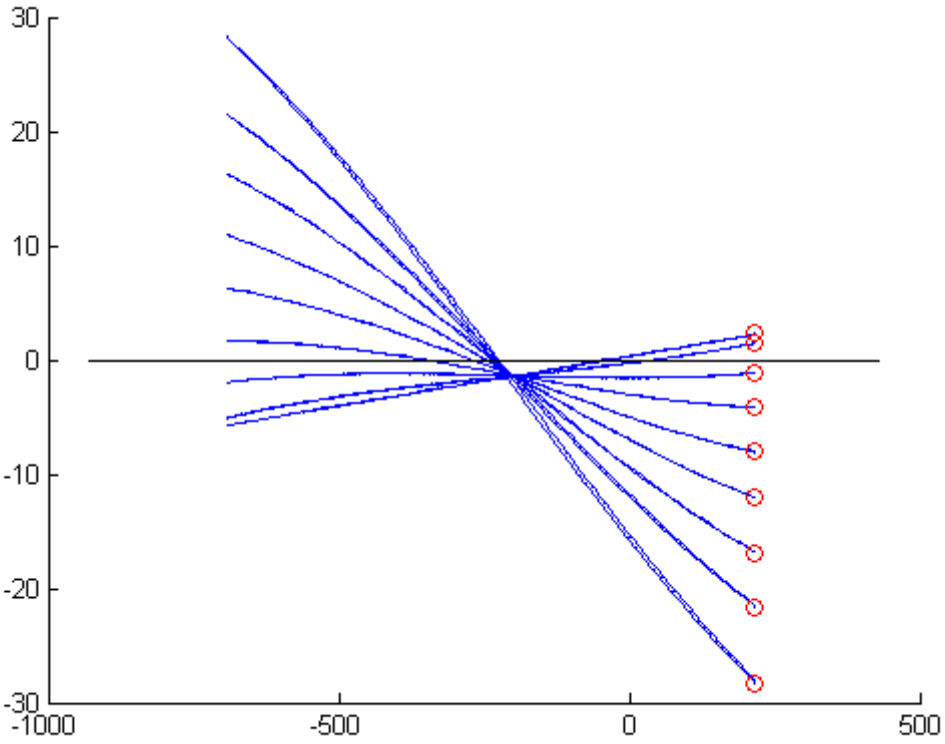

Negative stiffness with shifting equilibrium point.

The rotation point of the graph has dropped clearly below the zero force line. When preload is increased one can see a stable equilibrium point shifting to the right until it moves out of scope. A unstable equilibrium point is coming in from the left side. This means that when the monolithic mechanism is clamped to the base plate in the initial configuration and then the preload is applied a constant negative force behavior will occur.

concluding remarks

- Initial stresses are a sufficient condition for equilibrium shifting.
- Preloading is not a sufficient condition for equilibirum shifting for this particular design, only when it is combined with an initial stress distribution.

link naar bron data